



**University of  
Nottingham**

UK | CHINA | MALAYSIA

# **Overcoming emerging challenges in biocatalysis**

**David Roura Padrosa**

**Supervisor:**

**Prof. Francesca Paradisi**

**Thesis submitted to the University of Nottingham for the  
degree of Doctor of Philosophy**

**August 2019**



## Abstract

In the last few decades, biocatalysis has emerged as a promising path towards more cost-effective and sustainable chemical synthesis in the path of developing more environmentally friendly strategies. Biocatalysis offers a beneficial approach but its widespread application is hampered by the drawbacks associated with the use of enzymes; especially, their stability under industrial requirements and their reusability. New, more robust, biocatalysts have been identified from extremophiles and in parallel, protein immobilisation has advanced, permitting the reuse of the biocatalysts, facile separation from the reaction bulk and their application in continuous processes. In this work, several aspects linked to the use of biocatalysts in flow reactors have been investigated to solve relevant challenges and facilitate the application of biocatalytic methods for chemical synthesis.

In this sense, a new method for the immobilisation of challenging enzymes has been developed and applied to a carboxylesterase for the hydrolytic deracemization of naproxen butyl ester in flow. Moreover, substrate insolubility has been resolved with the addition of surfactants (Chapter 4). Transaminases, and further optimization of their stability and applications, have also been investigated. Specifically, residues involved in PLP binding have been studied identifying a poorly conserved asparagine as a key amino acid in PLP stabilization in dimeric transaminases (Chapter 5). Novel synthetic methods involving transaminases have also been developed, specifically looking at the combination of a novel halo adapted alanine dehydrogenase to shift the equilibrium and reduce the amount of amino donor generally required (Chapter 6). Finally, the deamination of lysine was investigated for the synthesis of pipercolic acid. Here, the use of a transaminase was explored as well as a redox neutral cascade. This last system was co-immobilised in the same support and successfully applied in flow, achieving a volumetric yield of up to 2.5 g/h/L, 10-fold improvement from the fermentation-based production used up to date (Chapter 7).

# Table of contents

<b>Abstract</b>	<b>III</b>
<b>Table of contents</b>	<b>IV</b>
<b>Abbreviations</b>	<b>VII</b>
<b>Chapter 1: Introduction</b>	<b>- 10 -</b>
1.1. Enzymes as biocatalysts	- 10 -
1.2. Carboxylesterases	- 12 -
1.3. Aminotransferases	- 15 -
1.4. Oxidoreductases	- 17 -
1.5. Extremophiles as source of new biocatalysts	- 20 -
1.6. Enzyme immobilisation	- 22 -
1.7. Flow biocatalysis	- 25 -
1.8. Bibliography	- 28 -
<b>Chapter 2: Aims and objectives</b>	<b>- 41 -</b>
<b>Chapter 3: Material and methods</b>	<b>- 42 -</b>
3.1. Reagents	- 42 -
3.2. General instrumentation	- 42 -
3.3. Cell cultures and manipulation	- 44 -
3.3.1. Bacterial strains	- 44 -
3.3.2. Culture mediums	- 44 -
3.3.3. Preparation of chemically competent cells	- 45 -
3.3.4. Preparation of electro competent cells	- 45 -
3.3.5. Transformation of competent <i>E. coli</i> cells	- 46 -
3.4. General procedures	- 46 -
3.4.1. Gene cloning	- 46 -
3.4.2. Agarose gel electrophoresis	- 47 -
3.4.3. Protein overexpression and purification	- 48 -
3.4.4. Protein quantification	- 50 -
3.4.5. SDS-PAGE	- 50 -
3.4.6. Size exclusion chromatography	- 51 -
3.4.7. Enzymatic activity assay	- 51 -
3.4.8. Kinetic characterisation	- 53 -
3.4.9. Batch reactions	- 53 -
3.4.10. Covalent enzyme immobilisation	- 53 -
3.4.11. Preparation of Agarose with epoxide groups	- 54 -
3.4.12. Preparation of dextran-aldehyde	- 54 -
3.4.13. Flow reactions	- 54 -
3.4.14. HPLC analysis	- 56 -
3.5. Bibliography	- 57 -

**Chapter 4: Esterase immobilisation and flow assisted  
bioconversion of water insoluble substrates \_\_\_\_\_ - 58 -**

4.1.	Introduction _____	- 59 -
4.2.	HeE cloning and characterisation _____	- 61 -
4.3.	Profen hydrolysis _____	- 68 -
4.4.	Immobilisation of BS2m _____	- 72 -
4.4.1.	T4L strategy _____	- 74 -
4.5.	Flow deracemization of naproxen butyl ester _____	- 76 -
4.6.	Experimental procedures _____	- 79 -
4.6.1.	Synthesis of p-nitrophenyl esters _____	- 79 -
4.6.2.	Synthesis of NSAID butyl-ester _____	- 79 -
4.6.3.	NMR characterization of butyl esters _____	- 79 -
4.6.4.	HPLC analysis to determine the enantioselectivity _____	- 80 -
4.6.5.	Computational analysis of tunnels _____	- 81 -
4.7.	Bibliography _____	- 82 -

**Chapter 5: PLP binding in class-III  $\omega$ -transaminases \_\_\_\_\_ - 89 -**

5.1.	Introduction _____	- 90 -
5.2.	PfTA crystal structure determination _____	- 92 -
5.3.	Computational analysis of PLP-binding pocket _____	- 93 -
5.4.	Functional characterisation of the single mutants _____	- 97 -
5.5.	Cofactor release study _____	- 100 -
5.6.	Temperature stability under PLP limiting conditions _____	- 101 -
5.7.	Melting temperature _____	- 103 -
5.8.	Structural rearrangements after PLP binding _____	- 104 -
5.9.	Experimental procedures _____	- 106 -
5.9.1.	Crystallization, data collection and structure determination of PfTA _____	- 106 -
5.9.2.	Model building, refinement and validation _____	- 107 -
5.9.3.	Computational analyses _____	- 107 -
5.9.4.	MSA and conservation scores _____	- 107 -
5.9.5.	Apo and holo-form calculations _____	- 108 -
5.9.6.	Cofactor release study _____	- 108 -
5.9.7.	Temperature stability assays _____	- 108 -
5.9.8.	Melting temperature and dissociation constant calculations _____	- 109 -
5.10.	Bibliography _____	- 110 -

**Chapter 6: In situ recycling of the amino donor for transaminase  
catalysed reactions \_\_\_\_\_ - 115 -**

6.1.	Introduction _____	- 116 -
6.2.	Introduction _____	- 116 -
6.3.	Alanine dehydrogenase cloning and characterisation: _____	- 118 -

<b>6.4.</b>	<b>Co-substrate recycling for TA catalysed reactions:</b>	_____	<b>- 123 -</b>
<b>6.5.</b>	<b>HeAlaDH immobilisation:</b>	_____	<b>- 127 -</b>
<b>6.6.</b>	<b>Post-immobilisation stabilisation:</b>	_____	<b>- 129 -</b>
6.6.1.	Flow assisted amination with a mixed packed-bed reactor	_____	- 133 -
6.6.2.	Co-immobilisation of AlaDH and FDH:	_____	- 134 -
<b>6.7.</b>	<b>Experimental procedures</b>	_____	<b>- 139 -</b>
6.7.1.	Coating of immobilised HE-AlaDH with polyethyleneimine	_____	- 139 -
6.7.2.	Coating of immobilised HE-AlaDH with glutaraldehyde	_____	- 139 -
6.7.3.	Coating of immobilised AlaDH with dextran poly-aldehyde:	_____	- 139 -
6.7.4.	Co-immobilisation of HeAlaDH and CbFDH:	_____	- 139 -
<b>6.8.</b>	<b>Bibliography</b>	_____	<b>- 141 -</b>
<b>Chapter 7: Synthesis of pipecolic acid by a multi-enzymatic cascade</b>			<b>- 147 -</b>
<b>7.1.</b>	<b>Introduction</b>	_____	<b>- 148 -</b>
<b>7.2.</b>	<b>HeP5C cloning and characterization</b>	_____	<b>- 150 -</b>
<b>7.3.</b>	<b>Combination of HeP5CR with HeTA catalysed reaction</b>	_____	<b>- 152 -</b>
<b>7.4.</b>	<b>Combination of HE-P5C with Lys6DH</b>	_____	<b>- 161 -</b>
7.4.1.	Lysine 6 dehydrogenase candidate selection and characterisation:	_____	- 161 -
7.4.2.	Batch biotransformation of L-lysine into L-PA:	_____	- 164 -
<b>7.5.</b>	<b>Immobilisation of GsLys6DH and HeP5C:</b>	_____	<b>- 165 -</b>
<b>7.6.</b>	<b>Optimisation of HeP5CR immobilisation, co-immobilisation with GsLys6DH and flow-assisted synthesis of L-PA:</b>	_____	<b>- 166 -</b>
<b>7.7.</b>	<b>Experimental procedures</b>	_____	<b>- 173 -</b>
7.7.1.	Synthesis of pyrroline-6-carboxylate:	_____	- 173 -
7.7.2.	Co-immobilisation of BsLys6DH and HeP5CR:	_____	- 173 -
<b>7.8.</b>	<b>Bibliography</b>	_____	<b>- 174 -</b>
<b>Chapter 8: Conclusions and final remarks</b>			<b>- 182 -</b>
<b>Acknowledgments</b>			<b>- 186 -</b>

## Abbreviations

AADH	Amino acid dehydrogenases
MECN	Acetonitrile
AlaDH	Alanine dehydrogenase
BCE	<i>Bacillus coagulans</i> esterase
BmGDH	<i>Bacillus megaterium</i> glucose dehydrogenase
BS2m	<i>Bacillus subtilis</i> esterase
CALB	<i>Candida antarctica</i> lipase B
CbFDH	<i>Candida boidinii</i> formate dehydrogenase
CLEA	Cross-linked enzyme aggregates
COX	Cyclooxygenase
CvTA	<i>Chromobacterium violaceum</i> transaminase
DAAT	D-amino acid transferase
DCC	Dicyclohexylcarbodiimide
dexCHO	Dextran aldehyde
DMSO	Dimethyl sulfoxide
DNA	Deoxyribonucleic acid
DSF	Differential scanning fluorimetry
DTT	Dithiothreitol
EDTA	Ethylenediaminetetraacetic acid
EtOH	Ethanol
FAD	flavin adenine nucleotide
Fmoc	Fluorenylmethyloxycarbonyl
GA	Glutaraldehyde
GsLys6DH	<i>Geobacillus stearothermophilus</i> lysine-6-dehydrogenase
HeAlaDH	<i>Halomonas elongata</i> alanine dehydrogenase
HeE	<i>Halomonas elongata</i> esterase
HeP5CR	<i>Halomonas elongata</i> pyrroline-5-carboxylate reductase
HEPES	4-(2-hydroxyethyl)-1-piperazineethanesulfonic acid
HeTA	<i>Halomonas elongata</i> transaminase
HLADH	Horse liver alcohol dehydrogenase
HPLC	High pressure liquid chromatography
IDA	Iminodiacetic acid
IPA	Isopropyl amine
iPrOH	Isopropanol
IPTG	1-thio- $\beta$ -D-galactopyranoside
IREC	Imine reductase
LB	Lysogeny broth medium
m.c.	Molar conversion
MeOH	Methanol
NAD(H)	Nicotinamide adenine dinucleotide
NADP(H)	Nicotinamide adenine dinucleotide phosphate
NSAID	Non-steroidal anti-inflammatory drug
O/N	Overnight
P2C	$\Delta^1$ -piperidine-2-carboxylate
P5C	Pyrroline-5-carboxylate

P6C	$\Delta^1$ -piperideine-6-carboxylate
PA	Pipecolic acid
PCR	Polymerase chain reaction
PDB	Protein data bank
PEG	Polyethylene glycol
PEI	Polyethyleneimine
PfTA	<i>Pseudomonas fluorescens</i> transaminase
PLE	Pig liver esterase
PLP	Pyridoxal-5'-phosphate
PMP	Pyridoxamine-5'-phosphate
pNPA	<i>p</i> -nitrophenyl acetate
pNPB	<i>p</i> -nitrophenyl butyrate
P2P	Phenyl-2-propanoate
PPQ	Pyrrroloquinoline quinone
PVDF	Polyvinylidene fluoride
RIN	Residue interaction network
RMSD	Root mean square deviation
SDS-PAGE	Sodium dodecyl sulphate polyacrylamide gel electrophoresis
SHMT	Serine hydroxymethyl transferase
SMBA	<i>S</i> -methylbenzyl amine
SOB	Super optimal broth
T4C	<i>L</i> -thiazolidine-4-carboxylate
T4L	Bacteriophage T4 lysozyme
TA	Transaminase
TAE	Tris-acetate-EDTA
TB	Terrific broth
TEMED	Tetramethyl ethylenediamine
TFA	Trifluoroacetic acid
THF	Tetrahydrofuran
UV	Ultraviolet
WT	Wild type



### **Amino acids**

A	Ala	Alanine
C	Cys	Cysteine
D	Asp	Aspartic acid
E	Glu	Glutamic acid
F	Phe	Phenylalanine
G	Gly	Glycine
H	His	Histidine
I	Ile	Isoleucine
K	Lys	Lysine
L	Leu	Leucine
M	Met	Methionine
N	Asn	Asparagine
P	Pro	Proline
Q	Gln	Glutamine
R	Arg	Arginine
S	Ser	Serine
T	Thr	Threonine
V	Val	Valine
W	Trp	Tryptophan
Y	Tyr	Tyrosine

### **DNA and RNA nucleotides**

A	Adenine
C	Cytosine
T	Thymine
G	Guanine
U	Uracil

### **Units of measure**

bp	Base pair
g	Gram
mol	Mole
Da	Dalton
L	Litre
h	Hour
s	Second
min	Minute
M	Molarity
rpm	Rotation per minute

# Chapter 1: Introduction

## 1.1. Enzymes as biocatalysts

When developing processes for chemical manufacturing, there has been an increasing awareness of the need to consider not only the efficiency and scalability of the process, but more importantly its environmental metrics. In a growing society as ours, where the demand of fine and bulk chemicals is increasing, the development of new tools and techniques for their synthesis is of paramount importance. In this direction, the use of catalysts, greatly increase the economic feasibility of these reactions. Catalysts are molecules which, by lowering the energetic barrier of a certain reaction, speed up the transformation remaining unaltered during the process.

In an effort to give clear guidance in new synthetic process development, the concept of Green Chemistry was defined by Anastas *et al.* [1–2]. They defined the techniques enclosed inside green chemistry as those focused “to allow the formation of the desired products avoiding and eliminating the use of hazardous substances in the process”. This approach is based on 12 principles which every reaction should comply with, which go from the prevention of waste, to the use of benign solvents without leaving behind the use of renewable feedstock or benign chemicals (Figure 1.1).

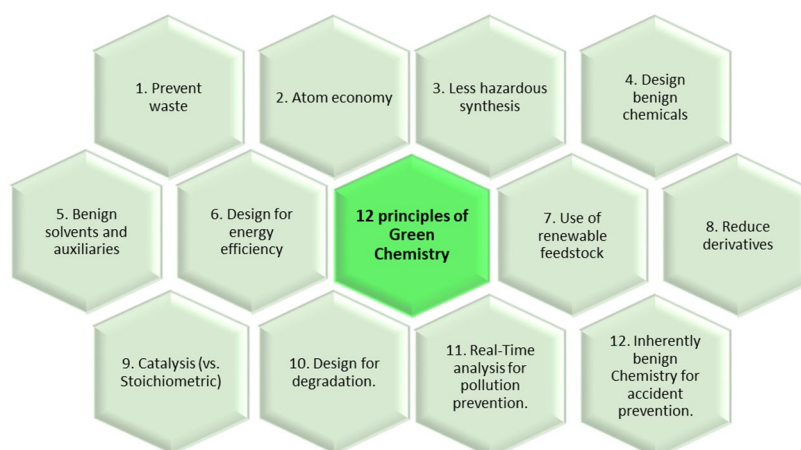


**Figure 1.1.** The twelve principles of green chemistry, as specified by Anastas *et al.* [1].

In nature, the role of the catalyst is played by different biomolecules, with utmost importance for enzymes. In fact, enzymes have been used for bioconversions since ancient times. Such biotransformations are found, for example, in the fermentation of alcoholic beverages for instance wine or beer. With the first identification and discovery of enzymes, a new path opened up for their use in chemical transformations isolated from the cell. This new use of enzymes as catalysts, was investigated soon after their first identification. The first synthesis performed with enzymes was done by Emil Fisher in 1894, establishing one of their important characteristics: an extremely high substrate specificity [3]. Emil Fisher, also foresaw the arrival of biocatalysis, stating that synthetic methods should evolve, following nature, to be undertaken in milder conditions [4]. Enzyme catalysed reactions comply with almost all the demands of Green Chemistry: they normally exhibit excellent atom economies, preventing the formation of waste and undesired products, and in addition, biocatalysts normally operate in mild conditions and aqueous systems, avoiding the use of hazardous solvents and facilitating the handling of the reaction.

While their implementation in industrial relevant reactions was targeted since the first enzyme discovery, only in the early 1970s some biocatalytic commercial processes were starting to get implemented, mainly in the food processing industry [5]. More recently, with the development of protein engineering techniques and more importantly, the revolutionary directed evolution [6–7], the enzymatic toolbox as well as their potential application has increased exponentially. These techniques do not only enable us to enhance the activity or stability of promising biocatalysts to meet the industrial requirement [8], but also allows for the creation of enzymes with new substrate scope or even with new activities [9–10]. Therefore, in recent years the efforts to effectively implement industrial biocatalysis have increased [11–13]. In the following sections, the groups of enzymes with more industrial potential are presented and some of their possible applications detailed.

## 1.2. Carboxylesterases

One of the most used, promising and versatile enzymes used in biocatalysis are hydrolases (EC 3), and inside this group of particular relevance are the carboxylesterases (EC 3.1.1.X) [14–15]. This large group is formed by a vast number of hydrolases which catalyse the cleavage or formation of ester bonds. These enzymes are ubiquitous as the reaction they perform is needed in all levels of life. Moreover, most esterases have a wide substrate range, closely related to their biological function. The tertiary structure of these enzymes is defined as the  $\alpha/\beta$  hydrolase fold [16–17]. This fold, depicted in Figure 1.2, is typically formed by eight  $\beta$ -sheets, mostly in parallel arrangement, linked together by  $\alpha$ -helices and disordered regions. Enzymes within this fold share striking similarities in their central catalytic domain, with the catalytic residues placed in specific positions of the primary sequence, corresponding to a definite geometry of the active site. Normally, the catalytic triad is formed by a catalytic nucleophile, a histidine, which acts as a base activating the catalytic serine, and an acid residue, normally an aspartic or glutamic acid, which polarizes the histidine.

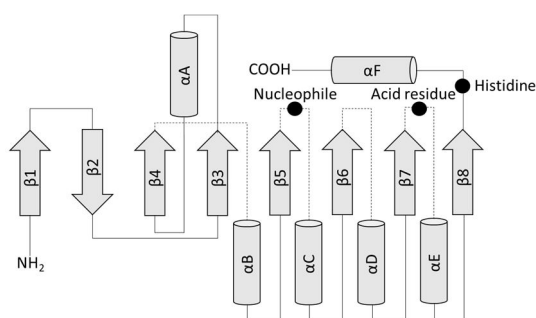


**Figure 1.2.** Scheme of the typical  $\alpha/\beta$  hydrolase fold. The position of the catalytic residues in the structure are indicated.

To cleave the ester bond, once the substrate has entered the active site, the catalytic serine performs a nucleophilic attack, forming an acyl-enzyme intermediate. This tetrahedral intermediate is stabilised by both interaction with the catalytic histidine and with the oxyanion hole. The intermediate is then attacked by a second nucleophile (water for the hydrolysis) releasing the alcohol. The resulting intermediate is finally resolved forming the carboxylic acid and restoring the free enzyme (Figure 1.3). Some lipases, when used in organic media, can also

perform the reverse reaction, the formation of an ester bond from the alcohol and carboxylic acid, known as esterification. In this case, instead of water being the second nucleophile, the alcohol performs the attack.

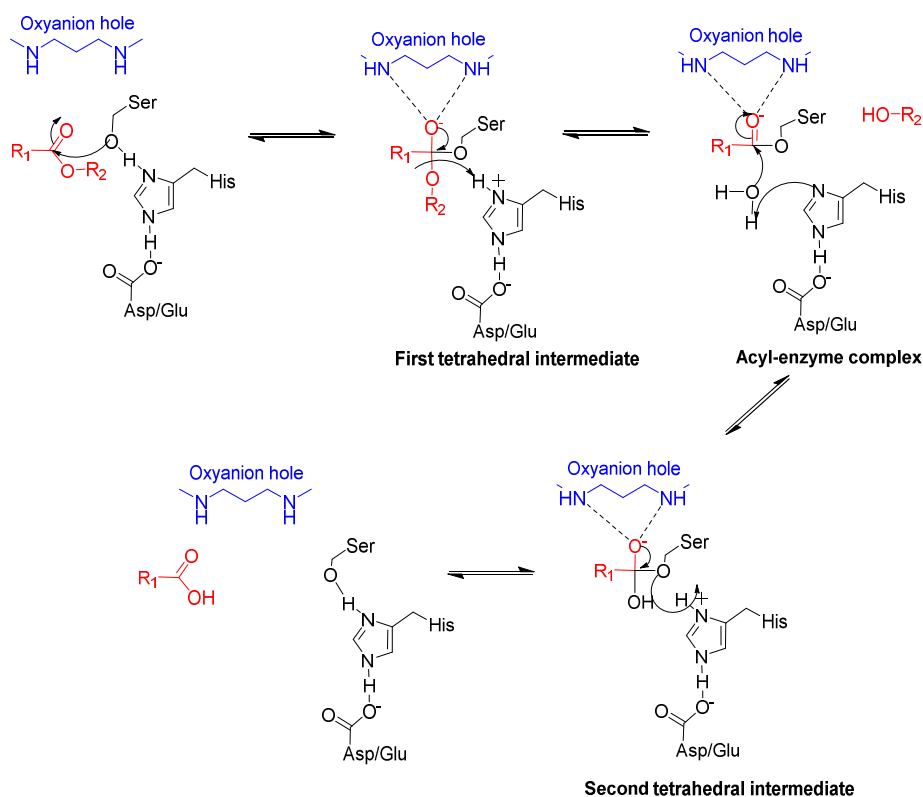


**Figure 1.3.** Catalytic mechanism of esterases and lipases. The red structure exemplifies the substrate and the blue coloured corresponds to the oxyanion hole.

As for their classification, carboxylesterases are divided into several classes, but the most important examples are mainly in two classes: carboxylesterases (EC 3.1.1.1) and lipases (EC 3.1.1.3). While lipases prefer more hydrophobic and large chain esters, such as triacyl fatty acids, carboxyl esterases tend to work better with more water soluble, small chain esters. Initially, the classification of carboxylesterases into one of these two groups was based on their substrate specificity [18] but with the increasing number of sequences and structures becoming available, further differences were observed at the structural level too. This suggestive differences were used by Arpingy *et al.*, to classify bacterial lipolytic enzymes into eight different families, based not only on their substrate specificity but taking also into account the sequence and structural differences [19]. One of the main structural differences used, was the presence of a “lid” covering the active site, typical of lipases.

More recent studies, though, show that the presence of the lid is not exclusive to lipases and does not define the substrate scope of the enzyme and, therefore, it cannot be used as a clear indicator of the enzyme classification as a carboxylesterase or a lipase class [20–22].

Hydrolases in general, and esterases in particular, have been used in food, beverage, bioenergy and detergent industries for a long time now [23–25]. Their application to industry is facilitated by their commercial availability, their inherent high stability, and their uncomplicated application, as they do not require any cofactor for the catalysis. More recently, the potential of esterases for the synthesis of different active pharmaceutical ingredients (APIs) or chiral building blocks has gained interest due to their regio-, enantio- and stereoselectivity [25–26] (Figure 1.4). For example, one of the first esterases identified, pig liver esterase (PLE) [27], was used as early as 1975 by Sih *et al.*, for the synthesis of enantiopure (*R*)-mevalonic acid [28]. Since then, the application of PLE and other esterases for the hydrolysis of prochiral esters has steadily increased [29–31]. Similarly, taking advantage of the capacity of some lipases to perform the esterification reaction, recently, the use of CALB, a lipase from *Candida antarctica*, has been reported for the enantioselective preparation of important building blocks for pharmaceuticals such as (*S*)-atenolol [32–33] and also, for the deracemization of flurbiprofen [34].

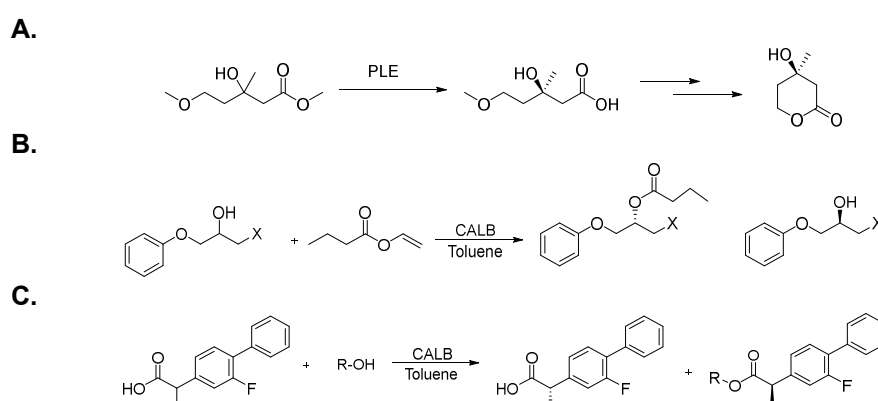


**Figure 1.4.** Examples of the use of lipases and esterases for the synthesis of relevant chemical intermediates or APIs. A. First reported use of PLE for the enantioselective synthesis of (*R*)-mevalonic acid [28]. B. Stereoselective formation of the alcohol building block for (*S*)-atenolol ( $\beta$ -blocker) [32]. C. Flurbiprofen deracemization using CALB for the stereospecific esterification [34].

### 1.3. Aminotransferases

Another group which has come to the fore during the last decades are aminotransferases. These enzymes are involved in the amino acid metabolism in biological systems and, since their discovery, they caught the attention for their potential in the production of a variety of aminated compounds, such as chiral amines, broadly used as building blocks in the nutraceutical industry [35–36]. Aminotransferases, also known as transaminases (TA), catalyse the transfer of an amino group to a molecule containing a carbonyl group, which will be the amino acceptor, from an amino donor. To catalyse this reaction, transaminases depend on pyridoxal-5-phosphate (PLP), a derivate of vitamin B<sub>6</sub>. The reaction mechanism proceeds through a ping-pong mechanism, as the reaction can be divided into two half-reactions [37–38]. In short, the amino donor reacts with the PLP molecule initially bound to a catalytic lysine in the active site, yielding pyridoxamine-5'-phosphate or PMP and the deaminated amino-donor. PMP then reacts with the amino acceptor to form the final amine and recover PLP (Figure 1.5).

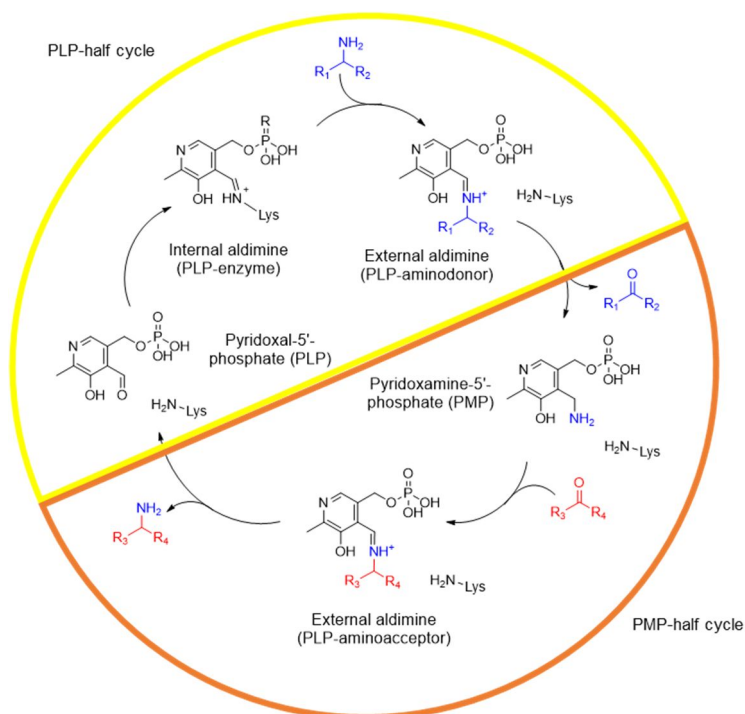


**Figure 1.5.** Reaction mechanism of aminotransferases. The key intermediates, as well as the two forms of the cofactor (PLP and PMP) are shown.

Transaminases, broadly speaking, are part of the largest fold-type in PLP dependent enzymes, type I or aminotransferase superfamily [39]. Inside this group, a functional distinction between transaminases can be made, dividing them mainly into  $\alpha$ - and  $\omega$ -transaminases, depending on the position of the amino group transferred with respect to the carboxyl group of the substrate [40] and moreover, based on their amino acid sequence, transaminases are classified in VI different groups [41], where  $\omega$ -transaminases fall inside class-III [42].

This class of enzymes has been successfully applied to industrially relevant biocatalytic processes (Figure 1.6). One of the most relevant examples is the synthesis of sitagliptin, where a heavily engineered TA is used to aminate regio- and stereo-selectively pro-sitagliptin. This biocatalytic process led to a 13% increase in the overall yield and a 53% increase in the productivity with a 19% reduction in the total waste [43], proving the potential of transaminases for industrial production of specific fine chemicals. Transaminases can also be applied for the synthesis of non-natural amino acids from achiral materials, chiral amines [44], and also aldehydes which by conventional synthetic methods may be difficult to access. By coupling TAs with a redox system, the aldehydes can be reduced to the corresponding alcohols [45].

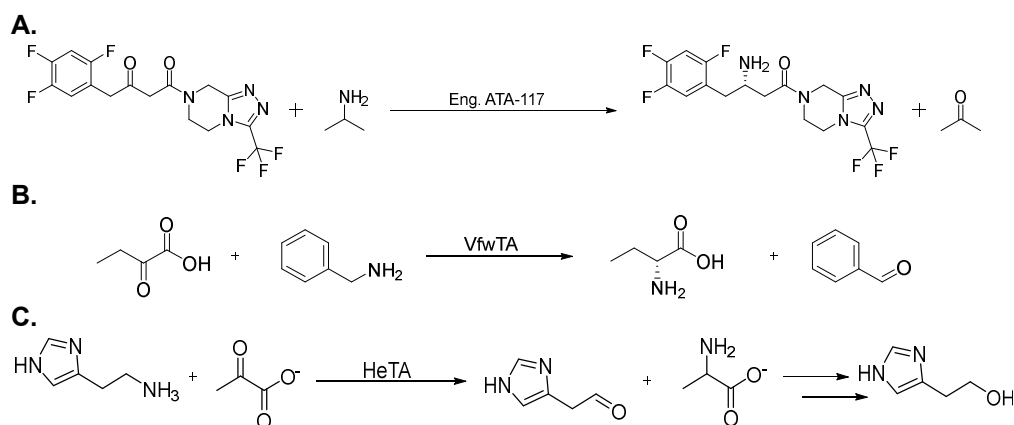


**Figure 1.6.** **A.** Schematic representation of the synthesis of sitagliptin using ATA-117 [43]. **B.** Synthesis of unnatural amino acid by *Vibrio fluvialis* transaminase [46]. **C.** Synthesis of aldehyde from amines and their reduction to chiral alcohols using *Halomonas elongata* transaminase [45–47].



## 1.4. Oxidoreductases

A third class of enzymes with relevant applications in industrial biotechnology are oxidoreductases. These enzymes are ubiquitous in all domains of life and are particularly interesting because they catalyse a very wide variety of different chemical transformations: from electron transfer to oxygen insertion [48]. The catalysis involves electron transfer (or another redox equivalent) between an acceptor molecule and the donor. Therefore, they act in two half reactions, one comprising an oxidation and a concomitant reduction. To achieve that, oxidoreductases harbour various redox-active partners, such as coenzymes (FAD, NAD, PPQ) or metal complexes (Fe-S cluster, heme) (Figure 1.7) [49].

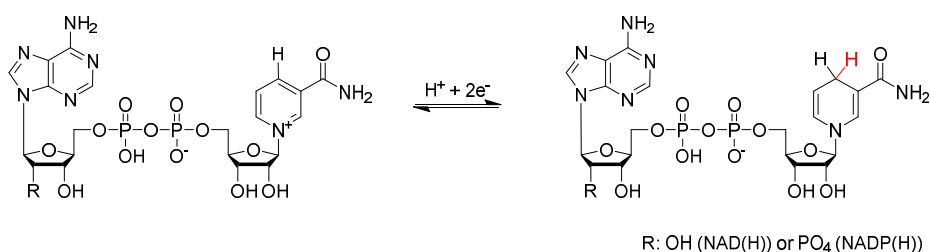


**Figure 1.7.** General reaction of oxidoreductases. In the figure, NAD(P) dependent oxidation or reduction is depicted.

Due to the heterogeneity in this class, there are several approaches to classify them in subgroups. They can be classified according to their sequence and three-dimensional structure, which is of special importance to the structure-function relationship and functional genomics, but more commonly, they are classified according to the catalytic properties and their co-enzyme dependence. This classification generally divides oxidoreductases in 4 main groups: oxidases, peroxidases, oxygenases/hydroxylases, and dehydrogenases/reductases [50].

One of the main challenges hampering their application on an industrial scale, is their cofactor dependence. Not only are cofactors expensive, but normally this product is not recycled within the catalytic cycle, unlike with TAs. Therefore, strategies for the cofactor regeneration are needed to increase the economic viability of the reaction. One option is to perform the reaction on a natural environment using whole cell

biocatalysis, which by means of the natural apparatus of the organism will recycle the cofactor used by the enzyme [51–52]. If the reaction is done with purified enzymes though, the most commonly used strategies consist on coupling the main reaction either with a second enzyme, which in a parallel reaction recycles the cofactor, or more simply with a co-substrate that the main redox enzyme is capable of transforming in the reverse reaction. These coupled systems, ideally use inexpensive co-substrates which do not interfere with the downstream purification of the desired product [53–55].

For their wide variety of chemical reactions, several oxidoreductases can be applied in industrially relevant biotransformations (Figure 1.8). Laccases and other oxidoreductases can be used for the degradation or biotransformation of lignin (Figure 1.8A) [56] or the biodegradation and decontamination for example, degrading recalcitrant toxic waste [57–58]. Again, mainly because of their versatility and high stereoselectivity, oxidoreductases can also be used for the asymmetric synthesis of demanding chemicals or active pharmaceuticals ingredients (APIs). One of the first described dehydrogenases, the horse liver alcohol dehydrogenase (HLADH), identified in the late 60s [59], has been successfully used for the kinetic resolution of aromatic aldehydes taking advantage of its stereospecificity (Figure 1.8B). As discussed in the previous section, alcohol dehydrogenases can also be coupled with a transaminase to perform the transformation of the generated aldehydes from the amines, to their corresponding alcohols [45]. Moreover, in this direction, the same enzyme can be used to recycle the cofactor by adding ethanol as the sacrificing substrate [60]. More recently, the identification of imine reductases (IREDs) opened up new routes to access chiral amines (Figure 1.8C). These type of enzymes, were first applied for the reduction of 3,4-dihydroisoquinones [61] and soon after, they were combined in a one pot reaction to synthesize pyrrolidines and piperidines from ketoacids [62] (Figure 1.8D).

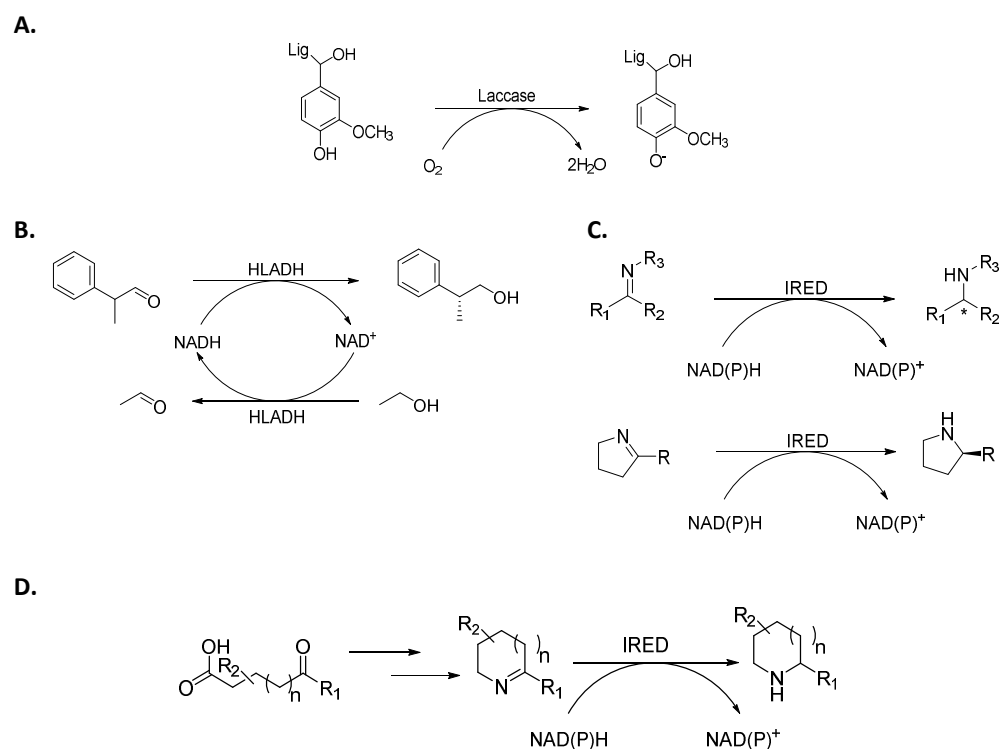


**Figure 1.8. A.** Detail of the laccase catalysed conversion of lignin aromatic ligands to the corresponding free phenoxy radical. Lig refers to the lignin scaffold. [56]**B.** Kinetic resolution of a chiral aldehyde using HLADH [59]. **C.** General reactivity of IREDs. **D.** Synthesis of pyrrolidines and piperidines from ketoacids by a multi-enzymatic system. The first two reactions are performed by a carboxylic acid reductase and a transaminase [62].

### 1.5. Extremophiles as source of new biocatalysts

Despite the main advantages of the use of enzymes in catalysis and their broad synthetic utilisations, there are also several drawbacks for their wider industrial application. Normally, they are only active at certain conditions and their stability and reusability is greatly affected by the harsher industrial required conditions. Enzymes tend to operate in mild conditions (temperatures of 30-40°C, in aqueous solvent and near neutral pH) which, normally, do not match the requirements of industrial syntheses. In this direction, enzyme mining from extremophiles has gained interest in the recent years to identify catalysts with higher compliance with industrial requirements [63–64].

Extremophiles are organisms that live in extreme environments [65], for example, they are exposed to extreme temperature, pressure, high salinity or harsh pH. Often, more than one “extreme” is present in the same environment. As a consequence, the cell machinery and enzymes coming from these organisms normally exhibit higher stability when compared to their mesophilic counterparts [66]. These organisms are named accordingly to their environment, as depicted in Table 1.1.

**Table 1.1.** Brief classification of the most important groups of extremophiles depending on the environmental condition needed for their growth.

Environment	Type	Definition
Temperature	Hyperthermophile	Growth over 80°C
	Thermophile	Growth from 60-80°C
	Mesophile	Growth from 15-60°C
	Psychrophile	Growth under 15°C
Salinity	Halophile	Growth over 1.5M NaCl
pH	Alkaliphile	Growth at pH over 8
	Acidophile	Growth at pH under 4
Oxygen	Anaerobe	Obligate growth without oxygen

From the different groups of extremophiles, the kind that has been more thoroughly investigated is that comprising thermophiles and psychrophiles. Specially, hydrolytic enzymes coming from these

organisms have been tested for their use in detergents, starch degradation and stereo-specific synthesis. Thermophilic enzymes can act, and in some cases only be activated, at high temperatures which minimises the problems associated with poor substrate solubility when using complex polymers, and/or biological contamination [67].

Another interesting group of enzymes are the ones from halophilic organisms. To survive in environments with high osmotic pressure, halophiles have adopted two main strategies: the first one, used for example by halobacterium a genus of *Archaea*, consists in accumulating inorganic salts ( $K^+$  and  $Cl^-$ , mainly) inside the cytoplasm by an energy dependent antiporter transport system present in their cellular membrane [68]. Alternatively, the other strategy consists of maintaining the cytoplasm at low salt concentration compared to the outer media but enriching it with high amounts of compatible solutes. These compounds are derived from sugars, polyols, betaines, ectoines or modified peptides and they are typically zwitterionic or negatively charged [68–69]. Both strategies, to different degrees, require adaptation of the cellular machinery and proteins to this cellular environment. Therefore, most of these organisms have evolved proteins with a sparse number of basic residues exposed and low hydrophobic surface [69]. Their enzymes, consequently, normally exhibit higher resistance to the presence of compatible solutes in the reaction media, a very common strategy in industrial biotransformation to avoid poor solubility of the substrate or enable direct and efficient purification of the product.

The accumulation of compatible solutes is the strategy used by *Halomonas elongata*. This species of bacteria was first described in 1980 by Vreeland, R.H., *et al.* [70] and is found in solar salterns. It mainly accumulates ectoine and other amino acidic derivatives depending on the salinity of the surrounding medium [71]. Enzymes from this organism have the advantage that, since it is a halo-tolerant bacterium and thus does not require salt to grow, its proteins can be easily expressed in typical biological expression systems such as *Escherichia coli*.

## 1.6. Enzyme immobilisation

Another issue with enzyme based biocatalysis is their long-term operational stability and difficulties for their recycling and recovery after the reaction has been completed. To overcome these problems and to facilitate their handling, immobilisation has emerged as a promising strategy [72–73].

In general, immobilisation is based on the interaction between the protein and a stabilising agent, such as a carrier or a solid support. Normally, carriers are composed of small porous particles and their nature can influence the behaviour of the newly generated biocatalyst. In general, immobilisation techniques can be divided in chemical binding (either covalent or by adsorption) and encapsulation (Figure 1.9). The choice of the immobilisation strategy is crucial and depends mainly on the protein resistance and the desired application.

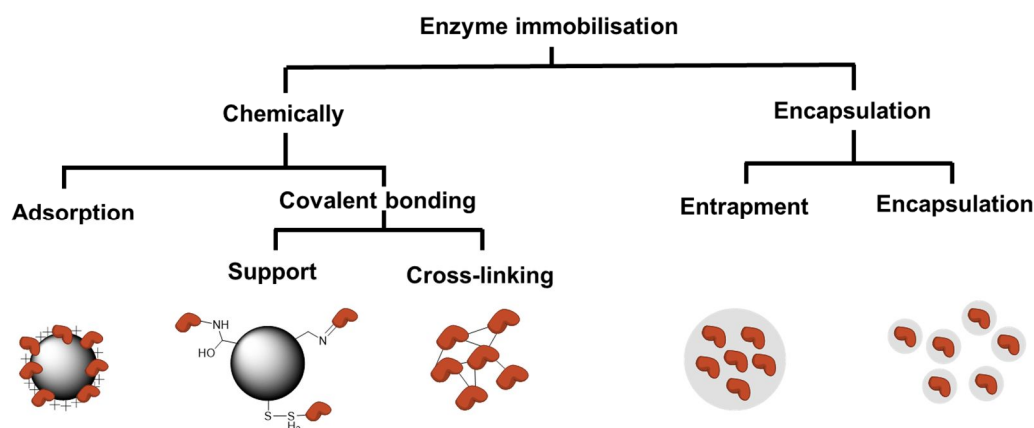


**Figure 1.9.** Schematic overview of the main immobilisation strategies.

With encapsulation the enzyme is trapped into a macroscopic matrix. Either individually or by encapsulating more than one enzymatic unit, this technique is normally used when the enzyme does not tolerate changes on its flexibility or binding to a support. This technique is essentially mimicking the natural environment of proteins, protected by a supramolecular structure (i.e. the cell) [74–76].

On the other hand, chemically immobilised enzymes can be linked onto the surface of a support or to each other by crosslinking. In cross-linked enzyme aggregates (CLEAs), the enzyme is normally first forced

to precipitate and then, by adding a cross-linker, for instance glutaraldehyde, the different proteins are covalently connected to each other creating a net. These preparations have been successfully used in industrial manufacturing, mostly hydrolytic reactions related to food processing [77–78]. Interestingly, the possibility to create multi-CLEAs by co-immobilising more than one enzyme in the same preparation has also been explored [79]. These preparations, while outperforming the free enzyme form, have been only extensively applied to hydrolases and often yield biocatalysts with poor physical robustness.

Alternatively, to obtain more robust biocatalysts, the enzymes can be immobilised onto a support. In this case, the nature of the interaction between the support and the enzyme defines the type of immobilisation. In adsorption, the enzyme is not covalently bound to the resin and is only kept in place by weak interactions; the most two common being ionic interaction and hydrophobic interaction. This technique normally yields biocatalysts with a high recovered activity as no major distortion of the protein structure occurs but, on the other hand, changes in the environment can cause enzyme leaching, breaking the weak interaction that kept it attached to the support.

Immobilisation generally has an effect on the activity of the protein as well as on its stability and in some cases, also on the selectivity [72–80]. Hence, it is important to tailor the immobilisation technique to specific enzymes to yield the best catalyst with minimal loss of activity. This loss of activity can be caused by two main factors: the enzyme itself (enzyme distortion or blockage of the active site) or linked to the type of support (diffusion or mass-transfer limitations). One of the most popular immobilisation methods for industrial application of biocatalysts is by covalent immobilisation onto a support or carrier. This method fixes tightly the enzyme to the support and prevents enzyme leaching during the process as well as its denaturation when stronger conditions are used, as the covalent bond reduces the conformational flexibility of the protein, creating a very robust heterogeneous biocatalyst.

Several commercially available supports can be used for covalent enzyme immobilisation. Epoxy resins, such as Sepabeads or Purolite have been extensively reported in the literature [81–82]. To increase the reproducibility of the technique and taking advantage of the His-tagged proteins to ease their purification, these supports can be modified to enable the directed immobilisation of the enzyme [83]. In this strategy, the epoxy groups of the support are partially modified using iminodiacetic acid followed by metal loading, similarly to the preparation of metal affinity chromatography resins. In this way, the His-tag of the protein will coordinate to the metal driving the covalent bonding between nucleophilic residues (-NH<sub>2</sub>) and unreacted epoxides by physical proximity. After immobilising the enzyme, any residual epoxy group is blocked to avoid side-reactivity (Figure 1.10). This approach not only allows the creation of robust biocatalyst but the reproducibility and control over the immobilisation is greatly enhanced.

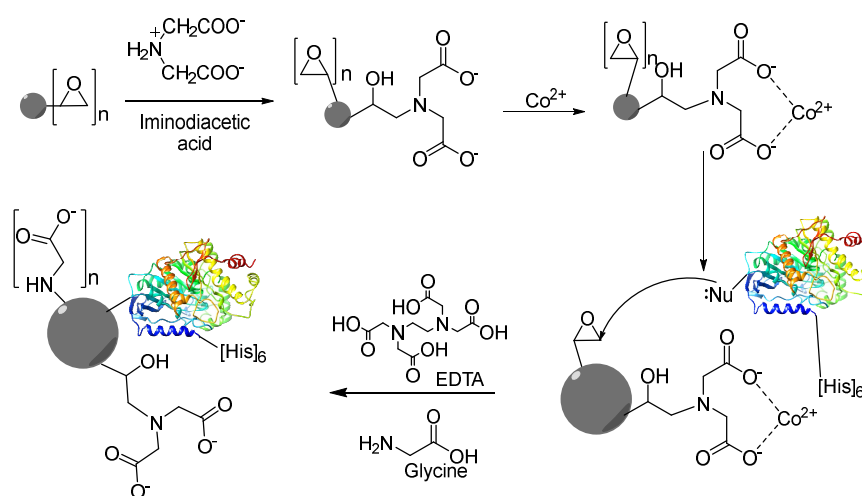


**Figure 1.10.** Representation of the epoxy group-based immobilisation.



## 1.7. Flow biocatalysis

In parallel to biocatalysis, from another perspective, flow chemistry has also emerged as a new strategy to advance in the field of developing more sustainable methods for synthesis.

Batch processes have been the standard development approach for the synthesis of pharmaceuticals or fine chemicals during the last years, as flow equipment developed specifically for laboratory scale only became available in the last 15 years [84]. Lately, this innovative technique showed many advantages compared to batch methods: improved heat and mass transfer, efficient mixing of substrates, shorter reaction times, and safer and scalable routes for bulk or fine chemical production [85–86]. Moreover, the flexibility of this technique allows for the introduction of scavenger columns and/or the application of catch and release strategies for in-line purifications, which could greatly increase the level of automation (Figure 1.11) and would translate in an easier method for the isolation of high-purity products in a faster and more economical way.

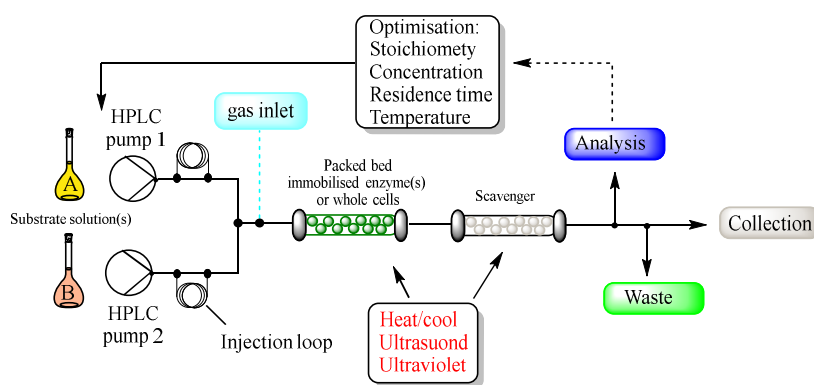


**Figure 1.11.** Schematic representation of the possibilities of the set-up for a flow system.

A landmark work by Ley and co-workers, demonstrated the full synthesis of Grossamide, a natural neolignane, using a fully automated flow reactor [87]. This work opened up the possibility to substitute traditional batch-based methods for the synthesis of pharmaceutically relevant products in flow. For example, the full synthesis of imatinib, a compound used for the treatment of chronic myeloid leukaemia [88] or Oxomaritidine, a cytotoxic alkaloid have also been reported in flow

chemistry [89]. This technique is also highly flexible and not limited to total synthesis; for example, as an alternative to solid phase peptide synthesis, the use of microfluidic flow systems, can overcome problems of scalability and cost-efficiency related to solid-phase peptide synthesis [90].

With all these examples, the combination of flow-reactors and biocatalysis seems a logical step to merge both technologies in a synergistic way. Early on, this approach was applied for the production of ethanol via fermentation of cellulosic mass, which showed better yields when compared to the batch reactions [91]. These initial biotransformation in flow were mostly performed by using whole cell biocatalyst, but the major limitation was the flow rate that could be achieved, which translated in low productivities [92]. Using whole cells also hampers the use of some substrates due to their membrane permeability and is limited to very specific conditions to maintain the cell integrity.

Further advances were made with the use of purified immobilised enzymes as a packed-bed reactor. Many of these examples, use an immobilised version of the lipase B from *Candida antarctica* (CALB) commercially available under the name of Novozym435®. Here, the lipase is immobilised through adsorption and this heterogeneous biocatalyst has been successfully used for the synthesis of geraniol esters [93], deracemization of flurbiprofen [34] and transesterification reactions [95]. Nonetheless, flow assisted bioconversions have not been limited to the use of hydrolases, though there are still limited examples in the literature. Pioneering work to expand the reaction scope of flow assisted biocatalysis has been led by our group. By exploiting an immobilised transaminase from *Halomonas elongata*, the first example of efficient amine synthesis from their corresponding aldehydes was reported by Planchestainer *et al.*, with an in-line purification step to recover the pure amine without further work-up [44]. Using a similar approach, in the reverse reaction catalysed by the same enzyme, a panel of aldehydes were synthesized from their corresponding amines. In this

case, a segmented flow generated by the intermittent addition of toluene not only eased the recovery of the aldehyde but also greatly facilitated their isolation [47]. To expand the cost-efficiency of these reactions, a self-sufficient biocatalyst was created by co-immobilisation of PLP on the same support, enhancing the system productivity and efficiency for the synthesis of different biogenic amines [95–96]. Nevertheless, flow synthesis is not limited to single enzymatic reactions. Contente and Paradisi, reported a multistep reaction for the synthesis of optically pure secondary alcohols starting from (S)-amines [45]. In addition, the synthesis of alcohols from amines through a two-step enzymatic reaction proved to be extremely efficient in the production of a manifold of chiral and biogenic alcohols through deamination and further reaction with the horse liver alcohol dehydrogenase (HLADH), without the need to isolate the aldehyde intermediate. Moreover, through in-line purification of the waste-water stream and recirculation, a closed loop system was achieved to reuse the cofactors, which greatly increased the system efficiency.

These few reviewed examples, prove the advantages of flow bioreactors for process intensification [97] but despite the multiple examples rapidly appearing in the literature, flow-based transformations are still facing some limitations. For example, in-line purification systems although starting to get attention, are still not efficiently coupled in flow due to the lack of an efficient universal technique [91–98]. Another issue to be surpassed, is the solubility of the substrates or intermediates, which poses a big challenge due to channel clogging and poor reactivity. For example, in the synthesis of imatinib, several intermediates are known to be insoluble and therefore, an extensive solvent screening was needed in order to avoid the associated problems [99]. This indicates, that while the combination of biocatalysis with flow systems has already been proved to offer a more sustainable and fully scalable methodology for the synthesis of APIs, bulk chemicals and industrially relevant products in the laboratory scale, further investigation is needed to overcome its limitations and provide a robust procedure for its effective application.

## 1.8. Bibliography

1. P. Anastas & N. Eghbali, Green chemistry: Principles and practice. *Chemical Society Reviews*, **39** (2010) 301–312. <https://doi.org/10.1039/b918763b>.
2. I. T. Horváth & P. T. Anastas, Introduction: Green chemistry. *Chemical Reviews*, **107** (2007) 2167–2168. <https://doi.org/10.1021/cr0783784>.
3. E. Fischer, Einfluss der Configuration auf die Wirkung der Enzyme. *Berichte der deutschen chemischen Gesellschaft*, **27** (1894) 2985–2993. <https://doi.org/10.1002/cber.18940270364>.
4. K. Freudenberg, Emil fischer and his contribution to carbohydrate chemistry. *Advances in Carbohydrate Chemistry*, **21** (1967) 1–38. [https://doi.org/10.1016/S0096-5332\(08\)60314-8](https://doi.org/10.1016/S0096-5332(08)60314-8).
5. J. James, B. K. Simpson, & M. R. Marshall, Application of enzymes in food processing. *Critical Reviews in Food Science and Nutrition*, **36** (1996) 437–463. <https://doi.org/10.1080/10408399609527735>.
6. F. H. Arnold, Design by Directed Evolution. *Accounts of Chemical Research*, **31** (1998) 125–131. <https://doi.org/10.1021/ar960017f>.
7. K. Chen & F. H. Arnold, Tuning the activity of an enzyme for unusual environments: sequential random mutagenesis of subtilisin E for catalysis in dimethylformamide. *Proceedings of the National Academy of Sciences*, **90** (1993) 5618–5622. <https://doi.org/10.1073/pnas.90.12.5618>.
8. R. DiSanto, D. Shonnard, S. Pannuri, S. Kamat, A. R. Martin, & I. Plotnikov, Improved activity and thermostability of (S)-aminotransferase by error-prone polymerase chain reaction for the production of a chiral amine. *Biochemical Engineering Journal*, **37** (2007) 246–255. <https://doi.org/10.1016/j.bej.2007.05.001>.
9. P. J. O'Brien & D. Herschlag, Catalytic promiscuity and the evolution of new enzymatic activities. *Chemistry and Biology*, **6**

(1999). [https://doi.org/10.1016/S1074-5521\(99\)80033-7](https://doi.org/10.1016/S1074-5521(99)80033-7).

10. D. Meyer, L. Walter, G. Kolter, M. Pohl, M. Müller, & K. Tittmann, Conversion of pyruvate decarboxylase into an enantioselective carboligase with biosynthetic potential. *Journal of the American Chemical Society*, **133** (2011) 3609–3616. <https://doi.org/10.1021/ja110236w>.
11. A. Wells & H. P. Meyer, Biocatalysis as a strategic green technology for the chemical industry. *ChemCatChem*, **6** (2014) 918–920. <https://doi.org/10.1002/cctc.201402065>.
12. B. M. Nestl, S. C. Hammer, B. A. Nebel, & B. Hauer, New generation of biocatalysts for organic synthesis. *Angewandte Chemie - International Edition*, **53** (2014) 3070–3095. <https://doi.org/10.1002/anie.201302195>.
13. O. Kirk, T. V. Borchert, & C. C. Fuglsang, Industrial enzyme applications. *Current Opinion in Biotechnology*, **13** (2002) 345–351. [https://doi.org/10.1016/S0958-1669\(02\)00328-2](https://doi.org/10.1016/S0958-1669(02)00328-2).
14. Uwe T. Bornscheuer and Romas J. Kazlauskas, Lipases and Esterases: Sections 5.3 - 5.4. *Hydrolases Org. Synth.* (Weinheim, FRG: Wiley-VCH Verlag GmbH & Co. KGaA, 2006), pp. 141–183. <https://doi.org/10.1002/3527607544.ch5b>.
15. U. T. Bornscheuer, Microbial carboxyl esterases: classification, properties and application in biocatalysis. *FEMS Microbiology Reviews*, **26** (2002) 73–81. <https://doi.org/10.1111/j.1574-6976.2002.tb00599.x>.
16. D. L. Ollis, E. Cheah, M. Cygler, B. Dijkstra, F. Frolow, S. M. Franken, M. Harel, S. J. Remington, I. Silman, & J. Schrag, The alpha/beta hydrolase fold. *Protein engineering*, **5** (1992) 197–211. <https://doi.org/10.1093/protein/5.3.197>.
17. M. Holmquist, Alpha Beta-Hydrolase Fold Enzymes Structures, Functions and Mechanisms. *Current Protein and Peptide Science*,

- 1 (2000) 209–235. <https://doi.org/10.2174/1389203003381405>.
18. *Lipases for biocatalysis for smarter chemical synthesis* (2014).
  19. J. L. Arpigny & K. E. Jaeger, Bacterial lipolytic enzymes: classification and properties. *The Biochemical journal*, **343 Pt 1** (1999) 177–83. <https://doi.org/10.1042/0264-6021:3430177>.
  20. A. Hjorth, F. Carrière, C. Cudrey, H. Wöldike, E. Boel, D. M. Lawson, F. Ferrato, C. Cambillau, G. G. Dodson, & L. Thim, A structural domain (the lid) found in pancreatic lipases is absent in the guinea pig (phospho)lipase. *Biochemistry*, **32** (1993) 4702–4707. <https://doi.org/10.1021/bi00069a003>.
  21. J. Uppenberg, M. T. Hansen, S. A. Patkar, & T. a Jones, The sequence, crystal structure determination and refinement of two crystal forms of lipase B from *Candida antarctica*. *Structure*, **2** (1994) 293–308. [https://doi.org/10.1016/S0969-2126\(00\)00031-9](https://doi.org/10.1016/S0969-2126(00)00031-9).
  22. V. De Vitis, C. Nakhnoukh, A. Pinto, M. L. Contente, A. Barbiroli, M. Milani, M. Bolognesi, F. Molinari, L. J. Gourlay, & D. Romano, A stereospecific carboxyl esterase from *Bacillus coagulans* hosting nonlipase activity within a lipase-like fold. *FEBS Journal*, (2018). <https://doi.org/10.1111/febs.14368>.
  23. Y. Gaber, *Hydrolases as Catalysts for Green Chemistry and Industrial Applications Esterase , Lipase and Phytase* Doctoral Thesis, University of Lund, 2008.
  24. R. Singh, M. Kumar, A. Mittal, & P. K. Mehta, Microbial enzymes: industrial progress in 21st century. *3 Biotech*, **6** (2016) 1–15. <https://doi.org/10.1007/s13205-016-0485-8>.
  25. B. D. Ribeiro, A. M. de Castro, M. A. Z. Coelho, & D. M. G. Freire, Production and Use of Lipases in Bioenergy: A Review from the Feedstocks to Biodiesel Production. *Enzyme Research*, **2011** (2011) 1–16. <https://doi.org/10.4061/2011/615803>.
  26. E. Busto, V. Gotor-Fernández, & V. Gotor, *Hydrolases: catalytically*

promiscuous enzymes for non-conventional reactions in organic synthesis. *Chemical Society reviews*, **39** (2010) 4504–23. <https://doi.org/10.1039/c003811c>.

27. W. Junge & E. Heymann, Characterization of the Isoenzymes of Pig-Liver Esterase Kinetic Studies. *European Journal of Biochemistry*, **95** (1979) 519–525.
28. F. C. Huang, L. F. H. Lee, R. S. D. Mittal, P. R. Ravikumar, J. A. Chan, C. J. Sih, E. Caspi, & C. R. Eck, Preparation of (*R*)- and (*S*)-Mevalonic Acids. *Journal of the American Chemical Society*, **97** (1975) 4144–4145. <https://doi.org/10.1021/ja00847a054>.
29. M. J. Homann, R. Vail, B. Morgan, V. Sabesan, C. Levy, D. R. Dodds, & A. Zaks, Enzymatic Hydrolysis of a Prochiral 3-Substituted Glutarate Ester, an Intermediate in the Synthesis of an NK1/NK2 Dual Antagonist. *Advanced Synthesis & Catalysis*, **343** (2001) 744–749. [https://doi.org/10.1002/1615-4169\(200108\)343:6/7<744::aid-adsc744>3.3.co;2-5](https://doi.org/10.1002/1615-4169(200108)343:6/7<744::aid-adsc744>3.3.co;2-5).
30. S. Iriuchijima, K. Hasegawa, & G. I. Tsuchihashi, Asymmetric Hydrolysis of Prochiral Diesters with Pig Liver Esterase. Preparation of Optically Active Intermediates for the Synthesis of (+)-Biotin and (+)- $\alpha$ -Methyl-3,4-dihydroxyphenylalanine. *Agricultural and Biological Chemistry*, **46** (1982) 1907–1910. <https://doi.org/10.1271/bbb1961.46.1907>.
31. M. Chartrain, P. Maligres, D. Cohen, V. Upadhyay, V. Pecore, D. Askin, & R. Greasham, Porcine liver esterase-catalyzed enantioselective hydrolysis of a prochiral diester into its optically pure (*S*)-ester acid, a precursor to a growth hormone secretagogue. *Journal of Bioscience and Bioengineering*, **87** (1999) 386–389. [https://doi.org/10.1016/S1389-1723\(99\)80051-6](https://doi.org/10.1016/S1389-1723(99)80051-6).
32. I. T. Lund, P. L. Bøckmann, & E. E. Jacobsen, Highly enantioselective CALB-catalyzed kinetic resolution of building blocks for  $\beta$ -blocker atenolol. *Tetrahedron*, **72** (2016) 7288–7292.

<https://doi.org/10.1016/j.tet.2016.02.018>.

33. E. E. Jacobsen, B. H. Hoff, A. R. Moen, & T. Anthonsen, Enantioselective enzymatic preparation of chiral glutaric monocarboxylic acids and amides. *Journal of Molecular Catalysis B: Enzymatic*, **21** (2003) 55–58. [https://doi.org/10.1016/S1381-1177\(02\)00138-8](https://doi.org/10.1016/S1381-1177(02)00138-8).
34. L. Tamborini, D. Romano, A. Pinto, A. Bertolani, F. Molinari, & P. Conti, An efficient method for the lipase-catalysed resolution and in-line purification of racemic flurbiprofen in a continuous-flow reactor. *Journal of Molecular Catalysis B: Enzymatic*, **84** (2012) 78–82. <https://doi.org/10.1016/j.molcatb.2012.02.008>.
35. D. Ghislieri & N. J. Turner, Biocatalytic approaches to the synthesis of enantiomerically pure chiral amines. *Topics in Catalysis*, **57** (2014) 284–300. <https://doi.org/10.1007/s11244-013-0184-1>.
36. H. Kohls, F. Steffen-Munsberg, & M. Höhne, Recent achievements in developing the biocatalytic toolbox for chiral amine synthesis. *Current Opinion in Chemical Biology*, **19** (2014) 180–192. <https://doi.org/10.1016/j.cbpa.2014.02.021>.
37. W. W. Umbreit, D. J. O’Kane, & I. C. Gunsalus, Function of the vitamin B6 group; mechanism of transamination. *The Journal of biological chemistry*, **176** (1948) 629–37.
38. B. Witkop & T. W. Beiler, Studies on Schiff Bases in Connection with the Mechanism of Transamination. *Journal of the American Chemical Society*, **76** (1954) 5589–5597. <https://doi.org/10.1021/ja01651a002>.
39. R. Percudani & A. Peracchi, The B6 database: A tool for the description and classification of vitamin B6-dependent enzymatic activities and of the corresponding protein families. *BMC Bioinformatics*, **10** (2009) 273. <https://doi.org/10.1186/1471-2105-10-273>.



40. S. Mathew & H. Yun,  $\omega$ -Transaminases for the Production of Optically Pure Amines and Unnatural Amino Acids. *ACS Catalysis*, **2** (2012) 993–1001. <https://doi.org/10.1021/cs300116n>.
41. F. Steffen-Munsberg, C. Vickers, H. Kohls, H. Land, H. Mallin, A. Nobili, L. Skalden, T. van den Bergh, H. J. Joosten, P. Berglund, M. Höhne, & U. T. Bornscheuer, Bioinformatic analysis of a PLP-dependent enzyme superfamily suitable for biocatalytic applications. *Biotechnology Advances*, **33** (2015) 566–604. <https://doi.org/10.1016/j.biotechadv.2014.12.012>.
42. R. S. Phillips, Chemistry and diversity of pyridoxal-5'-phosphate dependent enzymes. *Biochimica et Biophysica Acta - Proteins and Proteomics*, **1854** (2015) 1167–1174. <https://doi.org/10.1016/j.bbapap.2014.12.028>.
43. C. K. Savile, J. M. Janey, E. C. Mundorff, J. C. Moore, S. Tam, W. R. Jarvis, J. C. Colbeck, A. Krebber, F. J. Fleitz, J. Brands, P. N. Devine, G. W. Huisman, & G. J. Hughes, Biocatalytic asymmetric synthesis of chiral amines from ketones applied to sitagliptin manufacture. *Science*, **329** (2010) 305–309. <https://doi.org/10.1126/science.1188934>.
44. M. Planchestainer, M. L. Contente, J. Cassidy, F. Molinari, L. Tamborini, & F. Paradisi, Continuous flow biocatalysis: production and in-line purification of amines by immobilised transaminase from *Halomonas elongata*. *Green Chemistry*, **19** (2017) 372–375. <https://doi.org/10.1039/C6GC01780K>.
45. M. L. Contente & F. Paradisi, Self-sustaining closed-loop multienzyme-mediated conversion of amines into alcohols in continuous reactions. *Nature Catalysis*, **1** (2018) 452–459. <https://doi.org/10.1038/s41929-018-0082-9>.
46. J. S. Shin & B. G. Kim, Transaminase-catalyzed asymmetric synthesis of L-2-aminobutyric acid from achiral reactants. *Biotechnology Letters*, **31** (2009) 1595–1599.

<https://doi.org/10.1007/s10529-009-0057-7>.

47. M. L. Contente, F. Dall'Oglio, L. Tamborini, F. Molinari, & F. Paradisi, Highly Efficient Oxidation of Amines to Aldehydes with Flow-based Biocatalysis. *ChemCatChem*, **9** (2017) 3843–3848. <https://doi.org/10.1002/cctc.201701147>.
48. S. W. May & S. R. Padgette, Oxidoreductase enzymes in biotechnology: Current status and future potential. *Bio/Technology*, **1** (1983) 677–686. <https://doi.org/10.1038/nbt1083-677>.
49. A. W. Munro, P. Taylor, & M. D. Walkinshaw, Structures of redox enzymes. *Current Opinion in Biotechnology*, **11** (2000) 369–376. [https://doi.org/10.1016/S0958-1669\(00\)00112-9](https://doi.org/10.1016/S0958-1669(00)00112-9).
50. F. Xu, Applications of oxidoreductases: Recent progress. *Industrial Biotechnology*, **1** (2005) 38–50. <https://doi.org/10.1089/ind.2005.1.38>.
51. T. Ishige, K. Honda, & S. Shimizu, Whole organism biocatalysis. *Current Opinion in Chemical Biology*, **9** (2005) 174–180. <https://doi.org/10.1016/j.cbpa.2005.02.001>.
52. K. Goldberg, K. Schroer, S. Lütz, & A. Liese, Biocatalytic ketone reduction - A powerful tool for the production of chiral alcohols - Part II: Whole-cell reductions. *Applied Microbiology and Biotechnology*, **76** (2007) 249–255. <https://doi.org/10.1007/s00253-007-1005-x>.
53. X. Wang, T. Saba, H. H. P. Yiu, R. F. Howe, J. A. Anderson, & J. Shi, Cofactor NAD(P)H Regeneration Inspired by Heterogeneous Pathways. *Chem*, **2** (2017) 621–654. <https://doi.org/10.1016/j.chempr.2017.04.009>.
54. B. R. Riebel, P. R. Gibbs, W. B. Wellborn, & A. S. Bommarius, Cofactor Regeneration of both NAD<sup>+</sup> from NADH and NADP<sup>+</sup> from NADPH:NADH Oxidase from *Lactobacillus sanfranciscensis*.

- Advanced Synthesis & Catalysis*, **345** (2003) 707–712.  
<https://doi.org/10.1002/adsc.200303039>.
55. W. Liu & P. Wang, Cofactor regeneration for sustainable enzymatic biosynthesis. *Biotechnology Advances*, **25** (2007) 369–384.  
<https://doi.org/10.1016/j.biotechadv.2007.03.002>.
56. N. Cho, A. Leonowicz, J. Rogalski, D. Wesenberg, J. Luterek, M. Hofrichter, A. Matuszewska, & A. Wilkolazka, Fungal laccase: properties and activity on lignin. *Journal of Basic Microbiology*, **41** (2001) 185–227. [https://doi.org/10.1002/1521-4028\(200107\)41:3/43.O.CO;2-T](https://doi.org/10.1002/1521-4028(200107)41:3/43.O.CO;2-T).
57. R. C. Minussi, G. M. Pastore, & N. Durán, Potential applications of laccase in the food industry. *Trends in Food Science and Technology*, **13** (2002) 205–216. [https://doi.org/10.1016/S0924-2244\(02\)00155-3](https://doi.org/10.1016/S0924-2244(02)00155-3).
58. S. Camarero, D. Ibarra, M. J. Martinez, & A. T. Martinez, Lignin-Derived Compounds as Efficient Laccase Mediators of Different Types of Recalcitrant Dyes. *Applied and Environmental Microbiology*, **71** (2005) 1775–1784.  
<https://doi.org/10.1128/AEM.71.4.1775>.
59. H. Jörnvall, Horse liver alcohol dehydrogenase. The primary structure of the protein chain of the ethanol-active isoenzyme. *European journal of biochemistry*, **16** (1970) 25–40.
60. D. Giacomini, P. Galletti, A. Quintavalla, G. Gucciardo, & F. Paradisi, Highly efficient asymmetric reduction of arylpropionic aldehydes by Horse Liver Alcohol Dehydrogenase through dynamic kinetic resolution. *Chemical Communications*, (2007) 4038–4040. <https://doi.org/10.1039/b712290j>.
61. T. Huber, L. Schneider, A. Präg, S. Gerhardt, O. Einsle, & M. Müller, Direct reductive amination of ketones: Structure and activity of S-selective imine reductases from streptomyces. *ChemCatChem*, **6** (2014) 2248–2252.

<https://doi.org/10.1002/cctc.201402218>.

62. S. P. France, S. Hussain, A. M. Hill, L. J. Hepworth, R. M. Howard, K. R. Mulholland, S. L. Flitsch, & N. J. Turner, One-Pot Cascade Synthesis of Mono- and Disubstituted Piperidines and Pyrrolidines using Carboxylic Acid Reductase (CAR),  $\omega$ -Transaminase ( $\omega$ -TA), and Imine Reductase (IRED) Biocatalysts. *ACS Catalysis*, **6** (2016) 3753–3759. <https://doi.org/10.1021/acscatal.6b00855>.
63. B. Van den Burg, Extremophiles as a source for novel enzymes. *Current Opinion in Microbiology*, **6** (2003) 213–218. [https://doi.org/10.1016/S1369-5274\(03\)00060-2](https://doi.org/10.1016/S1369-5274(03)00060-2).
64. D. W. Hough & M. J. Danson, Extremozymes. *Current Opinion in Chemical Biology*, **3** (1999) 39–46. [https://doi.org/10.1016/S1367-5931\(99\)80008-8](https://doi.org/10.1016/S1367-5931(99)80008-8).
65. L. J. Rothschild & R. L. Mancinelli, Life in extreme environments. *Nature*, **409** (2001) 1092–1101. <https://doi.org/10.1038/35059215>.
66. R. Jaenicke & G. Böhm, The stability of proteins in extreme environments. *Current Opinion in Structural Biology*, **8** (1998) 738–748. [https://doi.org/10.1016/S0959-440X\(98\)80094-8](https://doi.org/10.1016/S0959-440X(98)80094-8).
67. M. T. Madigan & A. Orent, Thermophilic and halophilic extremophiles. *Current Opinion in Microbiology*, **2** (1999) 265–269. [https://doi.org/10.1016/S1369-5274\(99\)80046-0](https://doi.org/10.1016/S1369-5274(99)80046-0).
68. M. de Lourdes Moreno, D. Pérez, M. García, & E. Mellado, Halophilic Bacteria as a Source of Novel Hydrolytic Enzymes. *Life*, **3** (2013) 38–51. <https://doi.org/10.1016/j.ihe.2014.05.002>.
69. A. Siglioccolo, A. Paiardini, M. Piscitelli, & S. Pascarella, Structural adaptation of extreme halophilic proteins through decrease of conserved hydrophobic contact surface. *BMC structural biology*, **11** (2011) 50. <https://doi.org/10.1186/1472-6807-11-50>.
70. R. H. Vreeland, C. D. Litchfield, E. L. Martin, & E. Elliot, *Halomonas elongata*, a New Genus and Species of Extremely Salt-Tolerant

- Bacteria. *International Journal of Systematic Bacteriology*, **30** (1980) 485–495. <https://doi.org/10.1099/00207713-30-2-485>.
71. K. Schwibbert, A. Marin-Sanguino, I. Bagyan, G. Heidrich, G. Lentzen, H. Seitz, M. Rampp, S. C. Schuster, H.-P. P. Klenk, F. Pfeiffer, D. Oesterhelt, & H. J. Kunte, A blueprint of ectoine metabolism from the genome of the industrial producer *Halomonas elongata* DSM 2581 T. *Environmental Microbiology*, **13** (2011) 1973–1994. <https://doi.org/10.1111/j.1462-2920.2010.02336.x>.
  72. R. A. Sheldon & S. Van Pelt, Enzyme immobilisation in biocatalysis: why, what and how. *Chemical Society Reviews*, **42** (2013) 6223–6235. <https://doi.org/10.1039/c3cs60075k>.
  73. U. Hanefeld, L. Gardossi, & E. Magner, Understanding enzyme immobilisation. *Chemical Society Reviews*, **38** (2009) 453–468. <https://doi.org/10.1039/B711564B>.
  74. L. Betancor & H. R. Luckarift, Bioinspired enzyme encapsulation for biocatalysis. *Trends in Biotechnology*, **26** (2008) 566–572. <https://doi.org/10.1016/j.tibtech.2008.06.009>.
  75. M. B. Majewski, A. J. Howarth, P. Li, M. R. Wasielewski, J. T. Hupp, & O. K. Farha, Enzyme encapsulation in metal–organic frameworks for applications in catalysis. *CrystEngComm*, **19** (2017) 4082–4091. <https://doi.org/10.1039/C7CE00022G>.
  76. C. Rother & B. Nidetzky, Enzyme Immobilization by Microencapsulation: Methods, Materials, and Technological Applications. *Encycl. Ind. Biotechnol.* (Hoboken, NJ, USA: John Wiley & Sons, Inc., 2014), pp. 1–21. <https://doi.org/10.1002/9780470054581.eib275>.
  77. R. A. Sheldon, Cross-linked enzyme aggregates as industrial biocatalysts. *Organic Process Research and Development*, **15** (2011) 213–223. <https://doi.org/10.1021/op100289f>.
  78. L. Wilson, L. Betancor, G. Fernández-Lorente, M. Fuentes, A.

- Hidalgo, J. M. Guisán, B. C. C. Pessela, & R. Fernández-Lafuente, Cross-linked aggregates of multimeric enzymes: A simple and efficient methodology to stabilize their quaternary structure. *Biomacromolecules*, **5** (2004) 814–817. <https://doi.org/10.1021/bm034528i>.
79. C. Ning, E. Su, Y. Tian, & D. Wei, Combined cross-linked enzyme aggregates (combi-CLEAs) for efficient integration of a ketoreductase and a cofactor regeneration system. *Journal of Biotechnology*, (2014). <https://doi.org/10.1016/j.jbiotec.2014.05.004>.
80. B. Brena, P. González-Pombo, & F. Batista-Viera, Immobilization of Enzymes and Cells. *Methods in Molecular Biology*. (2013).
81. C. Mateo, O. Abian, G. Fernández-Lorente, J. Pedroche, R. Fernández-Lafuente, J. M. Guisan, A. Tam, & M. Daminati, Epoxy Sepabeads: A novel epoxy support for stabilization of industrial enzymes via very intense multipoint covalent attachment. *Biotechnology Progress*, **18** (2002) 629–634. <https://doi.org/10.1021/bp010171n>.
82. C. Mateo, R. Torres, G. Fernández-Lorente, C. Ortiz, M. Fuentes, A. Hidalgo, F. López-Gallego, O. Abian, J. M. Palomo, L. Betancor, B. C. C. Pessela, J. M. Guisan, & R. Fernández-Lafuente, Epoxy-amino groups: A new tool for improved immobilization of proteins by the epoxy method. *Biomacromolecules*, **4** (2003) 772–777. <https://doi.org/10.1021/bm0257661>.
83. C. Mateo, V. Grazu, J. M. Palomo, F. Lopez-Gallego, R. Fernandez-Lafuente, & J. M. Guisan, Immobilization of enzymes on heterofunctional epoxy supports. *Nature Protocols*, **2** (2007) 1022–1033. <https://doi.org/10.1038/nprot.2007.133>.
84. L. Vaccaro, D. Lanari, A. Marrocchi, & G. Strappaveccia, Flow approaches towards sustainability. *Green Chemistry*, **16** (2014) 3680. <https://doi.org/10.1039/C4GC00410H>.

85. J. Wegner, S. Ceylan, & A. Kirschning, Ten key issues in modern flow chemistry. *Chemical Communications*, **47** (2011) 4583. <https://doi.org/10.1039/c0cc05060a>.
86. I. R. Baxendale, The integration of flow reactors into synthetic organic chemistry. *Journal of Chemical Technology & Biotechnology*, **88** (2013) 519–552. <https://doi.org/10.1002/jctb.4012>.
87. I. R. Baxendale, C. M. Griffiths-Jones, S. V. Ley, & G. K. Tranmer, Preparation of the neolignan natural product grossamide by a continuous-flow process. *Synlett*, (2006) 427–430. <https://doi.org/10.1055/s-2006-926244>.
88. M. D. Hopkin, I. R. Baxendale, & S. V. Ley, A flow-based synthesis of Imatinib: The API of Gleevec. *Chemical Communications*, **46** (2010) 2450–2452. <https://doi.org/10.1039/c001550d>.
89. I. R. Baxendale, J. Deeley, C. M. Griffiths-Jones, S. V. Ley, S. Saaby, & G. K. Tranmer, A flow process for the multistep synthesis of the alkaloid natural product oxomaritidine: A new paradigm for molecular assembly. *Chemtracts*, **20** (2007) 462–463. <https://doi.org/10.1039/b600382f>.
90. I. R. Baxendale, S. V. Ley, C. D. Smith, & G. K. Tranmer, A flow reactor process for the synthesis of peptides utilizing immobilized reagents, scavengers and catch and release protocols. *Chemical Communications*, (2006) 4835–4837. <https://doi.org/10.1039/b612197g>.
91. F. M. Akwi & P. Watts, Continuous flow chemistry: where are we now? Recent applications, challenges and limitations. *Chemical Communications*, **54** (2018) 13894–13928. <https://doi.org/10.1039/c8cc07427e>.
92. L. H. Andrade, W. Kroutil, & T. F. Jamison, Continuous Flow Synthesis of Chiral Amines in Organic Solvents: *Organic letters*, **16** (2014) 6092–6095.

<https://doi.org/dx.doi.org/10.1021/ol502712v>.

93. H. M. Salvi, M. P. Kamble, & G. D. Yadav, Synthesis of Geraniol Esters in a Continuous-Flow Packed-Bed Reactor of Immobilized Lipase: Optimization of Process Parameters and Kinetic Modeling. *Applied Biochemistry and Biotechnology*, **184** (2017) 1–14. <https://doi.org/10.1007/s12010-017-2572-7>.
94. D. Yu, X. Zhang, D. Zou, T. Wang, T. Liu, L. Wang, W. Elfalleh, & L. Jiang, Immobilized CALB Catalyzed Transesterification of Soybean Oil and Phytosterol. *Food Biophysics*, **13** (2018) 208–215. <https://doi.org/10.1007/s11483-018-9526-7>.
95. A. I. Benítez-Mateos, M. L. Contente, S. Velasco-Lozano, F. Paradisi, & F. López-Gallego, Self-Sufficient Flow-Biocatalysis by Coimmobilization of Pyridoxal 5'-Phosphate and  $\omega$ -Transaminases onto Porous Carriers. *ACS Sustainable Chemistry & Engineering*, **6** (2018) 13151–13159. <https://doi.org/10.1021/acssuschemeng.8b02672>.
96. M. L. Contente & F. Paradisi, Transaminase-Catalyzed Continuous Synthesis of Biogenic Aldehydes. *ChemBioChem*, (2019) 1–5. <https://doi.org/10.1002/cbic.201900356>.
97. L. Tamborini, P. Fernandes, F. Paradisi, & F. Molinari, Flow Bioreactors as Complementary Tools for Biocatalytic Process Intensification. *Trends in Biotechnology*, **36** (2018) 73–88. <https://doi.org/10.1016/j.tibtech.2017.09.005>.
98. C. Wiles & P. Watts, Continuous flow reactors: a perspective. *Green Chemistry*, **14** (2012) 38–54. <https://doi.org/10.1039/C1GC16022B>.
99. M. D. Hopkin, I. R. Baxendale, & S. V. Ley, An expeditious synthesis of imatinib and analogues utilising flow chemistry methods. *Organic and Biomolecular Chemistry*, **11** (2013) 1822–1839. <https://doi.org/10.1039/c2ob27002a>.



## Chapter 2: Aims and objectives

As presented in the introduction, biocatalysis has proven to offer a more sustainable and environmentally friendly strategy for industrial relevant syntheses but its widespread industrial application is still hampered by a number of drawbacks. Problems associated with enzymatic stability can be solved through enzyme immobilisation techniques, but a universal methodology is not yet available. Nevertheless, enzyme immobilisation enables biocatalysis to take place in continuous flow systems, which are often advantageous when compared with both batch reactions and classical chemical synthesis. Therefore, resolving problems in both enzyme immobilisation and their efficient application in flow assisted biotransformations is of greatest importance for the future of biocatalysis.

My PhD thesis focusses on the identification of some of the issues encountered in flow based biocatalysis and proposes solutions to overcome these. To that end, the main objectives are:

1. The development of a covalent immobilisation strategy for carboxylesterase to allow their efficient combination with a flow reactor to perform hydrolytic reactions.
2. The development of a method to enhance substrate solubility to overcome the low reactivity of slurries in flow.
3. To gain structural insight of transaminases and enhance their PLP binding capacity which will minimise costs of large-scale processes.
4. The development of a robust recycling system for transaminase mediated amination of substrates with unfavourable equilibria avoiding the use of high amino-donor concentrations.
5. Finally, with a more synthetic focus, the development of a cascade for the efficient production of pipercolic acid using immobilised enzymes in combination with a flow-reactor.

## **Chapter 3: Material and methods**

### **3.1. Reagents**

All chemical reagents and cell growing medias were purchased from Sigma-Aldrich, U.K., Acros Organics, Thermo Fisher Scientific U.K or Merck Millipore. Organic solvents were purchased from Sigma-Aldrich or VWR. Enzyme carriers Sepabeads and ReliZyme were kindly donated by Resindion S.R.L. Plasmid DNA purification kit, PCR product purification and DNA purification from Agar-gel were purchased from Qiagen, Thermo or Macherey-Nagel. DNA ladder, Protein Marker, restriction enzymes and Q5 High Fidelity DNA polymerase were purchased from New England Biolab. QuickChange lightning multi-site directed mutagenesis kit was purchased from Agilent-Technologies.

When not specified, the manufacturer's protocol was used for the experiment.

### **3.2. General instrumentation**

- DNA amplification and temperature stability assays were performed in a PCR thermal Cycler SensoQuest® Labcycler 48 and Applied Biosystem® Verti®.
- DNA electrophoresis and Protein SDS-PAGE were carried out using a power supply EPS 301 from Amershan Bioscience.
- Plasmid purification was performed using the NucleoSpin Plasmid purification kit from Macherey-Nagel®, PCR product purification was performed with the QIAquick PCR purification kit from Qiagen® and agarose gel DNA extraction was performed using the QIAquick Gel Extraction kit from Qiagen®.
- Solid medium plates and liquid cultures were incubated in a static incubator Thermo Scientific MaxQ6000 with temperature control from 4 to 60°C or New Brunswick Scientific Model C24 for temperatures from 30 to 37°C.

- Cell debris were removed from cell lysate suspension using a centrifuge Thermo® Heraeus Multifuge with Thermo Fiberlite F15 for volumes larger than 2mL, at 4°C.
- General centrifuge cycles were performed using Thermo® Microcentrifuge Accuspin Micro 17R, with controlled temperature for volumes of 2mL or less.
- Cells were lysed by sonication using a Fisher brand Ultrasonic Liquid processor FB120 with timer and pulser from Fisher brand.
- Protein purifications were performed with a chromatography system AKTAPrime® Start from GE Healthcare using HisTrap FF 1mL, HisTrap FF 5mL (GE Healthchare) or Ni-NTA Superflow Cartridges (Qiagen).
- Size exclusion chromatography was performed using an AKTAPure® using a Superdex 200 Increase 10/300 GL (GE Healthcare) column.
- HPLC analysis were performed on an Agilent Technologies HPLC 1200 or a Thermo Scientific Dionex Ultimate 3000 Series HPLC coupled with a Waters X-Bridge C18 (3.5µm, 2.1 x 100 mm).
- Absorbance reading and scanning, as well as enzymatic tests, were performed on an EPOCH2 microplate and cuvette reader from BioTeck®.
- General pipetting was done with Micropipettes P5000, P1000, P200, P20, P10 and P2.5 from StarLab® and Eppendorf® Multipipette E2.
- pH-meter Orion Star A111, calibrated regularly with standard solutions (pH 4, pH 7 and pH 10 from Sigma-Aldrich).
- Chemicals were weighted using balances model PS5602, model CSC2000 or an analytical series PAS214C, all from Thermo Scientific®.

- Other common instruments used during the experiments: Lab-Line® Multi-Block Heater, Benchtop Shaker Carl Stuart Limited IKA®, Vortex mixer Wizard from FisherBrand® and microwave cooker from Daewoo®.

### 3.3. Cell cultures and manipulation

#### 3.3.1. Bacterial strains

The following bacterial strains were used:

- *E. coli* XL10-Gold for the construct replication and extraction. Genotype: endA1 glnV44 recA1 thi-1 gyrA96 relA1 lac Hte  $\Delta(\text{mcrA})183$   $\Delta(\text{mcrCB-hsdSMR-mrr})173$  tet<sup>R</sup> F'[proAB lacI<sup>q</sup>Z $\Delta$ M15 Tn10(Tet<sup>R</sup> Amy Cm<sup>R</sup>)]
- *E. coli* BL21 (DE3) as standard protein expression strain. Genotype: *E. coli* str. B F<sup>-</sup> ompT gal dcm lon hsdS<sub>B</sub>(r<sub>B</sub><sup>-</sup>m<sub>B</sub><sup>-</sup>)  $\lambda$  (DE3 [lacI lacUV5-T7p07 ind1sam7 nin5]) [malB<sup>+</sup>]<sub>K-12</sub>( $\lambda^S$ )
- *E. coli* BL21 (DE3) pLysS for the repression of the leak expression of the recombinant protein. Genotype: *E. coli* str. B F<sup>-</sup> ompT gal dcm lon hsdS<sub>B</sub>(r<sub>B</sub><sup>-</sup>m<sub>B</sub><sup>-</sup>)  $\lambda$  (DE3 [lacI lacUV5-T7p07 ind1sam7 nin5]) [malB<sup>+</sup>]<sub>K-2</sub>( $\lambda^S$ ) pLysS [T7p20 ori<sub>p15A</sub>] (Cm<sup>R</sup>)
- *E. coli* BL21(DE3) RIPL for the enhanced expression of the recombinant gene. Genotype: *E. coli* B F<sup>-</sup> ompT hsdS (r<sub>B</sub><sup>-</sup> m<sub>B</sub><sup>-</sup>) dcm<sup>+</sup> Tet<sup>r</sup> gal  $\lambda$ (DE3) endA Hte [argU proL Cam<sup>r</sup>] [argU ileY leuW Strep/Spec<sup>r</sup>]

#### 3.3.2. Culture mediums

- LB medium: N-Z amine (10g), yeast extract (5g), NaCl (10g) and distilled H<sub>2</sub>O (1 L).
- LB agar plates: N-Z amine (10g), yeast extract (5g), NaCl (10g), agar (15g) and distilled H<sub>2</sub>O (1 L).

- SOB medium: N-Z amine (5g), yeast extract (1.25g), NaCl (0.25g), KCl (0.05g), MgCl<sub>2</sub> 6H<sub>2</sub>O (0.5g), MgSO<sub>4</sub> 6H<sub>2</sub>O (0.6g) and distilled H<sub>2</sub>O (250 mL).
- TB medium: N-Z amine (12g), yeast extract (24g), glycerol (5g), K<sub>2</sub>HPO<sub>4</sub> (2.2g) and KH<sub>2</sub>PO<sub>4</sub> (9.4g) and distilled H<sub>2</sub>O (1L).
- ZYP-5052 auto-induction media: N-Z-Amine (3 g), yeast extract (1.5 g), 1M K<sub>2</sub>HPO<sub>4</sub> (15 mL), 1M KH<sub>2</sub>PO<sub>4</sub> (15 mL), 1M (NH<sub>4</sub>)<sub>2</sub>SO<sub>4</sub> (7.5 mL) 1000x trace element solution (0,6 mL) consists of: FeCl<sub>2</sub> (50 mM), CaCl<sub>2</sub> (20 mM), MnCl<sub>2</sub> (10 mM), ZnSO<sub>4</sub> (10 mM), CoCl<sub>2</sub> (2 mM), CuCl<sub>2</sub> (2 mM), NiCl<sub>2</sub> (2 mM), HCl (60 mM), Na<sub>2</sub>MoO<sub>4</sub> (2 mM), Na<sub>2</sub>SeO<sub>4</sub> (2 mM) and H<sub>3</sub>BO<sub>3</sub> (2 mM) (sterilized by filtration); 50x 5052 solution (6 mL) consists of: glycerol (25 g), glucose (2,5 g), α-lactose monohydrate (10 g) and dH<sub>2</sub>O (to 100 mL) in dH<sub>2</sub>O (to 300 mL).

### 3.3.3. Preparation of chemically competent cells

A single colony of *E. coli* of the desired strain was inoculated into LB medium (50 mL) and grown at 37°C, 150 rpm to an OD<sub>600</sub> of approximately 0.4. The culture was then placed on ice for 20 minutes and subsequently harvested by centrifugation at 3000 g for 15 minutes at 4°C. The cells were resuspended in 10 mL of an ice-cold 100 mM magnesium chloride solution and harvested again in the same conditions as before. The pellet was resuspended in 20 mL of an ice-cold solution of 100 mM calcium chloride and incubated in ice for 30 minutes. After the last harvesting by centrifugation (3000 G, 10 minutes, 4°C), resuspended in 0.5 mL of the previous solution and aliquoted in 80 µL in 1.5 mL microcentrifuge tubes and frozen at -80°C.

### 3.3.4. Preparation of electro competent cells

A single colony of *E. coli* of the desired strain was inoculated into LB medium (50 mL) and grown at 37°C, 150 rpm to an OD<sub>600</sub> of approximately 0.4. The cells were chilled in ice for 20 minutes and then harvested by centrifugation at 3000 rpm, 15 minutes at 4°C. The pellet was then carefully resuspended in ice-cold sterilised water followed by

centrifugation at the same conditions as before. The wash step was repeated with 25 mL of water and then 15 mL of water/glycerol 10%. The pellet was finally resuspended in 0.5 mL of water/glycerol 10% and aliquoted (50 µL) in 1.5 mL microcentrifuge tubes which were flash frozen and stored at -80°C.

### **3.3.5. Transformation of competent *E. coli* cells**

Transformation of chemically competent cells was performed by adding 0.2-2 µL (100 ng) of the plasmid to a microcentrifuge tube containing 40 µL of the chemically competent cells. The competent cells were left on ice for 30 minutes and after that, the sample was heat-shocked at 42°C for 60 seconds. The sample was then cooled in ice for 2 minutes and 250 µL of either SOB or LB media was added to the tube. The cells were then left 1h at 37°C and 180 rpm and then spread onto two LB-agar plates containing the appropriate antibiotic, where they were grown overnight at 37°C.

For the electroporation, 1 µL of DNA was added to 50 µL of electrocompetent cells and then transferred into an ice-cold electroporation cuvette. Cells were electroporated at 1.8 kV for approximately 5 ms, followed by the addition of 500 µL of SOC medium immediately after. Cells were left to grow for 1 hour at 37°C and 180 rpm before spreading onto LB-agar plates containing the appropriate antibiotic where they were grown overnight at 37°C.

## **3.4. General procedures**

### **3.4.1. Gene cloning**

HeE, HeP5CR and HeAlaDH were cloned by PCR from the genome of *Halomonas elongata* DSM2581 (strain: type strain: DSM 2581) [1] and BsLys6DH was subcloned from the commercially ordered construction from Thermo Fisher Scientific® containing the enzyme sequence of *Geobacillus stearothermophilus* lysine-6-dehydrogenase [2] optimised for expression in *Escherichia coli*.

When using PCR, the reaction was performed using Q5® High-Fidelity DNA polymerase from New England Biolabs. The primers,

ordered from Thermo Fisher Scientific, were designed to amplify the desired gene and incorporate restriction sites on both ends. After PCR, the product was purified using the PCR purification kit, and both the gene and the desired vector were digested with the appropriate restriction enzymes (Table 3.1). Ligation was performed overnight at 16°C using T4-DNA ligase from New England Biolabs. After ligation, either chemical or electro competent cells were used for the transformation. The correct assembly of the final construction was confirmed by sequencing.

**Table 3.1.** Detailed information of the cloning of the three genes from *H. elongata* DSM2581. The gene code from Ensembl [3] is shown, as well as the primers used and the restriction enzymes. The restriction sites are underlined.

Gene name	Primers and Restriction enzymes:	Final construction
helo_2889	5' CCC TGT GCG <u>GGATCC</u> TGA CGT CAT GCG CAA AGC TCA AGC 3' (BamHI) 5' ATA TAA A <u>GGTACCT</u> CAT CAG TTG ATC TGC AGG <u>CTG TCC</u> AGC GAC G 3' (KpnI)	pRSETB-HeE
helo_4115	5' AAA AA <u>GGATCC</u> CCC CAT GGC AAG CCA AGT CAC C 3' (BamHI) 5' AAA AA <u>GAATTC</u> TCA TCA GCG CTT GCC GAG TTC G 3' (EcoRI)	pRSETB-HeP5CR
helo_3819	5' AAA AA <u>GGATCC</u> CCC ATG AAG ATC GCC GTG CC 3' (BamHI) 5' AAT C <u>GAATTC</u> CCC TCA TCA GCC GAT CAA GCT GG C 3' (EcoRI)	pRSETB-HeAlaDH

### 3.4.2. Agarose gel electrophoresis

DNA assay gel electrophoresis was performed using an agarose concentration of 0.8% (w/v). The solution was made by dissolving agarose powder (0.32 g) in 40 mL of TAE buffer by heating it in a standard microwave oven until the solution was completely clear. When the temperature was low enough without leaving it solidify, 4 µL of SYBR safe DNA staining were added. The solution was then loaded into the mould and left to solidify. Samples were prepared appropriately mixing them with the Gel Loading Dye Purple (6x) from New England Biolabs. The electrophoresis was conducted routinely at 75V and 150 mA for 45 minutes.

### **3.4.3. Protein overexpression and purification**

Protein overexpression was performed after competent cells were transformed with the expression vector harbouring the desired protein.

For proteins expressed with autoinduction media, one single colony was inoculated directly in the flask with either 50 mL or 300 mL of ZYP-5052 media supplemented with the correct antibiotic. For proteins expressed with either LB medium or TB broth, an overnight pre-inoculum of at least 10 mL was prepared the day before and 1/100 of the final volume added to either 50 mL or 300 mL of the corresponding media supplemented with the desired antibiotic. Proteins were expressed in the conditions detailed in Table 3.2.

After the chosen time, cell cultures were harvested at 4000 rpm for 20 minutes at 4°C in the appropriate centrifuge tubes and the cells separated from the medium. The supernatant was carefully removed, and the cells resuspended in a minimum of 5 mL of loading buffer/g of pellet. The cell lysis was performed in ice using the sonicator in pulse mode (30 seconds on, 30 seconds off) for a minimum of 10 minutes. The lysate was then centrifuged at 14500 rpm, for a minimum of 45 minutes at 4°C. The collected supernatant was filtered with 0.45 µm Millex PVDF filters before loading onto the Ni<sup>2+</sup> preloaded columns.

The affinity chromatography was performed using an AKTA Start system with the appropriate column. The filtered crude extract was loaded and left washing until the non-specific proteins were completely eluted. After that, an isocratic wash step with only 5-10% of elution buffer was performed to elute the non-specific proteins still bound onto the column. Finally, 100% of elution buffer was passed through the column and protein elution monitored by UV. Fractions were collected and those containing the desired protein pooled and placed into dialysis tubing. The protein samples were dialysed at least for 20 hours replacing the buffer at least 2 times at 4°C. The pure proteins were stored at 4°C if not stated differently.



**Table 3.2.** Detail of the expression and purification conditions used for the various proteins investigated.

Protein	Expression conditions:	Loading buffer:	Elution buffer:
<b>HeE</b>	BL21(DE3) plyss - TB broth at 0.6-0.9 OD600, cold shock for 20mins and induction at with 1 mM IPTG O/N at 30°C.	50 mM Phosphate buffer pH8, 0.1 M NaCl, 30 mM imidazole, 0.1 mM PLP	50 mM Phosphate buffer pH8, 0.1 M NaCl, 300 mM imidazole
<b>BS2m</b>	BL21(DE3) plyss - TB broth at 0.6-0.9 OD600, induction at with 1 mM IPTG O/N at 30°C.	50 mM Phosphate buffer pH8, 0.1 M NaCl, 30 mM imidazole, 0.1 mM PLP	50 mM Phosphate buffer pH8, 0.1 M NaCl, 300 mM imidazole
<b>BS2mT4L1 / BS2mT4L2</b>			
<b>HeTA</b>	BL21(DE3) Star- Autoinduction ZYP media for 20h.		
<b>CVTA</b>	BL21(DE3) - LB medium at 0.6-0.9 OD600, induction at with 0.01 mM IPTG O/N at 30°C.	50 mM Phosphate buffer pH8, 0.1 M NaCl, 30 mM imidazole, 0.1 mM PLP	50 mM Phosphate buffer pH8, 0.1 M NaCl, 300 mM imidazole, 0.1 mM PLP
<b>PfTA</b>	BL21(DE3) Star- TB broth at 0.6-0.9 OD600, induction at 30°C with 1 mM IPTG O/N.	50 mM Phosphate buffer pH8, 0.1 M NaCl, 30 mM imidazole	50 mM Phosphate buffer pH8, 0.1 M NaCl, 300 mM imidazole
<b>BSlys6DH</b>	BL21(DE3) Star- Autoinduction ZYP media for 20h.		
<b>BmgDH</b>	BL21(DE3) - LB broth at 0.6-0.9 OD600, induction at 30°C with 1 mM IPTG O/N	50 mM Tris-HCl, 0.1M NaCl, 6 mM imidazole pH 8	50 mM Tris-HCl, 0.1M NaCl, 300 mM imidazole pH 8
<b>CbFDH</b>	BL21(DE3) Star - LB medium at 0.6-0.9 OD600, induction at 25°C with 1 mM IPTG O/N.	50 mM Phosphate buffer pH8, 0.1 M NaCl, 30 mM imidazole	50 mM Phosphate buffer pH8, 0.1 M NaCl, 30 mM imidazole
<b>HeAlADH</b>	BL21(DE3) Star - TB broth at 0.6-0.9 OD600, induction at 30°C with 1 mM IPTG O/N.	50 mM Phosphate buffer pH8, 0.1 M NaCl, 30 mM imidazole	50 mM Phosphate buffer pH8, 0.1 M NaCl, 300 mM imidazole
<b>HLADH</b>	BL21(DE3) Star- Autoinduction ZYP media for 20h.	20 mM phosphate buffer, 0.5 M NaCl, 20 mM imidazole pH 7.4	20 mM phosphate buffer, 0.5 M NaCl, 30 mM EDTA, pH 7.4

### 3.4.4. Protein quantification

The preferred method for protein quantification was by measuring absorbance at 280 nm. The concentration was then determined using the molar extinction coefficient for each protein calculated using ProtParam [4] and exploiting the Lambert-Beer law, in combination with their molecular mass. The extinction coefficient and molecular mass of all the proteins investigated is presented in Table 3.3.

**Table 3.3.** Extinction coefficient and molecular mass used for the calculation of protein concentration using a Take3 plate in combination with the EPOCH2.

Protein	Extinction coefficient ( $M^{-1} cm^{-1}$ )	Molecular mass (kDa)
HeE	72700	57
BS2m	80455	54
BS2mT4L1 / BS2mT4L2	108900	76.3
HeTA	62840	54.4
CvTA	81735	55.2
PfTA	68340	52.5
HeP5CR	18500	32
BsLys6DH	19400	46
BmGDH	28420	29
CbFDH	51402	42
HeAlaDH	24500	42
HLADH	18890	24

### 3.4.5. SDS-PAGE

SDS-PAGE assay was performed following the original procedure [5]. The running gel (12%: 1.95 mL of Tris HCl 1.5M pH 8.8, 2.25 mL acrylamide 40%, 3.125 mL of dH<sub>2</sub>O, 75  $\mu$ L SDS 10%, 75  $\mu$ L ammonium persulfate 10% (w/v) and 7.5  $\mu$ L TEMED) was prepared and loaded in between the two glass pieces, adding a few drops of isopropanol on top to avoid the formation of a meniscus. After the gel was polymerised, the stacking gel was prepared and loaded (0.25 mL 1M Tris pH 6.8, 0.33 mL acrylamide 40%, 1.4 mL dH<sub>2</sub>O, 20  $\mu$ L SDS 10%, 20  $\mu$ L ammonium persulfate 10% (w/v) and 3  $\mu$ L TEMED). Before loading, the samples were heated at 90°C for at least 5 minutes after mixed with an equal volume of the 2x loading buffer (0.18 M Tris-HCl buffer pH6, 3.8 mM  $\beta$ -mercaptoethanol, 7.2% (w/v) SDS, 36% (w/v) glycerol and 0.36 (w/v) bromophenol blue). The assay was run at 30 mA, 300V for 70 minutes.

The protein marker, unstained protein standard, Broad range (10-200 kDa) was loaded as a comparison. The gel was then removed from the mould and either stained with Coomassie blue staining solution (2% Coomassie brilliant blue R-250 in aqueous solution 50% methanol and 10% acetic acid) for 15-30 minutes following destaining with the destaining solution (aqueous solution 7.5% methanol and 10% acetic acid) overnight or with Instant Blue (Expedeon®) solution overnight.

#### **3.4.6. Size exclusion chromatography**

The molecular mass of the native proteins was determined by size exclusion chromatography on a Superdex 200 Increase 10/300 GL column with a total bed column of 24 mL from GE Healthcare. The column was equilibrated with 20 mM sodium phosphate buffer pH 8 with 150 mM NaCl. The purified enzymes (0.5-2 mg) were then injected and the experiment run at a flow of 0.8 mL/min. Fractions were collected and those corresponding to the eluted peak were assayed for concentration and activity to confirm the protein was still active and therefore, correctly folded. A calibration curve was prepared using the weight markers from Sigma-Aldrich:  $\beta$ -amylase (200 kDa), yeast alcohol dehydrogenase (150 kDa), bovine serum albumin (66 kDa) and the void volume indicated by blue dextran (2000 kDa).

#### **3.4.7. Enzymatic activity assay**

The activity of the different proteins was assessed by following the formation or depletion of a product or a substrate, in the case of the transaminases and esterases tested. The activity of the different oxidoreductases tested were assessed by the formation of NAD(P)H. One unit is defined as the amount of enzyme which catalyses the formation or depletion of 1  $\mu$ mol of product or substrate per minute. The standard assay conditions as well as the extinction coefficient used to assess the specific activity of the enzymes is shown in Table 3.4.

Activity assays on various conditions were performed using variations of the standard methods by varying the conditions of interest. In temperature activity assays, all components from the reaction except the

enzyme were heated to the desired temperature and the reaction was started by adding the enzyme. For pH activity assays, universal buffer was used from pH 3 to pH 12 instead of the standard buffer. For salt, cosolvent or metal toxicity activity assays, to the standard conditions the desired component was added, and the reaction performed in the standard conditions.

For the stability assays, typically, 0.1 mg/mL of the enzyme were incubated at the desired conditions. At regular times, a sample was taken, and the activity of the enzyme assessed using the standard activity assay. All stability assays apart from the temperature stability assays, if not stated otherwise, were performed at 4°C.

**Table 3.4.** Detail of the standard assay conditions used for the various enzymes tested. Extinction coefficient of the product or substrate monitored is also shown.

Protein	Standard assay conditions:	Extinction coefficient (mM <sup>-1</sup> cm <sup>-1</sup> )
<b>HeE</b> <b>BS2m</b> <b>BS2mT4L1 /</b> <b>BS2mT4L2</b>	0.5 mM <i>p</i> -nitrophenyl acetate, 50 mM phosphate buffer pH 8 at 30°C. Variation in absorbance at 420 nm was measured.	15
<b>HeTA</b> <b>CvTA</b> <b>PfTA</b>	2.5 mM S-MBA, 2.5 mM pyruvate, 0.1 mM PLP, 50 mM phosphate buffer pH 8 at 30°C. Variation in absorbance at 245 nm was measured	12.6
<b>HeP5CR</b>	10 mM <i>L</i> -thiazolidine carboxylate, 1 mM NAD <sup>+</sup> , 100 mM phosphate buffer pH 8 at 30°C. Variation in absorbance at 340 nm was measured.	
<b>BsLys6DH</b>	10 mM <i>L</i> -lysine, 1 mM NAD <sup>+</sup> , 100 mM phosphate buffer pH 8 at 30°C. Variation in absorbance at 340 nm was measured.	
<b>BmGDH</b>	40 mM glucose, 1 mM NAD <sup>+</sup> , 50 mM phosphate buffer pH 8 at 30°C. Variation in absorbance at 340 nm was measured.	
<b>CbFDH</b>	100 mM ammonium formate, 1 mM NAD <sup>+</sup> , 50 mM phosphate buffer pH 8- or 100-mM carbonate buffer pH 10 at 30°C. Variation in absorbance at 340 nm was measured.	6.22
<b>HeAlaDH</b>	40 mM <i>L</i> -alanine, 1 mM NAD <sup>+</sup> , 100 mM carbonate buffer pH 10 or 2.5 mM pyruvate, 250 mM NH <sub>4</sub> <sup>+</sup> , 0.1 mM NADH, 100 mM phosphate buffer pH 8 at 30°C. Variation in absorbance at 340 nm was measured.	
<b>HLADH</b>	40 mM ethanol, 1 mM NAD <sup>+</sup> , 50 mM Tris-HCl pH 8.8 at 30°C. Variation in absorbance at 340 nm was measured.	

### 3.4.8. Kinetic characterisation

To measure the kinetic properties of the studied enzymes, the concentration of the corresponding substrate was varied, and the enzymatic activity measured using the same method as in the standard activity assay. Data was then plotted and fitted to the standard Michaelis-Menten curve using GraphPad™. When the data did not have a good fit to the Michaelis-Menten curve ( $R < 0.95$ ), or it was not possible to reach saturation conditions, the data was transformed according to the Hanes-Woolf [6] plot to estimate both  $K_M$  and  $k_{cat}$ .

### 3.4.9. Batch reactions

Batch biotransformations, either with free enzyme or immobilised biocatalyst, were performed with the desired concentration of substrate, either in solution (0.1-2 mg/mL of enzyme) or suspension in the appropriate buffer system. Samples were withdrawn at different times and the reaction was quenched by adding 450  $\mu$ L of HCl 0.2% and 450  $\mu$ L of acetonitrile. The samples were analysed by HPLC (Dionex UltiMate 3000, Waters X-Bridge C18 (3.5  $\mu$ m, 2.1x100 mm), 0.8 mL/min, measuring at 210 nm, 250 nm and 265 nm) to assess the conversion.

### 3.4.10. Covalent enzyme immobilisation

Generally, 1g of Sepabeads or RelyZyme resin was treated with 2 mL of modification buffer (0.1M sodium borate and 2M of iminodiacetic acid in 50 mM phosphate buffer pH 8.5) under gentle shaking for 2h at room temperature. The resin was then filtered and washed three times with distilled water and mixed with 5 mL of the metal solution (1M sodium chloride and 5 mg/mL of the cation in 50 mM phosphate buffer pH 6) for another 2h. Following the same procedure, the sample was washed 3 times with distilled water and then the protein solution (2 to 10 mL) was added. The sample was kept under agitation (4-24h). The beads were then filtered and washed thoroughly with desorption buffer (50 mM EDTA and 0.5M NaCl in 20 mM phosphate buffer pH 7.4) and washed with distilled water. Finally, 4 mL of blocking buffer (3M glycine in 50 mM phosphate buffer pH 8.5) were added and the suspension left for agitation for 20 hours. The beads were washed, collected and conserved

in an appropriate volume of storage buffer at 4°C. Details of the supports used can be found in Table 3.5.

#### **3.4.11. Preparation of Agarose with epoxide groups**

Preparation of agarose with epoxide groups (Ag-ep) was prepared and the quantification of epoxide was conducted as described before [7]. In all batches, the resin contained  $60 \pm 4$   $\mu\text{mol}$ s of epoxides/g of dry resin.

#### **3.4.12. Preparation of dextran-aldehyde**

To obtain the 50% oxidised dextran-aldehyde, 10g of dextran (35-45 kDa) were dissolved in 100 mL water and mixed with 1g of periodate stirring at room temperature for 2h. After, it was dialysed against 50 times the volume of distilled water 4 times.

#### **3.4.13. Flow reactions**

Continuous flow biotransformations were performed using a R2+/R4 flow reactor commercially available from Vapourtec® equipped with an Omnifit ® glass column (6.6 mm i.d. x 100 mm length) filled with an appropriate volume of immobilised enzyme. When needed two solutions or solvents were mixed using a T tube before entrance to the column. The flow rate was varied and optimised for each reaction. The exiting flow stream was collected, and the results analysed by HPLC. The samples were analysed by HPLC (Dionex UltiMate 3000, Waters X-Bridge C18 (3.5  $\mu\text{m}$ , 2.1x100mm), 0.8 mL/min, measuring at 210 nm, 250 nm and 265 nm) to assess the conversion.

**Table 3.5.** List of all the immobilisation supports used.

<b>Resin</b>	<b>Matrix</b>	<b>Pore size</b>	<b>Particle size range</b>	<b>Functional group</b>	<b>Oxirane or aldehyde content</b>
<b>EC/EP-S</b>	Polymethacrylate	10-20 nm	100-300 µm	Epoxide	Min. 100 µmol/g wet
<b>EC403-S</b>	Polymethacrylate	40-60 nm	100-300 µm	Epoxide	Min. 30 µmol/g wet
<b>EC/HFA-S</b>	Polymethacrylate	10-20 nm	100-300 µm	Amino epoxide	Min 50 µmol/g wet
<b>HFA403-S</b>	Polymethacrylate	40-60 nm	100-300 µm	Amino epoxide	Min. 30 µmol/g wet
<b>HFA112-S</b>	Polymethacrylate	20-40 nm	100-300 µm	Amino epoxide	Min. 60 µmol/g wet
<b>EP112-S</b>	Polymethacrylate	20-40 nm	100-300 µm	Epoxide	Min. 60 µmol/g wet
<b>EP113-S</b>	Polymethacrylate	20-50 nm	100-300 µm	Epoxide	Min. 40 µmol/g wet
<b>EP400/SS</b>	Highly porous polymethacrylate	-	50-150 µm	Epoxide	Min. 100 µmol/g wet
<b>Agarose-glyoxyl</b>	Agarose 6BCL	24-70 nm	45-165 µm	Aldehyde	Max. of 70 µmol/g wet
<b>Agarose-epoxide</b>	Agarose 6BCL	24-70 nm	45-165 µm	Epoxide	60-65 µmol/g wet

### 3.4.14. HPLC analysis

Typically, for compounds with detectable fluorophores, samples were appropriately diluted in a solution of 1:1 (v/v) 0.1% HCl and 450  $\mu$ L of MeCN to stop the enzymatic reaction. These samples were then analysed by HPLC (Dionex UltiMate 3000, Waters X-Bridge C18 (3.5  $\mu$ m, 2.1x100mm), 0.8 mL/min, measuring at 210 nm, 250 nm and 265 nm) to assess the conversion.

For compounds with an amine functionality with no detectable fluorophore, FMOc derivatisation was used to enable their detection. Typically, 100  $\mu$ L of a maximum of 10 mM of the desired compound were mixed with 200  $\mu$ L of 100 mM borate buffer pH 9. To the mix, 400  $\mu$ L of 15 mM FMOc diluted in MeCN was added. The sample was properly mixed and left for at least 10 minutes before mixing 200  $\mu$ L of it with 400  $\mu$ L of MeCN and 400  $\mu$ L of 0.1% HCl. The retention times of the different compounds is detailed in Table 3.6.

**Table 3.6.** Retention times of the different compounds used. Compounds in table A were run using a gradient method from 5:95 to 95:5 (H<sub>2</sub>O:MeCN 0.1%TFA) over 4 minutes with a flow rate of 0.8 mL/min. Compounds in table B instead, were run using a gradient method from 40:60 to 95:5 (H<sub>2</sub>O:MeCN 0.1%TFA) over 4 minutes with a flow rate of 0.8 mL/min.

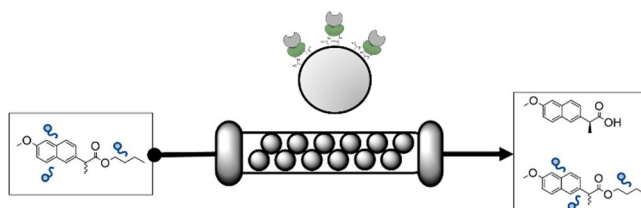
A.		B.	
Compound	Retention time (min)	Compound	Retention time (min)
$\alpha$ -methyl benzyl acetic acid butyl ester	5.47	Alanine-FMOc	1.58
$\alpha$ -methyl benzyl acetic acid	3.98	Glycine-FMOc	1.21
Flurbiprofen butyl ester	5.98	Pipecolate-FMOc	3.15
Flurbiprofen acid	4.86	Proline-FMOc	1.98
Ibuprofen butyl ester	6.22	Lysine-FMOc	4.11
Ibuprofen acid	5.05	Lysine ethyl ester – FMOc	4.02
Naproxen butyl ester	5.74	Ornithine-FMOc	4.00
Naproxen acid	4.52	Cyclohexylamine-FMOc	4.13
Benzaldehyde	3.60	Serinol-FMOc	0.78
Benzylamine	1.06		
Vanillin	3.09		
Cinnamaldehyde	4.14		
Cinnamyl amine	3.12		
S-methylbenzylamine	2.11		
Acetophenone	3.85		



### 3.5. Bibliography

1. R. H. Vreeland, C. D. Litchfield, E. L. Martin, and E. Elliot, Halomonas elongata, a New Genus and Species of Extremely Salt-Tolerant Bacteria, *International Journal of Systematic Bacteriology.*, vol. 30, no. 2, pp. 485–495, 1980. <https://doi.org/10.1099/00207713-30-2-485>
2. M. Heydari, T. Ohshima, and N. Nunoura-kominato, Highly Stable L-Lysine 6-Dehydrogenase from the Thermophile Geobacillus stearothermophilus Isolated from a Japanese Hot Spring : Characterization , Gene Cloning and Sequencing , and Expression, *Applied and Environmental Microbiology* vol. 70, no. 2, pp. 937–942, 2004. <https://doi.org/10.1128/AEM.70.2.937.942.2004>
3. P. J. Kersey *et al.*, Ensembl Genomes 2018: An integrated omics infrastructure for non-vertebrate species, *Nucleic Acids Research*, vol. 46, no. D1, pp. D802–D808, 2018. <https://doi.org/10.1093/nar/gkx1011>
4. E. Gasteiger *et al.*, *The Proteomics Protocols Handbook*. Totowa, NJ: Humana Press, 2005.
5. U. K. Laemmli, Cleavage of structural proteins during the assembly of the head of bacteriophage T4, *Nature*, vol. 227, no. 5259, pp. 680–5, Aug. 1970. <https://doi.org/10.1038/227680a0>
6. C. S. Hanes, Studies on plant amylases: The effect of starch concentration upon the velocity of hydrolysis by the amylase of germinated barley, *The Biochemical Journal*, vol. 26, no. 5, pp. 1406–21, 1932. <https://doi.org/10.1042/bj0261406>
7. C. Mateo *et al.*, Glyoxyl agarose: A fully inert and hydrophilic support for immobilization and high stabilization of proteins, *Enzyme and Microbial Technology*, vol. 39, no. 2, pp. 274–280, 2006. <https://doi.org/10.1016/j.enzmictec.2005.10.014>

## Chapter 4: Esterase immobilisation and flow assisted bioconversion of water insoluble substrates



#### 4.1. Introduction

As discussed in the introduction, esterases and lipases are among the most used enzymes in nutraceutical industry [1–3]. They can be used in a wide range of applications, from biopolymeric synthesis to the production of biodiesel or fine chemicals. In the latter case, most of the molecules tend to be chiral and so, taking advantage of the capacity of esterases and lipases to stereo selectively hydrolyse or form ester molecules, they can be applied for the synthesis of a plethora of pharmaceutical building blocks [4].

An important application of this type of hydrolases is the preparation of non-steroidal anti-inflammatory drugs (NSAIDs), one of the most broadly used chemicals in pharmaceuticals [5–7]. NSAIDs are a group of propionic acid derivatives which inhibit the cyclooxygenase (COX), responsible of the inflammatory response. Although normally commercialized as racemic mixtures, the specific biological effect of these drugs is closely linked to their chirality [8–10]. Therefore, their preparation as enantiopure compounds has been studied in the last years. The most common strategy applying hydrolases, consists on the deracemization by esterification in organic media. This strategy relies on lipases high stability in these conditions and it avoids the water solubility issues of NSAIDs and its derivatives [11–12]. This approach, has been applied combining an immobilized carboxylesterase and a flow system for the preparation of flurbiprofen in toluene, using a packed-bed reactor filled with Novozym435® (immobilised lipase B from *Candida Antarctica* (CALB)) [13]. However, the use of organic solvent displays some drawbacks for application at industrial scale, as conversion rates of these reactions are negatively affected by the presence of water. Another problem when the process is performed on larger scale is the reusability of the biocatalyst. For monomeric enzymes, such as esterases and lipases, covalent immobilisation remains a problematic issue. When immobilised onto a support, covalently or by adsorption, monomeric enzymes, such as esterases, tend to form a superficial layer, hampering the substrate diffusion and the mass transfer [14–15]. Therefore, the

obtained biocatalysts normally exhibit low recovered activity and high ratios of enzyme per resin are needed, lowering the economic benefits of their industrial application. The previously mentioned Novozym435®, is a preparation of immobilised CALB by adsorption. It is commercially available, and the loading of the biocatalyst has a ratio of 82 mg of enzyme/g of resin, yielding only a 7.5% recovered activity. Therefore, only a few examples are available on the bio-catalysed hydrolysis mediated by these enzymes in a continuous flow reactor due to the two main reasons discussed: (1) the challenging covalent-immobilization of esterases and (2) the low water solubility of NSAIDs acid and its esters derivatives in water.

In this chapter, to further expand the enzymatic toolbox of the Paradisi group, a new esterase from the moderate halophile *Halomonas elongata* was cloned and characterised. The capacity of the newly cloned esterase, compared to two other esterases from mesophilic counterparts (BS2m from *Bacillus subtilis* and BCE from *Bacillus coagulans*), to cleave NSAIDs was studied. Following the investigation of the performance in batch set ups, and comparing their structural characteristics, BS2m appeared to be the best candidate for its high activity and enantioselectivity for naproxen butyl ester. BS2m was immobilised with a new methodology and the resulting biocatalyst, used as a packed-bed reactor for the flow-assisted deracemization of naproxen butyl ester in a buffered water system and mild conditions.

The work presented in this chapter is my exclusive contribution unless otherwise stated and it has been included in two publications:

- M. Planchestainer, M. Contente, D. Roura Padrosa, and F. Paradisi, "Genetically Fused T4L Acts as a Shield in Covalent Enzyme Immobilisation Enhancing the Rescued Activity," *Catalysts*, vol. 8, no. 1, p. 40, Jan. 2018.
- D. Roura Padrosa, V. De Vitis, M. Contente, F. Molinari, and F. Paradisi, "Overcoming Water Insolubility in Flow: Enantioselective

Hydrolysis of Naproxen Ester,” *Catalysts*, vol. 9, no. 3, p. 232, 2019.

#### 4.2. HeE cloning and characterisation

helo\_2889 was identified in the genome of *Halomonas elongata* DSM 258. The hypothetical protein is classified as carboxylesterase and shared 51% similarity to EST55 [16], a carboxylesterase from *Geobacillus stearothermophilus* and 48% with BSE, a homologue from *Bacillus subtilis* [17]. Firstly, a model of the predicted protein, named HeE, was made using Phyre2 server [18]. The homology model compared to EST55 (PDB: 2OGS) and BSE (PDB: 1QE3) can be seen in Figure 4.1. The modelled structure for HeE had the typical  $\alpha/\beta$  hydrolase fold and the characteristic catalytic triad for hydrolases, formed by the catalytic serine, a histidine and an acid residue (Asp or Glu) [19]. In the case of HeE, the catalytic triad is formed by Ser213, Glu327 and His413. Its active site does not seem to be covered by any loop or helix, suggesting that HeE does not have a lipase-like fold, as it lacks the lid structure typical of this group of enzymes.

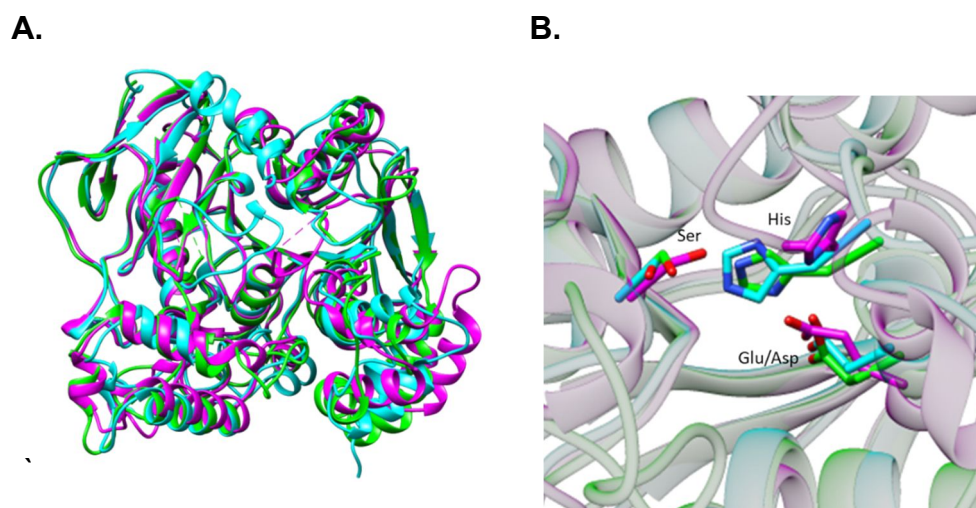


**Figure 4.1.** **A.** Modelled structure for HeE (light blue) compared to EST55 (green) and BSE (pink). **B.** Detail of the active site for the three enzymes.

With this information, and focussing on the discovery of industrially relevant enzymes, helo\_2889 gene was amplified and cloned into a pRSETB based vector for the expression of the new protein, named HeE.

Expression was successful and the enzyme was obtained in high purity with yields of 10-12 mg/L of culture (Figure 4.2).

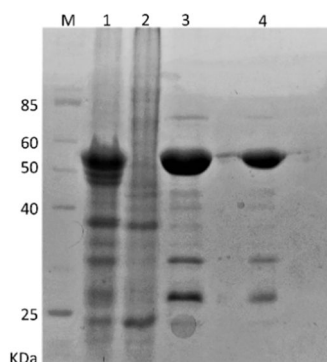


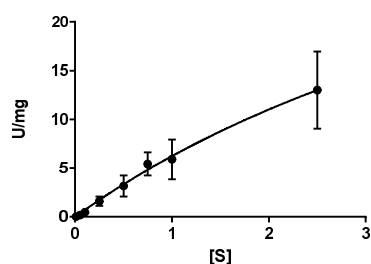
**Figure 4.2.** SDS-page gel of the purification of HeE. M. Molecular mass markers; 1. Whole cell fraction after expression; 2. Insoluble fraction; 3. Soluble fraction; 4. Pure enzyme.

After purification was achieved, the enzyme was characterised to better understand its resistance to different factors as well as its substrate scope.

Initially, short chain *p*-nitrophenol esters were assessed as substrate. Hydrolysis of this substrates is easily detectable using a UV-Vis spectrophotometer since the product of the hydrolysis, *p*-nitrophenol, has a maximum of absorbance at 420 nm, with an extinction coefficient of 15000 M<sup>-1</sup> cm<sup>-1</sup>. For the characterisation of the newly cloned carboxylesterase, the standard assay was performed with 0.5 mM *para*-nitrophenyl acetate at pH 8.

Firstly, kinetic characterisation of HeE was performed with both *p*-nitrophenyl acetate (*p*NPA) and *p*-nitrophenyl butyrate (*p*NPB). Due to instrument limitations, activity of the enzyme could not be assessed at concentrations higher than 2.5 mM and therefore, the data could not be fitted successfully to the Michaelis-Menten equation. As an alternative, both  $K_M$  and  $k_{cat}$  were assessed using the Hanes-Woolf plot [20–21] (Table 4.1). As any approximation, this method is prone to error since both variables are dependent on the substrate concentration but unlike the Lineweaver-Burk plot [22], it does not overestimate the error at low concentrations therefore giving a better indication of the parameters with the data obtained.

**Table 4.1.** Kinetic parameters calculated for HeE for both pNPA and pNPB. Values were estimated using the Lineweaver-Burk derivative. In the left, Michaelis-Menten fitting of the experimental data for HeE. Values correspond to the average of 3 replicates.



HeE		
Substrate	pNPA	pNPB
$K_M$ (mM)	$2.21 \pm 0.25$	$2.05 \pm 0.47$
$k_{cat}$ (s <sup>-1</sup> )	$15.53 \pm 0.89$	$29.53 \pm 3.40$

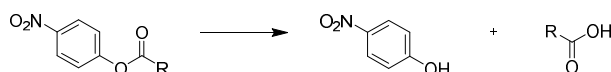
HeE shows similar affinity for both pNPA and pNPB, with the calculated  $K_M$  virtually identical. The turnover number ( $k_{cat}$ ), though, is almost twice for pNPB than for pNPA indicating a higher efficiency hydrolysing the longer chain ester.

To investigate HeE substrate scope, the activity of HeE against several different *p*-nitrophenyl esters was tested. Qian, L. *et al.* published in 2011 an array of *p*-nitrophenyl esters for the characterisation of lipolytic enzymes [23]. In their work, four different enzymes (CALB and 3 new enzymes obtained by genome mining) with the capacity to hydrolyse esters were evaluated against 17 different substrates. The substrate panel was formed by linear aliphatic esters, branched aliphatic esters, cycloalkyl esters and aromatic esters. Likewise, HeE activity was tested with at least, a representative molecule of each group. To that purpose, the different *p*-nitrophenol ester derivatives were prepared chemically by esterification and the activity against these substrates calculated at the same concentration as the standard activity assay. The results are shown in Table 4.2.

HeE shows a higher activity for the butyrate substrate (2) compared to the acetate version (1), with a two-fold increase of the specific activity. According to its classification as a true esterase and the absence of a lid in its structure, HeE shows a much lower activity with longer chain esters. Less than half of the activity is detected with *p*-nitrophenyl octanoate (6) and the activity is lower the longer the substituent is; with only 7.2% of the activity detected with the dodecanoate ester (7) and no activity with

the tetradecanoate substituent (8). This same trend is also observed with branched linear substrates, such as the pivalate (5). It is well known that while lipases prefer substrates with higher hydrophobicity, and therefore longer carbon chains, esterases work better when the substrates are water soluble short chain esters [24].

**Table 4.2.** Activity of HeEst against different *p*-nitrophenyl ester derivatives, following the general reaction shown. All substrates were used at 1 mM final concentration. All other conditions were kept as defined from the standard activity assay.



Entry	Name	R group	HeEst (U/mg)
1	4-nitrophenyl acetate	-CH <sub>3</sub>	3.60 ± 0.37
2	4-nitrophenyl butyrate		6.00 ± 0.83
3	4-nitrophenyl benzoate		4.33 ± 0.12
4	4-nitrophenyl cyclohexane carboxylate		5.23 ± 0.93
5	4-nitrophenyl pivalate		0.36 ± 0.04
6	4-nitrophenyl octanoate	(CH <sub>2</sub> ) <sub>6</sub> CH <sub>3</sub>	1.56 ± 0.14
7	4-nitrophenyl dodecanoate	(CH <sub>2</sub> ) <sub>10</sub> CH <sub>3</sub>	0.26 ± 0.02
8	4-nitrophenyl tetradecanoate	(CH <sub>2</sub> ) <sub>12</sub> H <sub>3</sub>	0

More interestingly, HeE shows a comparable activity when the acetate is replaced by a benzylic group (3). A similar trend is observed when the acidic part is occupied by cyclohexane (4). From these observations, it seems that HeE can accommodate bulky substrates in its active site, when the acidic chain is formed with either aromatic or cyclic structures, differently from the low activities detected with the bulky linear substituents such as the *p*-nitrophenyl pivalate or the *p*-nitrophenyl octanoate.

The effect of temperature on the activity and stability of HeE was then assessed (Figure 4.3). The halo-adapted enzyme rapidly loses activity at higher temperatures, with less than half of the activity at 55°C, and the same trend is observed in the stability test, where HeE does not



resist temperatures higher than 37°C, with a loss of 60% of its activity at 40°C after 4h. In milder conditions such as 25 or 37°C, it is significantly more stable with no apparent loss of activity after 24h.

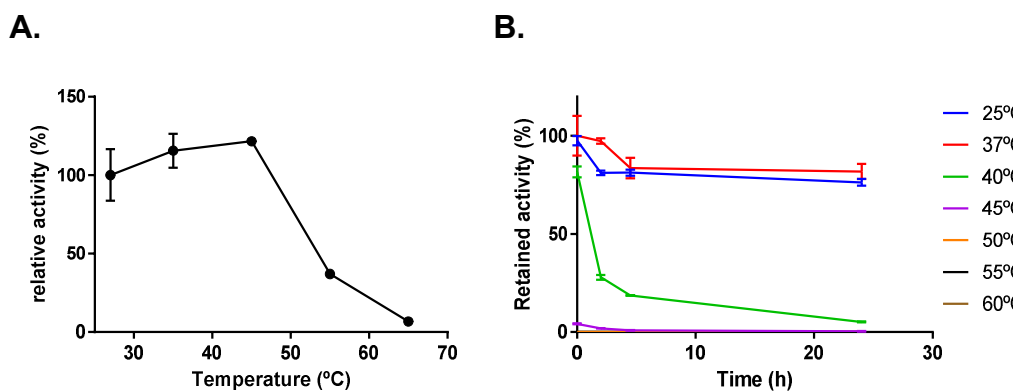


**Figure 4.3.** Temperature effect. **A.** Effect of the temperature on the activity of HeE. All reaction components were incubated at the desired temperature but the protein. The activity was tested using the standard activity assay. **B.** Stability at different temperatures of HeE. 0.1 mg/mL of the protein were incubated at the desired temperature. The activity was tested using the standard activity assay at different time points.

As for the pH (Figure 4.4), HeE showed a good stability from pH 7.5 to pH 9 and surprisingly, between pH 10 and 12, 40% of the activity was still detectable after 48h incubation. At acidic pH on the other hand, the retained activity was much lower. Therefore, the optimal pH for the storage and reaction was set as pH 8.

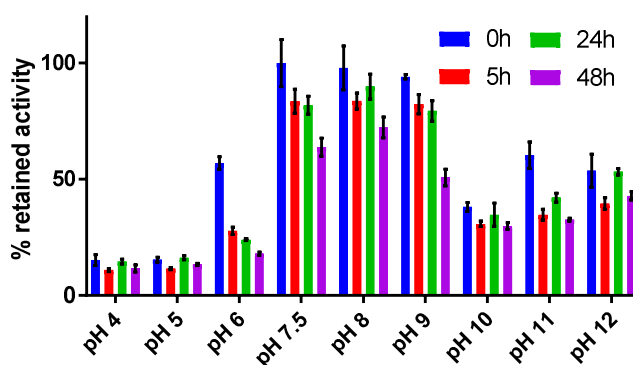


**Figure 4.4.** pH effect on the stability of HeE. The enzyme was incubated at 4°C for 48h and the activity determined at different time points using the standard activity assay. The values correspond to the average of 3 replicates.

One of the most interesting features of the enzymes originating from *H. elongata* is their capacity to resist to organic solvents, and this relates to the strategy this bacterium uses to counteract the high osmotic

pressure; the accumulation of compatible solutes in the cytoplasm [25–26]. This behaviour was observed for the transaminase cloned from the same organism [27]. The resistance of HeE to organic co-solvents up to 20% (v/v) is shown in Figure 4.5.

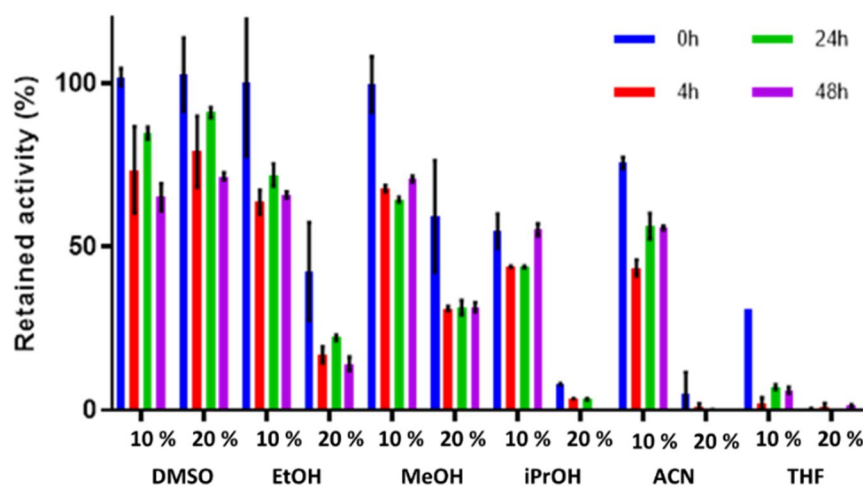


**Figure 4.5.** Cosolvent effect on the stability of HeE. 0.1 mg/mL of protein were incubated at 4°C for 48h in the presence of 10% or 20% (v/v) of the desired cosolvent. Activity was tested at different time points using the standard activity assay. The values correspond to the average of 3 replicates.

In general, a decrease of activity was observed with all the cosolvents used, but HeE shows good resistance to DMSO and other simple alcohols tested. Isopropanol (iPrOH), acetonitrile and tetrahydrofuran, on the other hand, have a much harsher effect at both 10 and 20%. The mild resistance to the organic cosolvents exhibited, indicates DMSO and alcohols as the best choice to use with HeE.

HeE activity and stability in high ionic strength environments was also tested. To have a better idea of its performance, it was compared with a mesophilic esterase from *Bacillus subtilis*, BS2m. This esterase was cloned by Schmidt *et al.*, and kindly provided by the Bornscheuer group [28]. HeE has a 51% similarity to BS2m. Both activity (Figure 4.6) and stability (Figure 4.7) were evaluated.

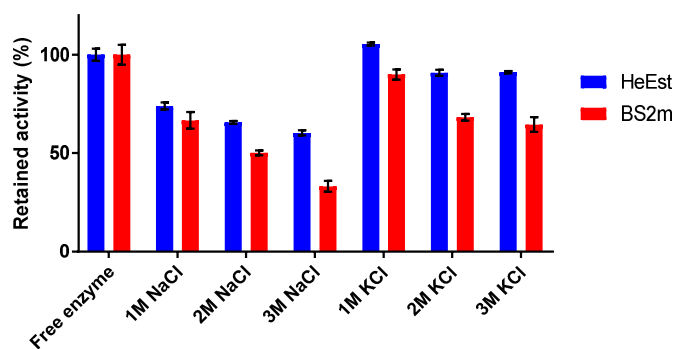
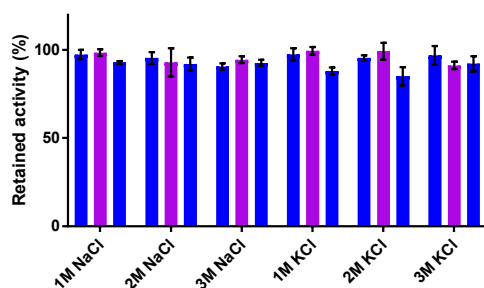


**Figure 4.6.** Salt concentration effect on the activity of HeE and BS2. Activity was determined with the standard activity assay with presence of the indicated concentration of salts.

**A.**



**B.**

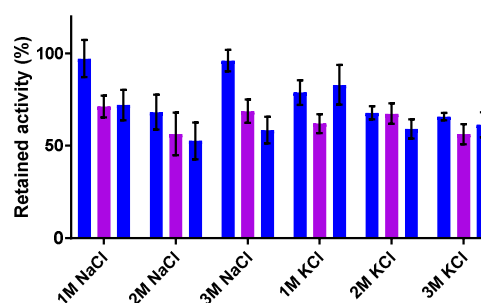


**Figure 4.7.** Salt concentration effect on the stability of HeE (A) and BS2m (B). 0.1 mg/mL of protein were incubated with the desired concentration of salt and the activity tested at different time points.

As expected, HeE shows a better behaviour in both cases compared to BS2m. The difference in activity is more obvious at the highest ionic strength tested (3M NaCl or KCl) where HeE exhibits a 30% higher retained activity. Moreover, HeE shows no loss of activity after 48h incubation at any of the tested concentrations while BS2m shows only 75% at 1M NaCl after 24h and only 52% of the activity after 48h with 3M NaCl.

In general, HeE shows good resistance to both organic solvents at low concentration and in environments with high ionic strength, confirming the trend observed previously with other halophilic enzymes. Moreover, it shows a surprising resistance at basic pHs compared to BSE (*Bacillus subtilis* esterase) with a more similar behaviour to Lip2, an organic solvent-resistant esterase from *Monascus purpureus* [29–30]. On the contrary, HeE is unstable at temperatures superior than 37°C. More

interestingly, HeE is capable of hydrolysing aromatic and cyclic bulky esters, feature which can be exploited for the hydrolysis of industrially relevant molecules, such as NSAIDs.

### 4.3. Profen hydrolysis

Since HeE showed a good activity against substrates with bulky substituents, its capacity to hydrolyse esters of 3 different NSAIDs (ibuprofen, naproxen and flurbiprofen) was tested, and to assess its stereoselectivity, the enantiomeric excess (e.e.) of the hydrolysed product was also calculated. As a comparison, an esterase from Prof. Molinari group in the University of Milan, BCE, and BS2m were used. BCE is an esterase cloned from *Bacillus coagulans* [31] which showed better activity against ethyl ester and consequently its capacity to hydrolyse racemic NSAIDs esters was tested with the ethyl ester version while both HeE and BS2m were tested against butyl esters. It is also important to note that while the amount of enzyme in the biotransformation was the same for the three proteins (0.1 mg/mL), they displayed different activities: BS2m showed an activity of  $61 \pm 3$  U/mg, HeE of  $3.5 \pm 0.2$  U/mg and BCE had an activity of 0.03 U/mg against 0.5 mM pNPA. The results are shown in Table 4.3.

HeE, although it has lower activity compared to BS2m, is capable of hydrolysing both flurbiprofen and ibuprofen esters with good yields under 24h however, it does not display any stereospecificity. Curiously, HeE shows a lower conversion with naproxen butyl ester. This trend is also followed by BCE, which cleaves ibuprofen and flurbiprofen selectively for the (S)-enantiomer but with low molar conversions but when tested with naproxen, no conversion was detected at all. BS2m in contrast, can hydrolyse the three NSAIDs esters but only shows stereoselectivity for naproxen. Naproxen butyl ester is the least flexible and bulkier NSAID of the selected ones and the peculiarity of BS2m, capable of hydrolysing it opposed to HeE and BCE, was further investigated.

**Table 4.3.** Maximum molar conversion and enantiomeric excess of the batch biotransformations with all three enzymes and the substrates tested. A general scheme of the hydrolysis reaction is shown. For conversions < 5% e.e. could not be detected (n.d.). All enzymes were used at 0.1 mg/mL.

**1a.**

**1b.**

**1c.**

Substrate	BCE <sup>1</sup>		HeE <sup>2</sup>		BS2m <sup>2</sup>	
	Conversion	e.e.	Conversion	e.e.	Conversion	e.e.
<b>1a. Naproxen ester</b>	< 5%	n.d.	35%	<5%	55%	80% ( <i>R</i> )
<b>1b. Ibuprofen ester</b>	22%	>97% ( <i>S</i> )	>95%	<5%	>95%	<5%
<b>1c. Flurbiprofen ester</b>	36%	>97% ( <i>S</i> )	88%	<5	81%	<5%

<sup>1</sup> Ethyl ester substrates were used. <sup>2</sup> Butyl ester substrates were used.

To explain the different capability of accepting highly bulky substrates, the architecture of the active site and surrounding of the three esterases was analysed. For HeE the homology model created using Phyre2 was used [18] while the crystal structure for BS2m (PDB: 1C7J) and the open conformation of BCE was retrieved from the Protein Data Bank (PDB: 5O7G).

The differences in the conversion could not be explained by the architecture of the active site. The three studied esterases are almost identical (Figure 4.8) with the only difference being an Asp instead of the Glu in BCE compared to both BS2m and HeE in the homologous position. The surrounding of the active site or other typical structures such as the oxyanion hole were also identically positioned, therefore the differences can be hardly explained by these factors. Moreover, docking of the three NSAID's esters in the active site of the three enzymes did not explain the difference as all three substrates fitted in a catalytically active conformation in the three proteins active site.

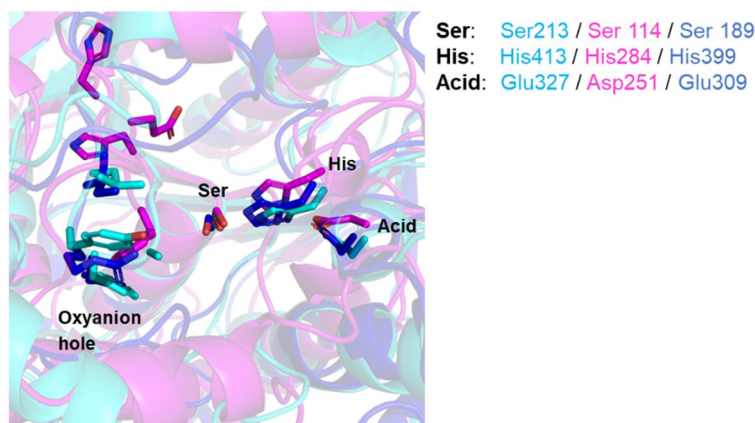


**Figure 4.8.** Detail of the catalytic triad for the three esterases studied: BCE (pink), HeE (dark blue) and BS2m (light blue).

The tunnels leading to the active site calculated using Caver in the static structure [32, 33], however, were more revealing (Figure 4.9). These tunnels were modelled from the protein surface to the catalytic serine, to better understand how the substrate would enter the active site. From the different options calculated by the program, the shortest and with the least restrictive bottleneck was chosen for all esterases. Correlating with their capability to cleave naproxen butyl ester, the most rigid and bulky of the NSAIDs tested, BS2m showed the least restrictive tunnel with no apparent bottleneck and a length of only 2 Å. As it can be seen in Figure 4.9B the tunnel is located very superficially on the protein, so the substrate can easily access the active site. For HeE and BCE, the tunnel was three and five times longer respectively, and both showed a bottleneck of less than 2 Å. Moreover, the tunnels for BCE and HeE do not appear to be straight, further hindering the movement of such a rigid substrate into the active site. Furthermore, the surroundings of the catalytic pocket can also be important for the substrate recognitions and its shuttling into the active site. BCE while the tunnel is formed by 60% hydrophobic chain amino acids which could facilitate the interaction with the naproxen ester, Phe38 and Trp190 create a very restrictive bottleneck, of only 1.29 Å. These two residues could act as a gate, characteristic previously seen in acetylcholine esterases [34]. In HeE, on the other hand, the entrance is surrounded by charged amino acids (Arg132, Asp288 and Glu327) and is less constricted with no obvious bottleneck. The different nature of the tunnel of this two esterases

suggests that the main factor affecting their catalytic efficiency towards naproxen esters relies on the length and bottleneck of the active site, rather to hydrophobic or hydrophilic interactions with the substrate when this one is entering the catalytic pocket. All together, these differences could explain the poor activity of HeE and BCE towards bulky, rigid substrates such as naproxen esters. HeE showed some hydrolytic activity as its tunnel is more flexible and prone to shuttle the substrate to the active site more easily than in the case of BCE. From these results, BS2m was chosen as the best candidate to further exploit its unique characteristics for naproxen deracemization.

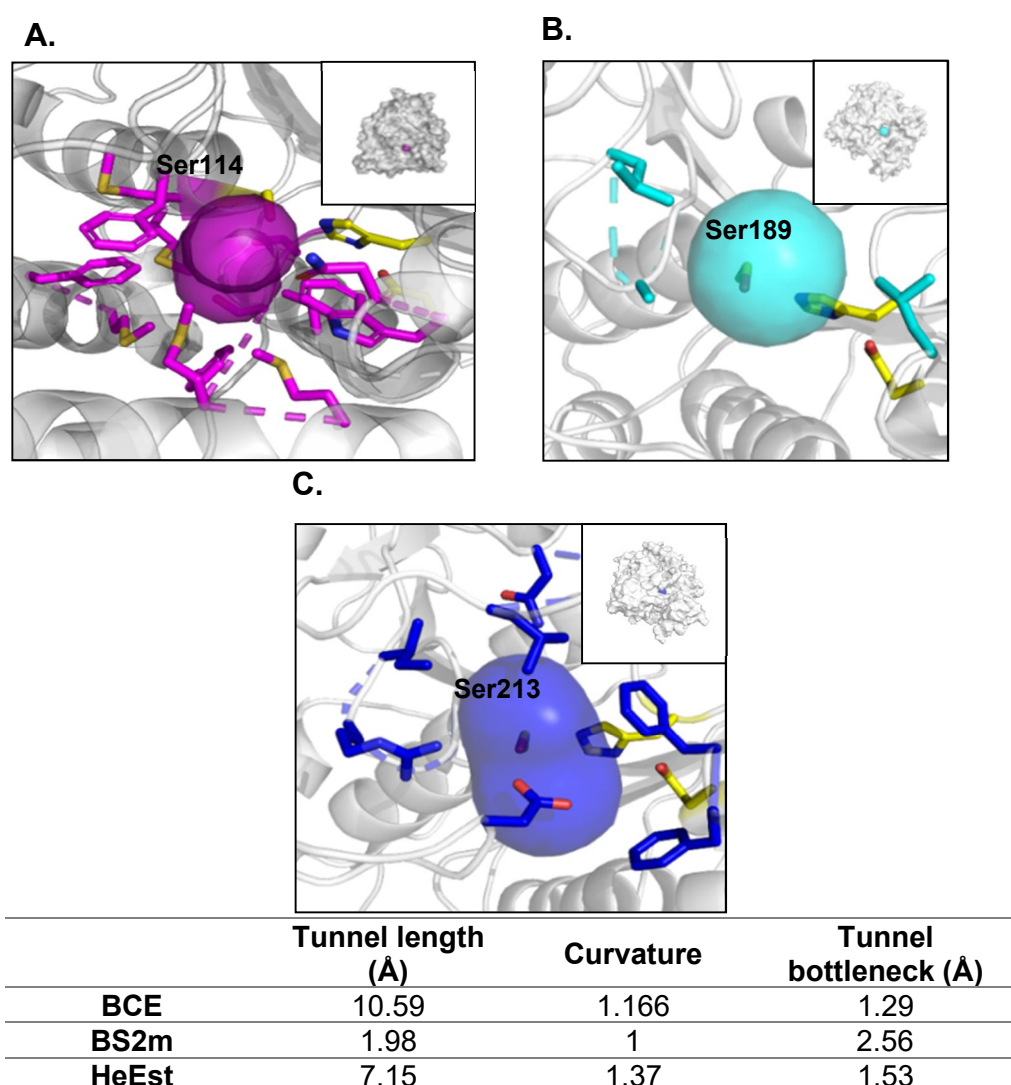


**Figure 4.9.** The catalytic triad is showed in yellow and the residues participating in the tunnel in pink for BCE (**A**), light blue for BS2m (**B**) and dark blue for HeE (**C**). The catalytic serine is labelled in all structures. The length, curvature and diameter of the bottleneck are shown. Curvature is calculated by dividing the minimum distance to the catalytic serine by the total distance of the tunnel.

#### 4.4. Immobilisation of BS2m

To enhance its reusability, stability and to allow its application as a packed-bed reactor in a flow system, BS2m was immobilised in a polymethacrylate resin functionalised with epoxy groups (for more details refer to Table 3.5 in Materials and Methods). Polymethacrylate resins are ideal for their use in flow reactors, as they have excellent resistance to temperature, pH and they are stable in mixed solvents containing organic solvents [35]. BS2m immobilisation was tried firstly using an epoxy derivatised resin, EC-EP/S from Resindion S.R.L. at different loadings (Figure 4.10) with a directional immobilisation technique through the coordination of the His-tag to cobalt bound to the resin [36]. The directionality of this method favours the correct positioning of the protein as the N-terminus His-tag is positioned on the other face of the active site. With this technique, and with the different loadings tested, less than 1% of the activity was recovered in all cases.

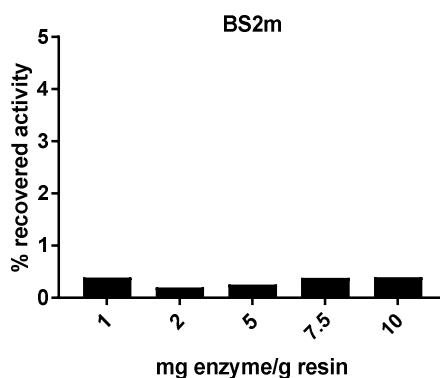


**Figure 4.10.** Percentage of recovered activity calculated for BS2m upon immobilisation relative to the activity of the free enzyme (62 U/mg).

As in the process of immobilisation a metal is used to direct the immobilisation, the effect of different metals to the activity of BS2m was tested (Figure 4.11). The metal used in the initial immobilisation is cobalt and indeed it seems to be the least toxic for the esterase. Both copper and nickel greatly affect the activity, but this is recovered following incubation with EDTA, following a similar protocol used during immobilisation. Therefore, the metal was excluded as a causing agent for the low recovered activity.



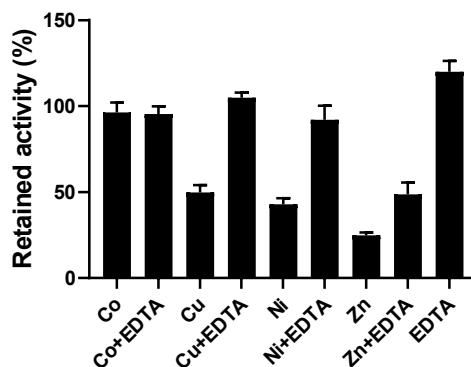


**Figure 4.11.** Effect of different metals on the activity of BS2m. Samples of 0.1 mg/mL of the protein were incubated for 2h with the metal solution and activity tested using the standard activity assay. 100 mM EDTA was added and the sample incubated for 10 minutes before testing the activity again (metal + EDTA samples).

Also, the directionality of the immobilisation could also provoke to protein active site to be facing the resin therefore affecting the expressed activity. This eventuality though, is not likely as the His-tag of BS2m is located in the other face of the protein in respect to the active site (Figure 4.12).

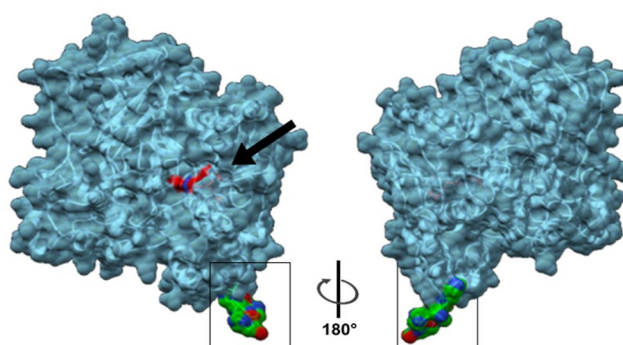


**Figure 4.12.** 3D surface representation of BS2m where the catalytic site is shown in red and with an arrow and the his-tagged in green inside the box.

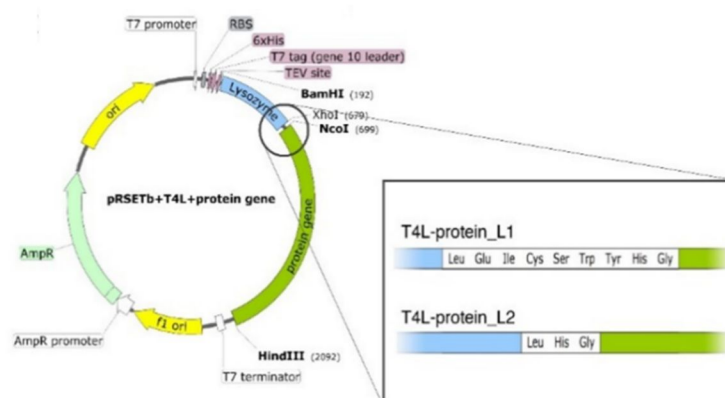
The problem of low recovered activity observed after covalent immobilisation of esterases has been previously reported. For example, the immobilisation of a thermophilic esterase from *Archeoglobus fulgidus* immobilised on the same resin used for BS2m, EC-EP showed only a 6% of the activity with 72 mg/g of resin [14]. Immobilisation of the pig liver esterase in hollow fibres with epoxides as terminal groups, reported by Sousa, H.A., *et al.*, led to only 3% recovered activity after 24h of immobilisation and by lowering the time of immobilisation a 26.5% was achieved (15). In our protocols, the immobilisation is routinely performed

for 4h but decreasing the time of immobilization did not have any influence in the recovered activity. This behaviour is not limited to esterases. This effect has been seen previously with monomeric enzymes with high rate of immobilisation. Although there are successful examples of immobilisation of esterases as cross-linked aggregates (CLEAs) or by adsorption, with high recovered activities [37–38] both systems lack the robustness typical of covalent immobilisation and therefore, the development of a new strategy for the covalent immobilisation of esterases was investigated.

#### 4.4.1. T4L strategy

To that end, a new strategy developed in the Paradisi group was adopted for the immobilisation of BS2m. This strategy consists in the engineering of a catalytically inactive variant of T4 lysozyme to create a fusion protein with the protein of interest, so that the T4L is cloned between the N-terminal His-tag and the target enzyme. The fusion protein is then immobilised following the same protocol as before, with the difference that the enzyme of interest is facing the bulk of the reaction and does not directly interact contact with the support (Figure 4.13). Moreover, the effect of the linker between the two enzymatic units was also assessed. The length of the linker can affect greatly the capacity of the fusion protein to fold correctly [39] and therefore two different linkers were evaluated: T4L1 composed of nine amino acids and T4L2 variant with only three amino acids between both proteins [40].

A.



**B.**



**Figure 4.13.** Representation of the T4L immobilisation strategy. **A.** Graphical representation of the plasmid construct for the spaced immobilisation. The two linkers are shown **B.** The initial strategy applied where the esterase is directly immobilised on the beads (left) whereas the T4L strategy is (right), where the esterase, BS2m, is shown in grey and the T4 lysozyme is shown in green.

Both variants, named BS2mT4L1 and BS2mT4L2, were successfully created and expressed following the same protocol of BS2m. Results of the immobilisation are shown in Table 4.4. In this case, another epoxy derivatised resin with bigger pores was also tested (EC403-S).

**Table 4.4.** Comparison of specific activities and expression levels of the original *Bacillus subtilis* esterase (BS2m) and the two chimeric proteins in the free enzyme form. Specific activities of the resin following immobilisation of enzymes (5 mg enzyme/g resin), and percentage of residual activity after immobilisation with respect to the free protein.

	Free enzyme		Sepabeads EC-EP/S (pore Ø 10-20 nm)		Sepabeads EP403/S (pore Ø 20-40 nm)	
	Specific activity (U/mg)	Expression (mg/L)	Specific activity (U/g)	Rescued activity (%)	Specific activity (U/g)	Rescued activity (%)
<b>BS2m</b>	61 ± 4	30	1.3 ± 0.1	0.4 ± 0.1	1.6 ± 0.4	0.5 ± 0.1
<b>BS2mT4L1</b>	31 ± 3	15	5.5 ± 0.8	3.6 ± 0.5	6.2 ± 0.8	3.9 ± 0.6
<b>BS2mT4L2</b>	35 ± 2	13	2.9 ± 0.6	1.7 ± 0.4	3.7 ± 0.4	2.1 ± 0.3

Although, both the activity and the level of expression decreased to almost half of the ones observed for BS2m, the best immobilised preparation of the biocatalyst was obtained with the BS2mT4L1 variant and had an activity of 6.2 U/g of resin, translating in an increase of the recovered activity by almost 10-fold.

Following these initial results, in an attempt to further optimise the biocatalyst, the loading of BS2mT4L1 was increased to 7.5 mg/g of resin. As seen in Table 4.5, the activity of the biocatalyst increased by almost

2-fold compared to the 5 mg/g of resin. In addition, as in the initial screening the use of a resin with larger pores translated into higher activities, two resins with larger pores but different matrix were tested: EP400/SS, a polymethacrylate based resin, and agarose CL6B with epoxide groups (Ag-ep) [41]. Immobilisation on the new supports resulted in higher recovered activity with almost twice of the specific activity and almost 10% of recovered activity, a 20-fold increase compared to the initial catalyst (EC-EP/S-BS2mT4L1).

**Table 4.5.** Comparison of specific activities and recovered activity of the BS2mT4L1 Specific activities of the resin following immobilisation of enzymes (7.5 mg enzyme/g resin), and percentage of residual activity after immobilisation (4 h, room temperature, in 50 mM phosphate buffer pH 8) with respect to the free protein.

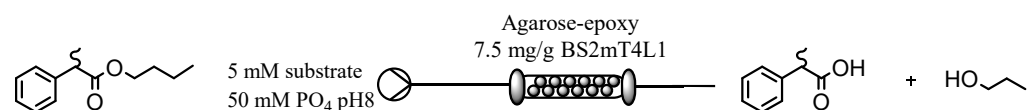
Support	Specific activity (U/g)	Rescued activity (%)
EC-403/S (pore Ø 20-40 nm)	11 ± 2	4.7 ± 0.2
EP400/SS (pore Ø 40-60 nm)	21 ± 3	9.0 ± 1.3
Ag-ep (pore Ø 24-70 nm)	22.1 ± 5	9.5 ± 2.1

#### 4.5. Flow deracemization of naproxen butyl ester

Once the biocatalyst was optimised, the flow assisted bioconversion of naproxen butyl ester in a buffered system was attempted. Despite the optimised immobilisation and increased residence times, the polymethacrylate resins did not produce any conversion of naproxen butyl ester. As naproxen butyl ester is a highly insoluble molecule [12] its implementation in flow chemistry is severely limited. Insoluble substrates can in fact cause blockages of the tubing and have poor contact time with the heterogenous biocatalyst, resulting in low mass transfer and low bioconversion [42]. To better understand the underlying limitations, propyl-2-phenylpropanoate (P2P) was tested as a model substrate. P2P has a higher solubility than naproxen butyl ester at low molarities (up to 5 mM), and therefore, its use in flow is more favourable. Moreover, cleavage of this substrate was faster than the naproxen butyl ester, allowing for shorter residence times. When this reaction was tested with both EC403-BS2mT4L1 and EP400-BS2mT4L1 in flow, very little or no conversion was observed. Different organic cosolvents and an inlet of toluene was evaluated, but it decreased

massively the activity of the biocatalyst and had no effect on the molar conversion. On the contrary, when Ag-ep-BS2mT4L1 was used with a 15 minutes residence time, 35% conversion was detected at the 1 mM scale (Table 4.6). To further improve the substrate solubility and therefore its availability for the enzyme, a surfactant, Triton® X-100 was added to the solution. Triton® X-100 has been previously proven to enhance the activity of esterases against NSAIDs esters [43]. It is also important to note that the presence of the surfactant could have undesired effects on the enzyme, affecting both its activity and stability by promoting denaturation of the enzyme [44–45] so only 0.5% (v/v) of the surfactant was added. Remarkably, in our case, the addition of a surfactant, such as Triton® X-100 to further improve the solubility of the substrate led to a higher conversion, with over 90% of the substrate hydrolysed at 1 mM scale and 60% at 5 mM scale.

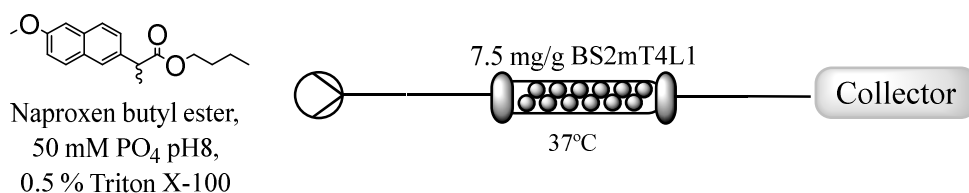
**Table 4.6.** Molar conversion for the flow-assisted biotransformation of P2P with Ag-ep/BS2mT4L1. A general scheme of the hydrolysis reaction is shown.



Substrate concentration (mM)	Residence time (minutes)	Molar conversion (%)
1 mM	15	35%
1 mM (0.5% Triton X-100)	15	> 90%
5 mM (0.5% Triton X-100)	15	60 %

Following these promising results, the hydrolysis of naproxen butyl ester was tested in presence of 0.5% of Triton X-100®. As with propyl-2-phenylpropanoate, the presence of the surfactant at low concentration increased massively the solubility of the ester, being able to obtain a clear solution at 5 mM scale. Results of the flow assisted bioconversion are shown in Table 4.7.

**Table 4.7.** Flow assisted hydrolysis of naproxen butyl ester. The substrate was prepared in 50 mM phosphate buffer pH 8 with 5% DMSO and 0.5% of Triton® X-100. All reactions were performed at 37 °C with 1.2 g of Ag-ep-BS2mT4L1 with a loading of 7.5 mg/g of resin.



Substrate (mM)	Residence time (minutes)	Molar conversion (%)	e.e. (%)
1 mM	30	>99 %	< 5%
	30	>99 %	< 5%
5 mM	10	65 %	40 %
	6	24 %	80 %

With a 30 minutes retention time, both at 1 mM and 5 mM scale, complete conversion of the substrate was obtained while the batch biotransformation led to only 55% conversion over 48h. To exploit the enantioselectivity observed by BS2m for naproxen butyl ester the residence times was decreased to give less contact time between the enzyme and the less favourable enantiomer. As the residence time decreased, the molar conversion also decreased but the enantioselectivity improved significantly. With 6 minutes retention time at 5 mM concentration, 24% of the substrate was hydrolysed but 80% e.e, the maximum observed previously in the batch biotransformations, was obtained. After the biotransformation, the activity of the biocatalyst was checked to assess the effect of Triton® X-100 on its stability. Following a total working time of six hours at a constant flow rate of 0.117 mL/min, the biocatalyst still retained 57% of its activity.

In conclusion, in this chapter, the combination of a better immobilisation method for BS2m with the presence of surfactant to enhance the solubility of naproxen butyl ester enabled the

enantioselective hydrolysis of this highly insoluble substrate in a buffered system and mild conditions for the first time in flow. Moreover, the biocatalyst exhibits good stability under these conditions, with 57% of the initial activity after 6h of use.

## **4.6. Experimental procedures**

### **4.6.1. Synthesis of *p*-nitrophenyl esters**

To a solution of *p*-nitrophenol (200 mg, 1.45 mmol) in CH<sub>2</sub>Cl<sub>2</sub> (10 mL) the corresponding acyl chloride was added (2.175 mmol) together with NEt<sub>3</sub> (30 μL, 0.2175 mmol). The reaction was stirred overnight at room temperature. Progress was monitored by TLC and upon completion, 10 mL of water were added. The organic layer was washed with deionised H<sub>2</sub>O and dried over Na<sub>2</sub>SO<sub>4</sub> and the solvent removed under reduced pressure. The residue was purified on silica by flash chromatography or recrystallized from an appropriate solvent

### **4.6.2. Synthesis of NSAID butyl-ester**

A solution of racemic or enantiopure acid (250 mg, 1 eq), butanol (1.5 eq) and 4-dimethylaminopyridine (DMAP 0.12 eq) in CH<sub>2</sub>Cl<sub>2</sub> (10 mL), was cooled down and 1.1 eq of dicyclohexylcarbodiimide (DCC) were added. The reaction was monitored by TLC (9:1 *n*-hexane/ethyl acetate) and once completed, filtered and washed with 5 mL of CH<sub>2</sub>Cl<sub>2</sub>. The crude was then purified by flash chromatography (9:1 *n*-hexane/ethyl acetate). All synthesized molecules purity was checked by HPLC and NMR.

### **4.6.3. NMR characterization of butyl esters**

The purity of butyl esters was assessed by HPLC and <sup>1</sup>H NMR. <sup>1</sup>H NMR spectra were recorded with a Varian Mercury (300 MHz) spectrometer. Chemical shifts (δ) are expressed in ppm.

- 4-nitrophenyl benzoate: white solid; <sup>1</sup>H NMR (400MHz, CDCl<sub>3</sub>) δ: 7.38-7.47 (m, 2 H), 7.5-7.59 (m, 2 H), 7.65-7.74 (m, 2 H), 7.88-7.92 (m, 1H), 8.11-8.17 (m, 2H) ppm.
- 4-nitrophenyl cyclohexanoate: pale yellow oil. <sup>1</sup>H NMR (400MHz, CDCl<sub>3</sub>) δ: 8.28 (d, J=8.3 Hz, 2H), 7.25-7.30 (m, 2H), 2.62 (tt,

J=11.1, 2.6, 1H), 2.06-2.12 (m, 2H), 1.82-1.89 (m, 2H), 1.67-1.75 (m, 1H), 1.55-1.64 (m, 2H), 1.24-1.47 (m, 3H) ppm.

- 4-nitrophenyl 4-nitrobenzoate: white solid. <sup>1</sup>H NMR (400MHz, DMSO) δ: 8.39-8.46 (m, 2H), 8.31-8.39 (m, 2H), 8.16-8.22 (m, 2H), 8.09-8.14 (m, 2H) ppm.
- Naproxen butyl ester: white solid. <sup>1</sup>H NMR (400 MHz, CDCl<sub>3</sub>) δ: 7.77 – 7.65 (m, 3H), 7.43 (dd, *J* = 8.4, 1.9 Hz, 1H), 7.24 – 7.09 (m, 2H), 4.09 (td, *J* = 6.7, 2.3 Hz, 2H), 3.93 (s, 3H), 3.86 (q, *J* = 7.1 Hz, 1H), 1.68 – 1.51 (m, 7H), 0.88 (t, *J* = 7.3 Hz, 3H) ppm.
- Ibuprofen butyl ester: clear oil. <sup>1</sup>H NMR (400 MHz, CDCl<sub>3</sub>) δ: 7.0-7.3 (m, 4H), 4.1 (t, *J* = 6.6 Hz, 2H), 3.70 (q, *J* = 7.2 Hz, 1H), 2.46 (d, *J* = 7.2 Hz, 2H), 1.86 (dp, *J* = 13.6, 6.8 Hz, 1H), 1.65 – 1.46 (m, 7H), 0.96 – 0.82 (m, 9H) ppm.
- Flurbiprofen butyl ester: clear oil. <sup>1</sup>H NMR (400 MHz, CDCl<sub>3</sub>) δ: 7.56 (dt, *J* = 8.1, 1.5 Hz, 2H), 7.51 – 7.34 (m, 4H), 7.16 (s, 1H), 7.16 (dd, *J* = 20.7, 1.8 Hz, 1H), 4.13 (td, *J* = 6.7, 1.1 Hz, 2H), 3.77 (q, *J* = 7.2 Hz, 1H), 1.68 – 1.53 (m, 5H), 1.42 – 1.26 (m, 2H), 0.92 (t, *J* = 7.4 Hz, 3H) ppm.
- α-methyl benzene acetic acid butyl ester: clear oil. <sup>1</sup>H NMR (400 MHz, CDCl<sub>3</sub>) δ: 7.42 – 7.16 (m, 5H), 4.1 (m, 2H), 3.73 (q, *J* = 7.2 Hz, 1H), 1.79 – 1.56 (m, 5H), 1.53 – 1.31 (m, 2H), 0.9 (t, *J* = 7.3 Hz, 3H) ppm.

#### 4.6.4. HPLC analysis to determine the enantioselectivity

HPLC analyses were performed with a Jasco PU-980 pump equipped with a UV-vis detector Jasco UV-975 (wavelength: 254 nm). Column: Lux Amylose-2, 4.60 mm i.d. × 150 mm, Phenomenex. Eluent: acetonitrile: water: formic acid (1:1:0.2, v/v/v). Flow: 1.0 mL/min. Retention times: (*R*)-Flurbiprofen 4.3 min; (*S*)-Flurbiprofen 5.7 min; (*R*)-Flurbiprofen ethyl ester 28.2 min; (*S*)-Flurbiprofen ethyl ester 36.1 min; (*R*)-Flurbiprofen butyl ester 29.8 min; (*S*)-Flurbiprofen butyl ester 37.8 min. Column Lux Cellulose-3, 4.60 mm i.d. x 150 mm, Phenomenex.



Eluent *n*-hexane:2-propanol: formic acid (98:2:0.1, v/v/v). Flow: 1.0 mL/min. Retention times: (*R*)-Ibuprofen butyl ester 4.0 min; (*S*)-Ibuprofen butyl ester 4.6 min; (*R*)-Ibuprofen ethyl ester 4.3 min; (*S*)-Ibuprofen ethyl ester 5.0 min; (*R*)-Ibuprofen 7.9 min; (*S*)-Ibuprofen ethyl ester 8.7 min. Column Lux Cellulose-1, 4.60 mm i.d. x 150 mm, Phenomenex. Eluent *n*-hexane:2-propanol: formic acid (92:8:0.1, v/v/v). Flow: 1.0 mL/min. Retention times: (*R*)-Naproxen butyl ester 5.0 min; (*S*)-Naproxen butyl ester 6.1 min; (*R*)-Naproxen ethyl ester 5.6 min; (*S*)-Naproxen ethyl ester 6.5 min; (*R*)-Naproxen 10.5 min; (*S*)-Naproxen 11.2 min.

#### **4.6.5. Computational analysis of tunnels**

The analysis of the tunnel leading to the catalytic site of the different esterases was performed using CAVER 3.0 plugin for Pymol [32] selecting as endpoint the catalytic serine. When available, crystal structures of the proteins were used or homology models were created using the Phyre2 server [18].

#### 4.7. Bibliography

1. K.-E. Jaeger & T. Eggert, Lipases for biotechnology. *Current Opinion in Biotechnology*, **13** (2002) 390–397. [https://doi.org/10.1016/S0958-1669\(02\)00341-5](https://doi.org/10.1016/S0958-1669(02)00341-5).
2. V. Gotor-Fernández, R. Brieva, & V. Gotor, Lipases: Useful biocatalysts for the preparation of pharmaceuticals. *Journal of Molecular Catalysis B: Enzymatic*, **40** (2006) 111–120. <https://doi.org/10.1016/j.molcatb.2006.02.010>.
3. P. Berglund, Hydrolases in Organic Synthesis: Regio- and Stereoselective Biotransformations. By Uwe T. Bornscheuer and Romas J. Kazlauskas. *ChemBioChem*, **7** (2006) 1280–1280. <https://doi.org/10.1002/cbic.200600269>.
4. A. C. L. de M. Carvalho, T. de S. Fonseca, M. C. De Mattos, M. D. C. F. De Oliveira, T. M. L. G. De Lemos, F. Molinari, D. Romano, & I. Serra, Recent advances in lipase-mediated preparation of pharmaceuticals and their intermediates. *International Journal of Molecular Sciences*, **16** (2015) 29682–29716. <https://doi.org/10.3390/ijms161226191>.
5. L. Steenkamp & D. Brady, Screening of commercial enzymes for the enantioselective hydrolysis of R,S-naproxen ester. *Enzyme and Microbial Technology*, **32** (2003) 472–477. [https://doi.org/10.1016/S0141-0229\(02\)00335-6](https://doi.org/10.1016/S0141-0229(02)00335-6).
6. Z. Habibi, M. Mohammadi, & M. Yousefi, Enzymatic hydrolysis of racemic ibuprofen esters using *Rhizomucor miehei* lipase immobilized on different supports. *Process Biochemistry*, **48** (2013) 669–676. <https://doi.org/10.1016/j.procbio.2013.02.020>.
7. L. Sie Yon, F. N. Gonawan, A. H. Kamaruddin, & M. H. Uzir, Enzymatic deracemization of (R, S)-ibuprofen ester via lipase-catalyzed membrane reactor. *Industrial and Engineering Chemistry Research*, **52** (2013) 9441–9453.

<https://doi.org/10.1021/ie400795j>.

8. P. J. Hayball, Chirality and nonsteroidal anti-inflammatory drugs. *Drugs*, **52 Suppl 5** (1996) 47–58.
9. I. T. Harrison, B. Lewis, P. Nelson, W. Rooks, A. Roszkowski, A. Tomolonis, & J. H. Fried, Nonsteroidal antiinflammatory agents. I. 6-Substituted 2-naphthylacetic acids. *Journal of Medicinal Chemistry*, **13** (1970) 203–205. <https://doi.org/10.1021/jm00296a008>.
10. S. Wynne & D. Djakiew, NSAID Inhibition of Prostate Cancer Cell Migration Is Mediated by Nag-1 Induction via the p38 MAPK-p75NTR Pathway. *Molecular Cancer Research*, **8** (2010) 1656–1664. <https://doi.org/10.1158/1541-7786.MCR-10-0342>.
11. R. Morrone, N. D'Antona, D. Lambusta, & G. Nicolosi, Biocatalyzed irreversible esterification in the preparation of S-naproxen. *Journal of Molecular Catalysis B: Enzymatic*, **65** (2010) 49–51. <https://doi.org/10.1016/j.molcatb.2010.01.014>.
12. A. Fini, Solubility and solubilization properties of non-steroidal anti-inflammatory drugs. *International Journal of Pharmaceutics*, **126** (1995) 95–102. [https://doi.org/10.1016/0378-5173\(95\)04102-8](https://doi.org/10.1016/0378-5173(95)04102-8).
13. L. Tamborini, D. Romano, A. Pinto, A. Bertolani, F. Molinari, & P. Conti, An efficient method for the lipase-catalysed resolution and in-line purification of racemic flurbiprofen in a continuous-flow reactor. *Journal of Molecular Catalysis B: Enzymatic*, **84** (2012) 78–82. <https://doi.org/10.1016/j.molcatb.2012.02.008>.
14. H. Ren, Z. Xing, J. Yang, W. Jiang, G. Zhang, J. Tang, & Q. Li, Construction of an Immobilized Thermophilic Esterase on Epoxy Support for Poly( $\epsilon$ -caprolactone) Synthesis. *Molecules*, **21** (2016) 796. <https://doi.org/10.3390/molecules21060796>.
15. H. A. Sousa, C. Rodrigues, E. Klein, C. A. M. Afonso, & J. G. Crespo, Immobilisation of pig liver esterase in hollow fibre

- membranes. *Enzyme and Microbial Technology*, **29** (2001) 625–634. [https://doi.org/10.1016/S0141-0229\(01\)00443-4](https://doi.org/10.1016/S0141-0229(01)00443-4).
16. P. Liu, H. E. Ewis, P. C. Tai, C. D. Lu, & I. T. Weber, Crystal Structure of the *Geobacillus stearothermophilus* Carboxylesterase Est55 and Its Activation of Prodrug CPT-11. *Journal of Molecular Biology*, **367** (2007) 212–223. <https://doi.org/10.1016/j.jmb.2006.12.067>.
  17. B. Spiller, A. Gershenson, F. H. Arnold, & R. C. Stevens, A structural view of evolutionary divergence. *Proceedings of the National Academy of Sciences of the United States of America*, **96** (1999) 12305–12310. <https://doi.org/10.1073/pnas.96.22.12305>.
  18. L. A. Kelly, S. Mezulis, C. Yates, M. Wass, & M. Sternberg, The Phyre2 web portal for protein modelling, prediction, and analysis. *Nature Protocols*, **10** (2015) 845–858. <https://doi.org/10.1038/nprot.2015-053>.
  19. D. L. Ollis, E. Cheah, M. Cygler, B. Dijkstra, F. Frolow, S. M. Franken, M. Harel, S. J. Remington, I. Silman, & J. Schrag, The alpha/beta hydrolase fold. *Protein engineering*, **5** (1992) 197–211. <https://doi.org/10.1093/protein/5.3.197>.
  20. C. S. Hanes, Studies on plant amylases: The effect of starch concentration upon the velocity of hydrolysis by the amylase of germinated barley. *The Biochemical journal*, **26** (1932) 1406–21. <https://doi.org/10.1042/bj0261406>.
  21. J. B. S. Haldane, Graphical Methods in Enzyme Chemistry. *Nature*, **179** (1957) 832–832. <https://doi.org/10.1038/179832b0>.
  22. H. Lineweaver & D. Burk, The Determination of Enzyme Dissociation Constants. *Journal of the American Chemical Society*, **56** (1934) 658–666. <https://doi.org/10.1021/ja01318a036>.
  23. L. Qian, J. Y. Liu, J. Y. Liu, H. L. Yu, C. X. Li, & J. H. Xu, Fingerprint lipolytic enzymes with chromogenic p-nitrophenyl esters of

structurally diverse carboxylic acids. *Journal of Molecular Catalysis B: Enzymatic*, **73** (2011) 22–26. <https://doi.org/10.1016/j.molcatb.2011.07.010>.

24. J. L. Arpigny & K. E. Jaeger, Bacterial lipolytic enzymes: classification and properties. *The Biochemical journal*, **343 Pt 1** (1999) 177–83. <https://doi.org/10.1042/0264-6021:3430177>.
25. D. Cánovas, C. Vargas, L. N. Csonka, A. Ventosa, & J. J. Nieto, Osmoprotectants in *Halomonas elongata*: high-affinity betaine transport system and choline-betaine pathway. *Journal of bacteriology*, **178** (1996) 7221–6. <https://doi.org/10.1128/JB.178.24.7221-7226.1996>.
26. V. Kindzierski, S. Raschke, N. Knabe, F. Siedler, B. Scheffer, K. P. Ger-Grau, F. Pfeiffer, D. Oesterhelt, A. Marin-Sanguino, & H. J. Kunte, Osmoregulation in the halophilic bacterium *halomonas elongata*: A case study for integrative systems biology. *PLoS ONE*, **12** (2017) 1–22. <https://doi.org/10.1371/journal.pone.0168818>.
27. L. Cerioli, M. Planchestainer, J. Cassidy, D. Tessaro, & F. Paradisi, Characterization of a novel amine transaminase from *Halomonas elongata*. *Journal of Molecular Catalysis B: Enzymatic*, **120** (2015) 141–150. <https://doi.org/10.1016/j.molcatb.2015.07.009>.
28. M. Schmidt, E. Henke, B. Heinze, R. Kourist, A. Hidalgo, & U. T. Bornscheuer, A versatile esterase from *Bacillus subtilis*: Cloning, expression characterization, and its application in biocatalysis. *Biotechnology Journal*, **2** (2007) 249–253. <https://doi.org/10.1002/biot.200600174>.
29. P. Kaiser, C. Raina, R. Parshad, S. Johri, V. Verma, K. I. Andrabi, & G. N. Qazi, A novel esterase from *Bacillus subtilis* (RRL 1789): Purification and characterization of the enzyme. *Protein Expression and Purification*, **45** (2006) 262–268. <https://doi.org/10.1016/j.pep.2005.08.030>.
30. L.-J. Kang, Z.-T. Meng, C. Hu, Y. Zhang, H.-L. Guo, Q. Li, & M. Li,

Screening, purification, and characterization of a novel organic solvent-tolerant esterase, Lip2, from *Monascus purpureus* strain M7. *Extremophiles*, **21** (2017) 345–355. <https://doi.org/10.1007/s00792-016-0907-x>.

31. V. De Vitis, C. Nakhnoukh, A. Pinto, M. L. Contente, A. Barbiroli, M. Milani, M. Bolognesi, F. Molinari, L. J. Gourlay, & D. Romano, A stereospecific carboxyl esterase from *Bacillus coagulans* hosting nonlipase activity within a lipase-like fold. *FEBS Journal*, (2018). <https://doi.org/10.1111/febs.14368>.
32. A. Pavelka, E. Sebestova, B. Kozlikova, J. Brezovsky, J. Sochor, & J. Damborsky, CAVER: Algorithms for Analyzing Dynamics of Tunnels in Macromolecules. *IEEE/ACM Transactions on Computational Biology and Bioinformatics*, **13** (2016) 505–517. <https://doi.org/10.1109/TCBB.2015.2459680>.
33. L. J. Kingsley & M. A. Lill, Substrate tunnels in enzymes: Structure-function relationships and computational methodology. *Proteins: Structure, Function, and Bioinformatics*, **83** (2015) 599–611. <https://doi.org/10.1002/prot.24772>.
34. A. Gora, J. Brezovsky, & J. Damborsky, Gates of enzymes. *Chemical Reviews*, **113** (2013) 5871–5923. <https://doi.org/10.1021/cr300384w>.
35. R. A. Sheldon, Enzyme immobilization: The quest for optimum performance. *Advanced Synthesis and Catalysis*, **349** (2007) 1289–1307. <https://doi.org/10.1002/adsc.200700082>.
36. C. Mateo, V. Grazu, J. M. Palomo, F. Lopez-Gallego, R. Fernandez-Lafuente, & J. M. Guisan, Immobilization of enzymes on heterofunctional epoxy supports. *Nature Protocols*, **2** (2007) 1022–1033. <https://doi.org/10.1038/nprot.2007.133>.
37. S. Montoro-García, F. Gil-Ortiz, J. Navarro-Fernández, V. Rubio, F. García-Carmona, & Á. Sánchez-Ferrer, Improved cross-linked enzyme aggregates for the production of desacetyl  $\beta$ -lactam

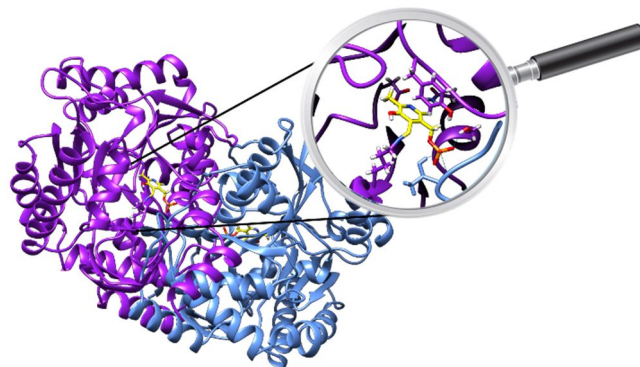
- antibiotics intermediates. *Bioresource Technology*, **101** (2010) 331–336. <https://doi.org/10.1016/j.biortech.2009.08.016>.
38. K. E. Cassimjee, R. Kourist, D. Lindberg, M. Wittrup Larsen, N. H. Thanh, M. Widersten, U. T. Bornscheuer, & P. Berglund, One-step enzyme extraction and immobilization for biocatalysis applications. *Biotechnology journal*, **6** (2011) 463–9. <https://doi.org/10.1002/biot.201000357>.
39. Y. Zou, W. I. Weis, & B. K. Kobilka, N-Terminal T4 Lysozyme Fusion Facilitates Crystallization of a G Protein Coupled Receptor. *PLoS ONE*, **7** (2012). <https://doi.org/10.1371/journal.pone.0046039>.
40. M. Planchestainer, M. Contente, D. Roura Padrosa, & F. Paradisi, Genetically Fused T4L Acts as a Shield in Covalent Enzyme Immobilisation Enhancing the Rescued Activity. *Catalysts*, **8** (2018) 40. <https://doi.org/10.3390/catal8010040>.
41. M. C. Nweke, R. G. McCartney, & D. G. Bracewell, Mechanical characterisation of agarose-based chromatography resins for biopharmaceutical manufacture. *Journal of Chromatography A*, **1530** (2017) 129–137. <https://doi.org/10.1016/j.chroma.2017.11.038>.
42. M. D. Hopkin, I. R. Baxendale, & S. V. Ley, An expeditious synthesis of imatinib and analogues utilising flow chemistry methods. *Organic and Biomolecular Chemistry*, **11** (2013) 1822–1839. <https://doi.org/10.1039/c2ob27002a>.
43. E. G. Lee, H. S. Won, H. S. Ro, Y. W. Ryu, & B. H. Chung, Preparation of enantiomerically pure (S)-flurbiprofen by an esterase from *Pseudomonas* sp. KCTC 10122BP. *Journal of Molecular Catalysis B: Enzymatic*, **26** (2003) 149–156. <https://doi.org/10.1016/j.molcatb.2003.05.004>.
44. S. Escobar, C. Bernal, & M. Mesa, Kinetic study of the colloidal and enzymatic stability of  $\beta$ -galactosidase, for designing its

encapsulation route through sol-gel route assisted by Triton X-100 surfactant. *Biochemical Engineering Journal*, **75** (2013) 32–38. <https://doi.org/10.1016/j.bej.2013.03.010>.

45. R. F. Perna, P. C. Tiosso, L. M. Sgobi, A. M. S. Vieira, M. F. Vieira, P. W. Tardioli, C. M. F. Soares, & G. M. Zanin, Effects of Triton X-100 and PEG on the Catalytic Properties and Thermal Stability of Lipase from Free and Immobilized on Glyoxyl-Agarose. *The Open Biochemistry Journal*, **11** (2017) 66–76. <https://doi.org/10.2174/1874091X01711010066>.



## Chapter 5: PLP binding in class-III $\omega$ -transaminases



## 5.1. Introduction

Transaminases (TAs), for their capacity to synthesize chiral amines have gained interest in the past years in the biocatalysis field [1]. In their catalytic cycle, these group of enzymes need pyridoxal-5-phosphate (PLP), the bioactive version of vitamin B6 as a cofactor. In the enzyme holo-form, PLP is not only bound through the catalytic lysine, but several residues participate in its stabilisation (Figure 5.1). A series of residues referred to as the phosphate binding cup interact through hydrogen bonding with the phosphate group of the cofactor [2] while an aromatic residue and a conserved non-polar aliphatic residue establish a  $\pi$ - $\pi$  stacking and hydrophobic interactions with the aromatic ring of PLP [3]. The combination of the covalent bond between the PLP and the lysine, together with the weaker interactions, help to maintain the cofactor in the correct position and, moreover, in the correct protonation state to catalyse the reaction. The most important interaction to maintain PLP protonated is between an acidic residue, a highly conserved aspartic acid in TAs, and the nitrogen of the pyridinium ring [4–5].

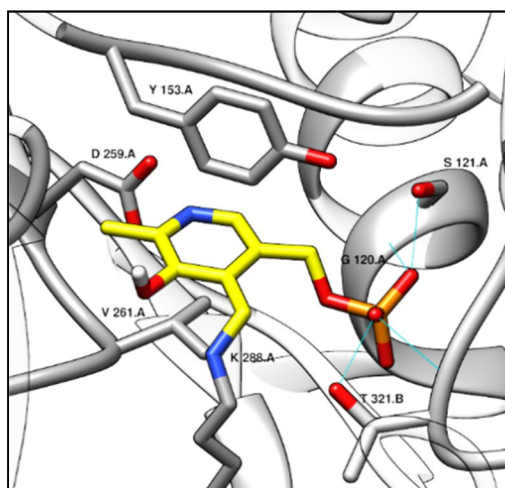


**Figure 5.1.** PLP binding motif of CvTA (PDB: 4A6T). A. 3d view of the most important residues interacting with PLP. Hydrogen bonds are depicted in light blue. Labels indicate the residue in one letter code, their position and the chain (A or B). PLP is shown in yellow.

During the catalytic cycle, PLP is converted into pyridoxamine-5-phosphate (PMP) which is no longer covalently bound and just kept in position through electrostatic and weak interactions. Due to the non-covalent nature interactions, PMP can leach from the active site to the

reaction bulk leaving the enzyme in its apo-form [6] which is more prone to denaturalisation and precipitation, and subsequently inactivation. Consequently, the applicability and scalability of the transaminase catalysed reactions are affected by their affinity for both forms of the cofactor, PLP and PMP.

Previous work in our group, proved that HeTA, a transaminase from *Halomonas elongata* [7] performed better when used in a flow reactor under PLP limiting conditions [8] than other homologous transaminases such as CvTA (from *Chromobacterium violaceum*) [9] and PfTA (from *Pseudomonas fluorescens*) [10–11] suggesting that HeTA possesses a higher affinity for PLP than their counterparts. A deeper understanding of the molecular interactions necessary to minimise the loss of PLP and therefore its exogenous requirement, would significantly impact the economics of large scale biotransformations involving transaminases.

In this chapter, to better understand the special features that could explain why HeTA exhibits a higher affinity for PLP than its homologues the PLP binding pocket of the three transaminases was studied by structural superposition and residue interaction network (RIN). HeTA displays an asparagine suitably positioned to interact with the aspartic acid that maintains the cofactor protonated. This position, occupied by a valine in CvTA and PfTA, could influence the aspartate residue, enhancing its capacity to interact with PLP. To investigate the effect of this position in the PLP binding, three different single mutants were constructed and their PLP affinity, stability, and functional characteristics were analysed. Additionally, the crystal structure of PfTA was determined for the first time.

The work presented in this chapter is my exclusive contribution unless otherwise stated. Raphael Alaux helped with the mutant construction and Philip Smith and Dr. Dreveny performed the crystallisation and assisted with the structure determination for PfTA.

This work has been included in one publication:

- D. Roura Padrosa, R. Alaux, P. Smith, I. Dreveny, F. Paradisi, F. López-Gallego, “Enhancing PLP-binding capacity of class-III  $\omega$ -transaminases by single residue substitution” (under revision).

## 5.2. PfTA crystal structure determination

To gain more information on PfTA and in order to compare the three enzymes at the molecular level, the transaminase from *Pseudomonas fluorescens* was crystallised in the presence of the cofactor PLP in collaboration with Dr. Ingrid Dreveny’s group (University of Nottingham). Crystals of PfTA were obtained when grown in a buffer with PEG6000 as the precipitant. The resulting crystals diffracted to 2.2 Å resolution and the structure was solved by molecular replacement (Table 5.1).

The crystal showed a tetrameric arrangement of PfTA, as a dimer of dimers, with the cofactor positioned at the interface between one of the dimeric units (Figure 5.2A). PfTA is structurally closely related to another transaminase from uncultivated *Pseudomonas sp.* (PDB: 5LH9 and 5LHA) with which it shares 49% sequence identity. As for the two other transaminases studied, CvTA and HeTA, the sequence similarity is 55% and 59% respectively (with an identity of 40% and 36%). When superposed with the two before mentioned TAs, the RMSDs are 1.5 and 1.8 Å, indicating as expected that the three enzymes show a very similar overall folding.

**Table 5.1.** Crystallographic data collection and refinement statistics.

Data collection		Refinement	
Space group	P2 <sub>1</sub> 2 <sub>1</sub> 2 <sub>1</sub>	Resolution range (Å)	88.07-2.21
Cell dimensions		<i>R</i> <sub>work</sub> / <i>R</i> <sub>free</sub>	0.211/0.243
<i>a</i> , <i>b</i> , <i>c</i> (Å)	92.02,94.54,242.22	No. atoms	
Resolution (Å)	2.21	Protein	13838
<i>R</i> <sub>pim</sub>	0.131 (0.723)	PLP	60
<i>I</i> / $\sigma$ <i>I</i>	3.9 (1.71)	Water	328
CC1/2	0.973(0.589)	<i>B</i> -factors (Å <sup>2</sup> )	
Completeness (%)	99.8 (88.07)	Protein	65.35
Redundancy	6.5 (6.5)	PLP	56.13
Wilson B-factor (Å <sup>2</sup> )	28.7	Water	38.86
No. of unique reflections	106548 (7759)	R.m.s. deviations	
		Bond lengths (Å)	0.009
		Bond angles (°)	1.062

Following the general observations, a more detailed study of the PLP binding pocket in PfTA was carried out. Four PLP molecules are present in the crystal structure, with all four cofactor molecules covalently bound to the enzyme through Lys293, forming the internal aldimine. The PLP binding site of this enzyme is very similar to other transaminases such as CvTA and HeTA (Figure 5.2B). The phosphate binding cup is formed by the residues of two different chains which are part of one dimeric unit. Gly125 and Ser126 from one chain, together with Tyr329 and Thr330 from the other, interact with the phosphate group of PLP through multiple hydrogen bonds. Moreover, hydrophobic interactions between Tyr158 and Val266 and the aromatic ring of PLP help stabilise the cofactor in the correct position. In addition, Asp264 is directed to the pyridinium nitrogen, in accordance to previous observations where this acidic residue is crucial for catalysis as it interacts with the cofactor to maintain in correct protonation state [4].

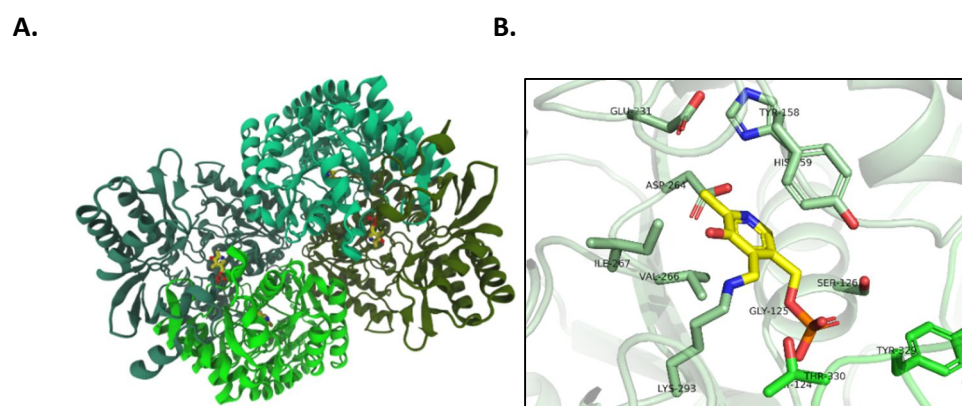


**Figure 5.2.** **A.** Overall structure of PfTA in cartoon representation and PLP shown in yellow sticks highlighting the tetrameric arrangement (subunits in different shades of green) **B.** Close-up view of the PLP (yellow) binding site with key residues labelled and Val129 highlighted in magenta. Residues from the two subunits forming the PLP binding site are coloured in green and teal, respectively.

### 5.3. Computational analysis of PLP-binding pocket

Once the crystal structure of PfTA was solved, to have a better understanding of the molecular interactions that govern the PLP binding in the three targeted TAs, the PLP binding sites of HeTA, CvTA and PfTA were analysed. By superimposing the three structures and focusing on the PLP-binding pocket, it was evident that the studied TAs shared

common traits, with nearly identical residues and architecture. However, a potentially significant difference between HeTA and the two other TAs, was the presence of an asparagine located in an  $\alpha$ -helix near the interface between the two monomers. The corresponding position in the structure of both CvTA and PFTA is occupied by a valine (Figure 5.3). This residue is at less than 3.5Å from the aspartate known to interact with the pyridinium nitrogen of PLP. Therefore, this asparagine could possibly affect the aspartic acid, further polarising it and enhancing its electrostatics to interact more strongly with PLP.

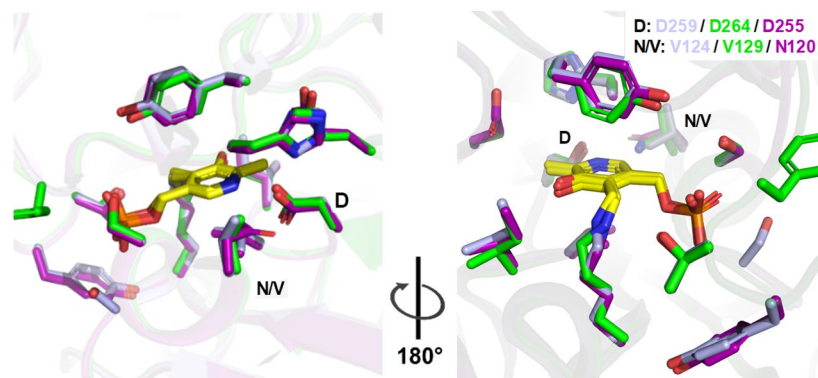
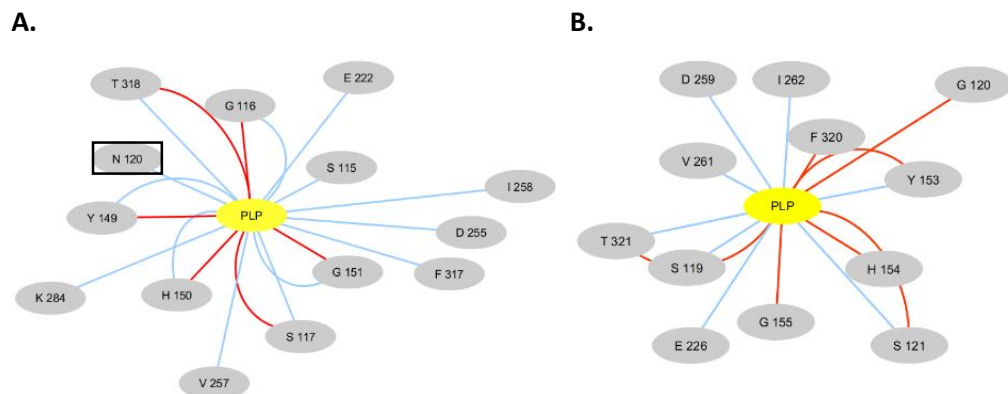


**Figure 5.3.** Superposition of the PLP binding pocket for HeTA (purple), CvTA (grey) and PFTA (green) created with Pymol.

To gain more evidence on the role of this asparagine, a residue interaction network (RIN) was computed. RINs are an alternative method to identify the possible covalent and non-covalent interactions that could affect, in this case, the PLP binding. Differently from direct visualisation of 3D structures, RINs provide a more easily interpretable layout, transforming the possible interactions that might occur in the 3D space in a scheme of connected nodes [12].



C.

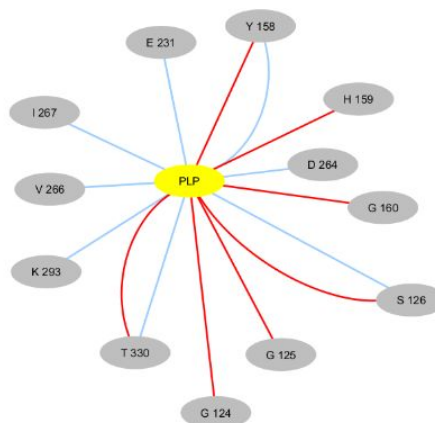


**Figure 5.4.** Residue interaction network (RIN) for PLP of HeTA (A), CvTA (B) and PfTA (C). Main chain interactions are indicated in red and side chain in light blue. Distance between residues and the central residue are representative of distances in the structure. N120 in HeTA is marked with a black square.

The RIN was performed using PLP as the main node to identify any predicted interactions. As depicted in Figure 5.4, the difference identified by superpositions was confirmed. In HeTA, N120 appears to be relevant in the PLP binding while both V124 in CvTA and V129 in PfTA do not appear in the interaction network.

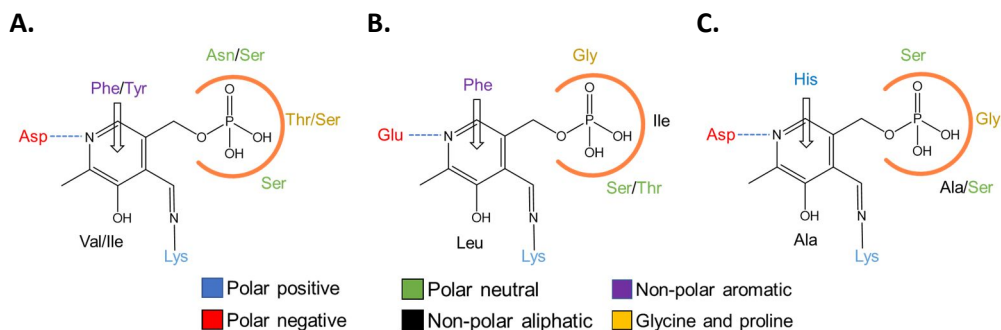


**Figure 5.5.** 2D representation of the main interaction of the PLP binding pocket in TAs (A), DAAT (B) and SHMT (C). Residues in each position were defined as the two more abundant amino acids (accounting for more than 80% of the variability) in each position. The phosphate cup is shown as an orange circle. Residues are coloured according to the legend.

A further study of different PLP binding enzymes revealed that within the same fold type, serine hydroxy methyltransferases (SHMT, EC 2.1.2.1) [13] and even more distant families such as D-amino acid aminotransferases (DAAT, EC 2.6.1.21) [14] share both the architecture and the nature of the residues participating in the PLP binding; the phosphate cup, the catalytic lysine, and the acidic residue to keep the

cofactor protonated (Figure 5.5). Although these two groups of enzymes catalyse very diverse reactions, their PLP binding pocket as well as the catalytic mechanism show significant similarities to the one of transaminases [15].

More interestingly, when further analysing the PLP binding site, in an equivalent position to N120 in HeTA, SHMT and DAAT presented a very conserved asparagine (Figure 5.6). This observation strongly suggest that the asparagine detected in HeTA and not present in CvTA or PFTA could indeed have an effect on the PLP binding. The fact that both DAAT and SHMT also present a highly conserved asparagine in an equivalent position suggests that this residue might play an important role, which is not been investigated before in TAs. In HeTA, similarly to DAAT and SHMT, the asparagine is predicted to interact via hydrogen-bonding with the aspartate. This hydrogen bonding might help the polarisation of PLP and further fix the position of the aspartic acid, enhancing the capacity of the enzyme to keep both forms of the cofactor in the active site, explain HeTA's better performance when used in flow with minimal concentration of PLP.

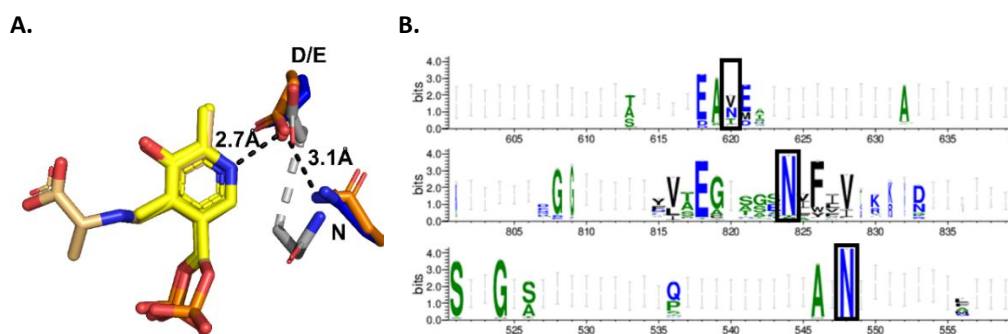


**Figure 5.6.** **A.** Detail of the interaction of the pyridinium nitrogen with the aspartic or glutamic residue for HeTA (blue), DAAT (gray) and SHMT (orange). PLP is depicted in yellow and the serine bound for SHMT in light yellow. Distances in angstroms are shown for HeTA with black lines. **B.** Amino acid frequency in the homologous position for w-TA (top), DAAT (middle) and SHMT (bottom).

To investigate the effect of the asparagine, three single mutants were designed: HeTA-N120V, which would disrupt the proposed interaction and CvTA-V124N and PFTA-V129N, to mimic WT-HeTA. All three mutants were successfully created and expressed in the same conditions as the WT enzymes.



#### 5.4. Functional characterisation of the single mutants

By purifying the enzymes without any supplementation of PLP in the buffer, the spontaneous the fraction of TA bound to PLP (holo-form) of the enzymes can be calculated by UV-Vis spectroscopy. The internal aldimine formed by PLP covalently bound to the catalytic lysine shows an absorption maximum at 415 nm, while free PLP has its maximum at 390 nm [16]. Based on the spectral differences, the holo-form in freshly purified enzymes before and after incubation with PLP was quantified by comparing their absorbance at 415 nm divided by the value at 280 nm. The samples after incubation were considered to be the maximum achievable holo-form and therefore fixed as the 100%. For the occupancy, the absorbance at 415 nm was compared to the mM of enzyme, considering the occupancy of the samples after incubation of PLP as the maximum (2 for the dimeric TAs, HeTA and CvTA and, 4 for the tetrameric PfTA) (Table 5.2).

**Table 5.2.** Holo-form percentage. Percentage of holo-form of each protein and its corresponding mutants without external PLP addition.

		Holo-form (%)	Occupancy <sup>1</sup> (PLP:enzyme ratio)	K <sub>d</sub> (μM)
HeTA	WT	69 ± 2	1.39 ± 0.04	12.4 ± 3.6
	N120V	42 ± 9	1.19 ± 0.02	30.3 ± 4.1
CvTA	WT	16 ± 2	0.33 ± 0.01	59.0 ± 15.8
	V124N	13 ± 1	0.22 ± 0.01	16.4 ± 5.6
PfTA	WT	39 ± 8	1.57 ± 0.27	14.1 ± 2.3
	V149N	37 ± 9	1.64 ± 0.04	14.8 ± 2.5

<sup>1</sup> Maximum occupancy is estimated as 2 for the two dimeric transaminases, HeTA and CvTA, and 4 for PfTA.

WT-HeTA exhibited the highest holo-form of all three enzymes, with almost 70%, and an occupancy of 1.39, meaning more than half of the protein units have a PLP molecule in their active site. The other dimeric transaminase, CvTA, only exhibited 16% of holo-form and an occupancy value of 0.3, indicating that most of the enzymatic units were not bound to PLP. PfTA, on the other hand, had almost 40% holo-form and an occupancy of 1.6. These results already suggest that for the WT variants, HeTA possesses a higher capacity to bind PLP, as most of the enzyme even under PLP limiting conditions, appears to have PLP bound in its

active site while CvTA and PfTA had less than half of their theoretical maximum occupancy.

For the mutants, however, different behaviours were seen. While HeTA-N120V had a decrease in both the holo-form and the occupancy, CvTA-V124N and PfTA-V129N did not change significantly. Altogether, it seems that N120 plays a role in HeTA binding of PLP but the fact that no difference was observed with the other two did not clarify if the binding capacity of HeTA was due to the presence of that Asn or if it could be mimicked in CvTA or PfTA.

To further investigate the effect of the mutation in the PLP affinity, the dissociation constant ( $K_d$ ) for PLP was calculated from the midpoint denaturation temperature ( $T_{1/2}$ ) at different concentrations of the cofactor [17].  $K_d$  is the equilibrium constant used to define the binding affinity of an enzyme for its substrate or cofactor, as in this case. Therefore, a lower  $K_d$  value translates into a higher affinity for the cofactor. The results are shown in Table 5.2.

In this case, WT-HeTA exhibited the lower  $K_d$  for PLP with a value of 12.4  $\mu\text{M}$ , 5 times lower compared to WT-CvTA, confirming that HeTA has a significantly better affinity for PLP than its homologous from *C. violaceum*. When the PLP affinity was determined for the mutants, differently from the holo-form, significant trends were observed. Replacing N120 for a valine in HeTA dramatically decreased its affinity for the cofactor, with a  $K_d$  value 3 times higher, correlating nicely with the initial hypothesis, as this mutant was designed to disrupt the interaction. More importantly, a similar behaviour was seen in CvTA-V124N, where the substitution for an asparagine decreased the  $K_d$  3-fold. This new variant showed a  $K_d$  comparable to WT-HeTA indicating the advantage offered by N120 in HeTA can also be mimicked in CvTA.

For PfTA, the tetrameric TA studied, the  $K_d$  was 14  $\mu\text{M}$  calculated for both WT-PfTA and PfTA-V129N, similar to the one exhibited by WT-HeTA. Unexpectedly, in this case, the mutation did not change significantly its affinity for the cofactor. This last observation could

indicate that such interaction is less relevant in tetrameric transaminases, where it is known that the main forces governing PLP binding are the tetrameric assembly which rigidifies more the PLP binding pocket [18–19].

To analyse in more detail the effect of the mutation, the activity of both variants of each protein, before and after incubation with PLP, were measured (Figure 5.7). For HeTA, the exogenous addition of PLP did not affect the specific activity of neither the WT nor N120V variant, indicating that the enzyme performs at its maximum when half of the active sites are occupied by PLP. On the contrary, for CvTA the exogenous addition of PLP had a significant effect, with only 10% of the activity expressed when no PLP was added. These results imply that CvTA performance is highly PLP-dependant, correlating with the low holo-form and occupancy observed for the WT and the V124N mutant. Unexpectedly, for PftA the WT exhibited a 2-fold increase in the activity after incubation with PLP while the mutant became insensitive to the presence of cofactor, similarly to HeTA.

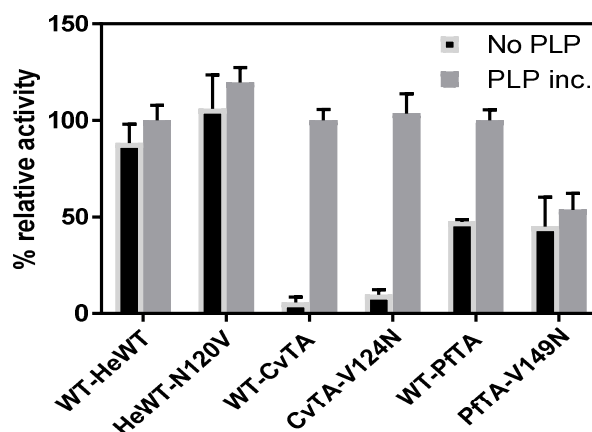


**Figure 5.7.** Activity percentage after PLP incubation. The change of activity after incubation with PLP as stated before is shown. 100% of activity corresponds to the WT activity after incubation with PLP.

These observations clearly indicate that HeTA is less dependent on exogenous PLP, which can be related to its higher affinity for PLP. Surprisingly, also the N120V variant exhibits this independency to PLP despite the affinity for the cofactor being 3 times lower suggesting that the mutation does not affect the catalytic efficiency of the enzyme. The

role of the studied Asn is also supported by CvTA-V124N behaviour, with a 3-fold increased affinity and the variant being slightly more active compared to the WT under PLP limiting conditions. Despite these, the role of the studied Asn seems to be restricted to dimeric transaminases, as for PfTA, this mutation does not affect the PLP binding and negatively affects the catalytic response to PLP of the enzyme, seen in the insensitivity of the V129N mutant in response to PLP.

### **5.5. Cofactor release study**

To further comprehend the implications of the Asn residue, we studied the release of PMP to the reaction bulk. To do so, the first half of the reaction was studied measuring absorbance at 390 nm, corresponding to free PLP, and 325 nm, which corresponds to free PMP [20]. Absorbance was then normalised to keep all values between 0 and 1. The minimum value was subtracted and the result, divided by the maximum difference, obtained by subtracting the minimum to the maximum value. To study just the first half reactions, only the amino donor was added in the reaction and no amino acceptor. Thus, the enzyme cannot complete the catalytic cycle, forcing the formation of PMP and its accumulation. PMP is only stabilised through non-covalent interactions and if not held tightly enough in the active site, will be released into the reaction bulk. Therefore, a higher affinity for PMP would translate into a slower release of it to the media while a higher rate of PMP detection in the bulk, would indicate the enzyme is exchanging more rapidly the aminated version of the cofactor to incorporate a new PLP molecule and start a new reaction half cycle.

As seen in Figure 5.8, HeTA-N120V produces PMP nearly 1.5 times faster than the WT over the first 60 minutes, with an especially steep increase in the first 20 minutes. The same phenomenon is observed in CvTA, where CvTA-N120V releases the aminated version of the cofactor nearly two times slower than the WT enzyme. It is clear from these results that the absence of the stabilising effect of the Asn residue, as seen in WT-CvTA and HeTA-N120V, triggers a faster release of PMP into the reaction bulk. This further supports that the Asn residue helps

also to keep PMP in the active site, preventing the destabilisation of the TAs as its release, leaves the enzyme in its apo-form, more unstable and prone to precipitation and moreover, when no PLP is available, catalytically inactive.

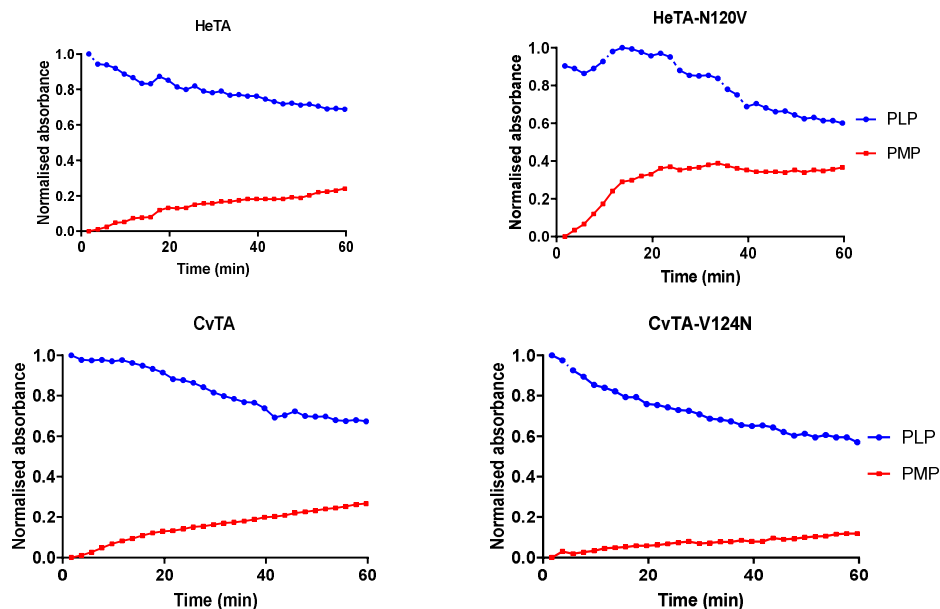


**Figure 5.8.** Time-courses of PMP formation during the first half of the transamination reaction. From a reaction containing 0.5 mM enzyme, 50 mM benzylamine and 0.5 mM PLP, the formation of PMP (red) was measured by following the increase of absorbance at 325 nm while PLP (blue) was monitored at 390 nm. Values of absorbance were normalized.

### 5.6. Temperature stability under PLP limiting conditions

Once functionally characterised and confirmed that the Asn does play a role in PLP and PMP binding for the two dimeric TAs, their resistance to temperature in the absence of PLP was investigated. The same assay was performed with PfTA to analyse if the mutation, in that case, provoked some effect that could explain the insensitivity to PLP observed in the activity assay. To that end, the three proteins and their mutants were incubated at the desired temperature for 30 minutes and after centrifugation to eliminate the possible precipitated proteins, the activity was assessed and compared to the one exhibited at 30°C, defined as 100%. This assay was performed with the enzymes freshly purified without any PLP to evaluate the resistance of the PLP-enzyme interaction (Figure 5.9).

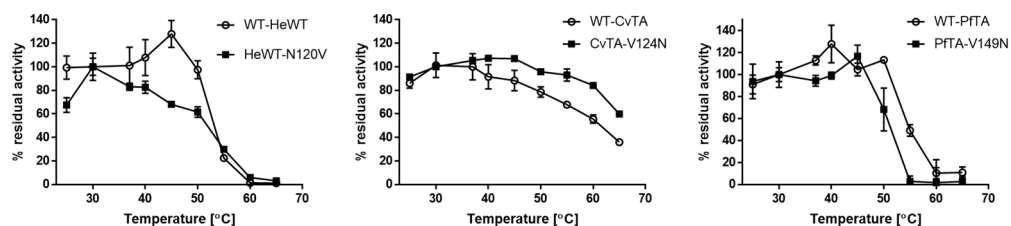


**Figure 5.9.** Temperature stability assays. The activity of the WT and the mutants for the three transaminases is presented in absence of PLP. 100% is defined as the activity at 30°C.

According to the initial hypothesis and previous observations, WT-HeTA and CvTA-V124N outperform their counterparts with a valine in the studied position. HeTA-N120V is significantly less stable than its WT counterpart, with substantial differences at temperatures ranging from 40 to 50°C. This same trend is observed in CvTA, where CvTA-V124N variant exhibits better stability at higher temperatures compared with the WT enzyme. This has to be due to the reinforcement of the PLP binding proved by the lower  $K_d$  in the variants that possess the asparagine.

On the other hand, PfTA-V129N has lower stability at temperatures of 50 and 55°C compared to the WT. This results, combined with the insensitivity exhibited by the enzyme to PLP regarding its activity, suggests that the mutation, although deleterious for the PLP binding, could be destabilising the quaternary structure of the enzyme, creating a more inactivation prone variant when the valine is substituted with an asparagine. This substitution might disrupt crucial hydrophobic interactions that may be important for the quaternary structure assembly, needed for the enzyme activity and affecting its stability.

It is important to note that the data from this assay might reflect conformational changes that translate in the loss of enzymatic activity, but such changes are not exclusively linked to the unfolding of the protein. The loss of activity may be related to the dissociation of PLP-enzyme or small structural rearrangements weakening the PLP-enzyme complex and promoting the cofactor release, which would yield an inactive version of the enzyme [18].

## 5.7. Melting temperature

While functional inactivation, as discussed before, does not directly correlate with protein denaturation, the midpoint denaturation temperature ( $T_m$ ) corresponds to the temperature at which half of the protein population is unfolded, assuming a two-state transition model.  $T_m$  were measured in absence and presence of PLP with freshly purified enzymes without PLP, to assess the effect of bound PLP as well as exogenous PLP on this parameter. Cofactor binding is generally related to a higher  $T_m$ , as it decreases the flexibility of the protein preventing its denaturation [21].

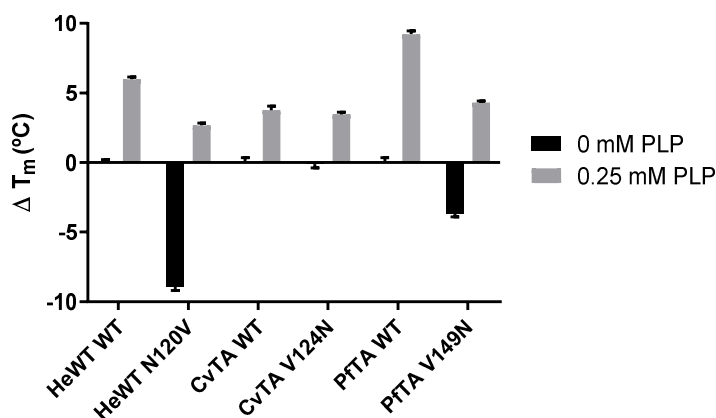


**Figure 5.10.**  $T_{1/2}$  of HeTA, CvTA and PftA mutants is presented without PLP and with 0.25 mM PLP in the reaction buffer as the difference from the WT  $T_{1/2}$  (53.3°C for WT-HeTA, 68.8°C for WT-CvTA and 62.9°C for PftA).

As shown in Figure 5.10, under limiting PLP conditions, the removal of N120 in HeTA caused a drop of the  $T_m$  of 9°C compared to the native enzyme. This difference was still present but reduced in PLP saturating conditions, where HeTA-N120V exhibited a  $T_m$  3°C lower. These results, combined with the previous observations, indicate that in HeTA, N120 plays a crucial role in the PLP binding which in turn greatly affects the stability of this TA and its resistance to denaturation.

In CvTA, however, the effect of the N124 in the thermal denaturation resistance is nearly negligible. Both mutant and the WT exhibit a similar  $T_{1/2}$  when no exogenous PLP is added and have an increase of 3°C in the  $T_{1/2}$  under saturation conditions. In this case, the increase in affinity for the cofactor does not neutralise enzyme inactivation by preventing

the unfolding of the quaternary structure, as proved here, but more probably by impeding the premature release of the cofactor from the active site in CvTA-N120V compared to the WT.

As for PfTA, in accordance to previous observations, the mutation provokes a destabilisation of the enzyme. PfTA-V129N has a  $T_{1/2}$  nearly 5°C lower than the WT both with and without PLP in solution. This indicates that while the mutation has a deleterious effect on the PLP binding affinity, it appears to have a negative effect on the stability of the enzyme.

### **5.8. Structural rearrangements after PLP binding**

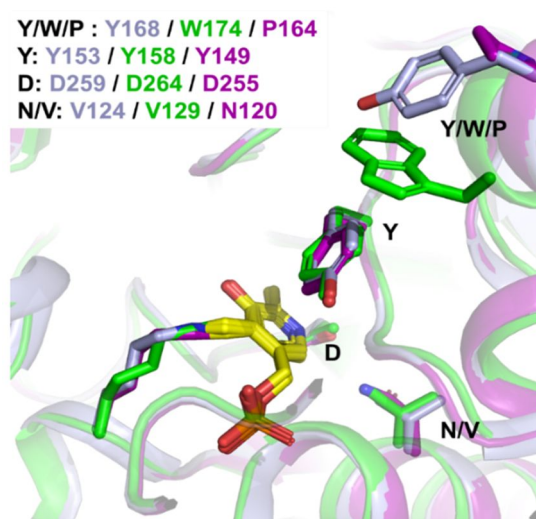
With all these results, it seems clear that HeTA N120 plays role in the binding of the cofactor. This interaction can be mimicked in CvTA but in PfTA, the high affinity for PLP cannot be explained by the presence of this residue and the beneficial effect cannot be mirrored. It is widely known that one of the major forces that governs the cofactor binding are supramolecular  $\pi$ - $\pi$  stacking interactions between the cofactor and the PLP-ring motif [22]. The most important interaction is established between a Tyr residue (Tyr149 in HeTA, Tyr153 in CvTA and Tyr158 in PfTA) (

Figure 5.11) and the PLP aromatic ring. The position of this residue though, is thought to change after PLP binding as seen for TAs from *Vibrio fluvialis* and *Pseudomonas sp.*[19–23]. This structural rearrangement contributes to the affinity for the cofactor and therefore, the study of this region can also help elucidate what are the governing factors that define the PLP affinity.

In this sense, CvTA possesses another tyrosine residue, Tyr168, which could act as a staple, fixing the loop where Tyr153 is located in the correct position after PLP binding. This could explain why, while CvTA-V124N exhibits a higher affinity for the cofactor, its  $T_{1/2}$  remains unaffected as the movement of the loop is more likely to affect in a major degree the unfolding of the protein.



Interestingly, in PfTA a Trp is present at the corresponding position. This residue could also stabilise Tyr159 once PLP is bound. Moreover, in PfTA the movement of this loop is constrained by the assembly of the tetramer. These two factors together, the presence of the Trp that could help the positioning of Tyr158 and the tetrameric quaternary structure which provide a more rigid environment, could explain the high PLP affinity shown by PfTA. Consequently, in both CvTA and PfTA it seems that larger macromolecular rearrangements are responsible of their affinity for PLP.



**Figure 5.11:** Detail of the flexible loop related to PLP binding. HeTA is shown in purple (PDB:6GWI), CvTA in light blue (PDB: 4A6T) and PfTA in green (PDB: 6S54). The residues forming the PLP-ring motif and the acid residues stabilizing the pyridinium ion.

On the contrary in HeTA, the homologous position is occupied by a proline. This residue can hardly interact with Tyr149 and due to its dimeric nature, there is no additional protein chain that can help to lock the position of Tyr153. Consequently, the stability of HeTA and its high affinity for PLP is better justified by local interactions formed by hydrogen bonding of PLP to the surrounding residues, where the presence of the studied asparagine has been proved to be beneficial.

To summarise, in this chapter, the role of N120 in HeTA related to its affinity for PLP and, consequently, to its thermal stability and midpoint denaturation temperature was confirmed. The same residue, when emulated in CvTA, produced a variant with similar affinity for PLP as WT-

HeTA and which showed a higher thermal stability than the WT. The fact this variant the same thermodynamic behaviour than the WT protein, indicates the higher affinity for PLP is important for the functionality of the enzyme independently of its denaturation. For PfTA, a tetrameric transaminase, the insertion of the asparagine caused deleterious effect considering the PLP binding but destabilised the enzyme, proved by lower thermal stability and  $T_{1/2}$ .

The identification of this position has introduced a new pathway for engineering dimeric TAs, aiming the reinforcement the cofactor interactions to ultimately achieve more robust biocatalysts with higher potential for industrial applications.

## **5.9. Experimental procedures**

### **5.9.1. Crystallization, data collection and structure determination of PfTA**

A full length PfTA synthetic construct, cloned in pET-28B vector, was expressed in the *E. coli* BL21 codon plus strain cultured at 37 °C in LB medium. Expression was induced by addition of 1-thio- $\beta$ -D-galactopyranoside at 0.5 mM and cells harvested after three hours. Cells were lysed by sonication in 45 mM phosphate, pH 7.2, 0.9 M NaCl, 0.09 mM PLP, 9 mM imidazole, 10% (v/v) glycerol. Samples were purified on a HisTrap HP chelating column (GE Healthcare) pre-charged with nickel sulphate. Further purification was carried out by size-exclusion chromatography using a Superdex 200 HiLoad 16/60 column (GE Healthcare) pre-equilibrated with 50 mM HEPES, pH 7.5, 300 mM NaCl, 0.1 mM PLP, 1% glycerol. Sitting drop vapor diffusion crystallization trials were carried out at 20 °C and the best hits were obtained in conditions G1 and G6 from the LMB screen (Molecular Dimensions), which were further optimized by varying protein and precipitant concentrations. Single crystals grew in under a week; the best condition being 6 mg/mL protein (in 50 mM HEPES, pH 7.5, 300 mM NaCl, 0.1 mM PLP, 1% glycerol, 20 mM DTT) mixed 1:1 0.1 M sodium citrate, pH 5.6, 12% w/v PEG 6000, 0.1 M lithium sulphate. Crystals were flash cooled after

soaking in cryoprotectant solution containing six parts precipitant mixture with four parts glycerol. Diffraction data for these crystals were collected on the I24 beamline at the Diamond Light Source and the structure was solved by molecular replacement using coordinates from the uncultivated *Pseudomonas sp.* transaminase (PDB: 5LHA) as a search model with PHASER.

### **5.9.2. Model building, refinement and validation**

Model building was conducted using COOT [35], and refinement using REFMAC5 [24]. Data collection and refinement statistics are summarized in supporting Table 1. The final model was validated using Molprobity and deposited into the Protein Data Bank (PDB: 6S54).

The asymmetric unit contained four molecules in a tetrameric arrangement, with an average interface of 5428.1 Å<sup>2</sup> between two subunits within a dimer and 1071.4 Å<sup>2</sup> between a subunit within one dimer and its nearest neighbour in the opposite dimer, using the PISA server [25]. Clear electron density for PLP linkage to K293 was observed in two chains (A and B), whereas the K293 side chain was less well defined in chains C and D, which may reflect a lower occupancy of the cofactor and/or a portion of the cofactor non-covalently bound to the enzyme. The latter two chains displayed higher B-factors overall. Figures were prepared using VMD [26] or Pymol [27].

### **5.9.3. Computational analyses**

3-dimensional structure analysis were done using the crystal structures of HeTA (PDB: 6GWI) [28], CvTA (PDB: 4A6T) and for PfTA (PDB: 6S54). Residue interaction analysis was performed using Cytoscape [29] in combination with StructureViz and RINalyzer.

### **5.9.4. MSA and conservation scores**

For aspartate aminotransferases, multiple sequence alignment was done retrieving all available sequences from the oTAED [30] annotated to be class III transaminases, corresponding to Pfam PF00202 (24998 sequences in total). Multiple sequence alignment was performed using ClustalW with two iterations. The PLP binding site was analysed using

HeTA, CvTA and PFTA crystal structures.

For D-alanine aminotransferases (PF01063) and serine hydroxy methyltransferase (PF00464), the alignment was retrieved from the Pfam database with a total number of 11689 sequences and 7460, respectively. The amino acid conservation in each position was analysed using Bioedit and the graphical visualization was performed with Web Logo [31]. Positions corresponding to the PLP binding site were visualized and analysed using DAAT from *Bacillus* sp. YM-1 crystal structure (PDB: 3DAA) as a model [14] and the serine hydroxy methyltransferase from *Bacillus stearothermophilus* (PDB: 1KKP) [13].

#### **5.9.5. Apo and holo-form calculations**

The ratio of absorbance Abs415/Abs280 was used to assess the percentage of holo-form after purification, with no external PLP. For HeTA, CvTA and its mutants the concentration range was from 5-7 mg/mL while for PFTA and its mutant concentration was 0.7 to 1.2 mg/mL. The values were compared with the same sample after incubation for 12h with 5 mM PLP at 4°C and 1h at 37°C after elimination of unbound or free PLP using gel filtration (PD-10 column purchased from GE Healthcare). The fractions containing the protein were collected and the ratio Abs415/Abs280 measured fixed as being the 100% holo-form.

#### **5.9.6. Cofactor release study**

To a solution of 0.5 mg/mL of the enzyme, 50 mM benzylamine and 0.5 mM of PLP were added. The absorbance was measured every 5 minutes for 4h at 395 nm to monitor the depletion of PLP and at 325 nm to measure the formation of PMP at 25°C using an Epoch 2 microplate reader. The absorbance values were normalized by subtracting the minimum absorbance and dividing by the maximum difference, so all values ranged between 1 and 0.

#### **5.9.7. Temperature stability assays**

The different proteins at a concentration of 1 mg/mL for CvTA and HeTA and 0.1 mg/mL of PFTA in their apo-form were incubated for 30 minutes at different temperatures ranging from 25 to 65 degrees in 50

mM phosphate buffer pH 8 without external PLP. After the incubation, samples were centrifuged to eliminate the precipitated protein and were left in ice for another 30 minutes. The activity was then tested following the formation of acetophenone at 245nm with the standard assay.

#### **5.9.8. Melting temperature and dissociation constant calculations**

Melting temperature ( $T_{1/2}$ ) values were calculated using differential scanning fluorimetry (DSF) using a BioRad C1000™ Thermal cycler and a CFX™96 Real Time System measuring the fluorescence in the range of the SYPRO Orange dye. The sample consisted of 1 mg/mL apo-form protein, 15x Sypro Orange with or without 0.25 mM PLP in 50 mM phosphate buffer pH 8. The melting temperatures were calculated fitting the data to a two-state Boltzmann function using GraphPad Prism™.

$K_d$  values of PLP for the apo form of each protein were calculated using different concentration of PLP (1  $\mu$ M to 250  $\mu$ M) in 50 mM phosphate buffer pH 8. Each sample was prepared with the desired amount of PLP in the same conditions as before. A single-site binding was then used to estimate the  $K_d$  from the  $T_{1/2}$  values obtained using GraphPad Prism™.

## 5.10. Bibliography

1. M. Höhne & U. T. Bornscheuer, Biocatalytic routes to optically active amines. *ChemCatChem*, **1** (2009) 42–51. <https://doi.org/10.1002/cctc.200900110>.
2. A. I. Denesyuk, K. A. Denessiouk, T. Korpela, & M. S. Johnson, Functional attributes of the phosphate group binding cup of pyridoxal phosphate-dependent enzymes. *Journal of Molecular Biology*, **316** (2002) 155–172. <https://doi.org/10.1006/jmbi.2001.5310>.
3. M. S. Humble, K. E. Cassimjee, M. Håkansson, Y. R. Kimbung, B. Walse, V. Abedi, H. J. Federsel, P. Berglund, & D. T. Logan, Crystal structures of the *Chromobacterium violaceum*  $\omega$ -transaminase reveal major structural rearrangements upon binding of coenzyme PLP. *FEBS Journal*, **279** (2012) 779–792. <https://doi.org/10.1111/j.1742-4658.2012.08468.x>.
4. A. C. Eliot & J. F. Kirsch, Pyridoxal Phosphate Enzymes: Mechanistic, Structural, and Evolutionary Considerations. *Annual Review of Biochemistry*, **73** (2004) 383–415. <https://doi.org/10.1146/annurev.biochem.73.011303.074021>.
5. G. Schneider, H. Käck, & Y. Lindqvist, The manifold of vitamin B6 dependent enzymes. *Structure*, **8** (2000) 1–6. [https://doi.org/10.1016/S0969-2126\(00\)00085-X](https://doi.org/10.1016/S0969-2126(00)00085-X).
6. S. Chen, J. C. Campillo-Brocal, P. Berglund, & M. S. Humble, Characterization of the stability of *Vibrio fluvialis* JS17 amine transaminase. *Journal of Biotechnology*, **282** (2018) 10–17. <https://doi.org/10.1016/j.jbiotec.2018.06.309>.
7. L. Cerioli, M. Planchestainer, J. Cassidy, D. Tessaro, & F. Paradisi, Characterization of a novel amine transaminase from *Halomonas elongata*. *Journal of Molecular Catalysis B: Enzymatic*, **120** (2015) 141–150. <https://doi.org/10.1016/j.molcatb.2015.07.009>.
8. A. I. Benítez-Mateos, M. L. Contente, S. Velasco-Lozano, F.

- Paradisi, & F. López-Gallego, Self-Sufficient Flow-Biocatalysis by Coimmobilization of Pyridoxal 5'-Phosphate and  $\omega$ -Transaminases onto Porous Carriers. *ACS Sustainable Chemistry & Engineering*, **6** (2018) 13151–13159. <https://doi.org/10.1021/acssuschemeng.8b02672>.
9. U. Kaulmann, K. Smithies, M. E. B. Smith, H. C. Hailes, & J. M. Ward, Substrate spectrum of  $\omega$ -transaminase from *Chromobacterium violaceum* DSM30191 and its potential for biocatalysis. *Enzyme and Microbial Technology*, **41** (2007) 628–637. <https://doi.org/10.1016/j.enzmictec.2007.05.011>.
  10. N. Ito, S. Kawano, J. Hasegawa, & Y. Yasohara, Purification and Characterization of a Novel ( S )-Enantioselective Transaminase from *Pseudomonas fluorescens* KNK08-18 for the Synthesis of Optically Active Amines. *Bioscience, Biotechnology, and Biochemistry*, **75** (2011) 2093–2098. <https://doi.org/10.1271/bbb.110240>.
  11. F. G. Mutti, C. S. Fuchs, D. Pressnitz, N. G. Turrini, J. H. Sattler, A. Lerchner, A. Skerra, & W. Kroutil, Amination of ketones by employing two new (S)-selective  $\omega$ -transaminases and the his-tagged  $\omega$ -TA from *Vibrio fluvialis*. *European Journal of Organic Chemistry*, (2012) 1003–1007. <https://doi.org/10.1002/ejoc.201101476>.
  12. Shcherbinin D., Veselovsky A. Analysis of Protein Structures Using Residue Interaction Networks. In: Mohan C. (eds) *Structural Bioinformatics: Applications in Preclinical Drug Discovery Process. Challenges and Advances in Computational Chemistry and Physics*, vol 27. (2019) Springer, Cham pp. 55–69. [https://doi.org/10.1007/978-3-030-05282-9\\_3](https://doi.org/10.1007/978-3-030-05282-9_3).
  13. V. Trivedi, A. Gupta, V. R. Jala, P. Saravanan, G. S. Jagannatha Rao, N. Appaji Rao, H. S. Savithri, & H. S. Subramanya, Crystal structure of binary and ternary complexes of serine hydroxymethyltransferase from *Bacillus stearothermophilus*.

- Insights into the catalytic mechanism. *Journal of Biological Chemistry*, **277** (2002) 17161–17169. <https://doi.org/10.1074/jbc.M111976200>.
14. D. Peisach, D. M. Chipman, P. W. Van Ophem, J. M. Manning, & D. Ringe, Crystallographic study of steps along the reaction pathway of D-amino acid aminotransferase. *Biochemistry*, **37** (1998) 4958–4967. <https://doi.org/10.1021/bi972884d>.
  15. R. S. Phillips, Chemistry and diversity of pyridoxal-5'-phosphate dependent enzymes. *Biochimica et Biophysica Acta - Proteins and Proteomics*, **1854** (2015) 1167–1174. <https://doi.org/10.1016/j.bbapap.2014.12.028>.
  16. S. Chen, P. Berglund, & M. S. Humble, The effect of phosphate group binding cup coordination on the stability of the amine transaminase from *Chromobacterium violaceum*. *Molecular Catalysis*, **446** (2018) 115–123. <https://doi.org/10.1016/j.mcat.2017.12.033>.
  17. F. H. Niesen, H. Berglund, & M. Vedadi, The use of differential scanning fluorimetry to detect ligand interactions that promote protein stability. *Nature Protocols*, **2** (2007) 2212–2221. <https://doi.org/10.1038/nprot.2007.321>.
  18. T. Börner, S. Rämisch, E. R. Reddem, S. Bartsch, A. Vogel, A. M. W. H. Thunnissen, P. Adlercreutz, & C. Grey, Explaining Operational Instability of Amine Transaminases: Substrate-Induced Inactivation Mechanism and Influence of Quaternary Structure on Enzyme-Cofactor Intermediate Stability. *ACS Catalysis*, **7** (2017) 1259–1269. <https://doi.org/10.1021/acscatal.6b02100>.
  19. T. Börner, S. Rämisch, S. Bartsch, A. Vogel, P. Adlercreutz, & C. Grey, Three in One: Temperature, Solvent and Catalytic Stability by Engineering the Cofactor-Binding Element of Amine Transaminase. *ChemBioChem*, **18** (2017) 1482–1486.



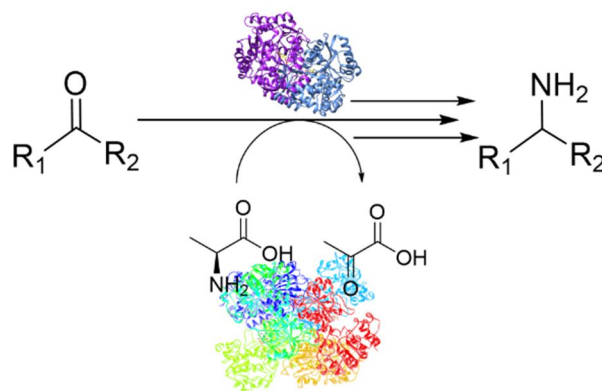
<https://doi.org/10.1002/cbic.201700236>.

20. T. Börner, C. Grey, & P. Adlercreutz, Generic HPLC platform for automated enzyme reaction monitoring: Advancing the assay toolbox for transaminases and other PLP-dependent enzymes. *Biotechnology Journal*, **11** (2016) 1025–1036. <https://doi.org/10.1002/biot.201500587>.
21. M. S. Celej, G. G. Montich, & G. D. Fidelio, Protein stability induced by ligand binding correlates with changes in protein flexibility. *Protein Science*, **12** (2003) 1496–1506. <https://doi.org/10.1110/ps.0240003>.
22. C. Sayer, M. N. Isupov, A. Westlake, & J. A. Littlechild, Structural studies of *Pseudomonas* and *Chromobacterium*  $\omega$ -aminotransferases provide insights into their differing substrate specificity. *Acta Crystallographica Section D: Biological Crystallography*, **69** (2013) 564–576. <https://doi.org/10.1107/S0907444912051670>.
23. Y.-C. Shin, H. Yun, & H. H. Park, Structural dynamics of the transaminase active site revealed by the crystal structure of a co-factor free omega-transaminase from *Vibrio fluvialis* JS17. *Scientific Reports*, **8** (2018) 11454. <https://doi.org/10.1038/s41598-018-29846-0>.
24. G. N. Murshudov, P. Skubák, A. A. Lebedev, N. S. Pannu, R. A. Steiner, R. A. Nicholls, M. D. Winn, F. Long, & A. A. Vagin, REFMAC5 for the refinement of macromolecular crystal structures. *Acta crystallographica. Section D, Biological crystallography*, **67** (2011) 355–67. <https://doi.org/10.1107/S0907444911001314>.
25. E. Krissinel, Stock-based detection of protein oligomeric states in jsPISA. *Nucleic Acids Research*, **43** (2015) W314–W319. <https://doi.org/10.1093/nar/gkv314>.
26. W. Humphrey, A. Dalke, & K. Schulten, VMD: Visual molecular dynamics. *Journal of Molecular Graphics*, **14** (1996) 33–38.

[https://doi.org/10.1016/0263-7855\(96\)00018-5](https://doi.org/10.1016/0263-7855(96)00018-5).

27. W. L. DeLano, Pymol: An open-source molecular graphics tool. *{CCP4} Newsletter On Protein Crystallography*, **40** (2002).
28. M. Planchestainer, E. Hegarty, C. Heckmann, L. Gourlay, & F. Paradisi, Widely applicable background depletion step enables transaminase evolution through solid-phase screening. *Chemical Science*, (2019). <https://doi.org/10.1039/C8SC05712E>.
29. P. Shannon, A. Markiel, O. Ozier, N. S. Baliga, J. T. Wang, D. Ramage, N. Amin, B. Schwikowski, & T. Ideker, Cytoscape: A Software Environment for Integrated Models of Biomolecular Interaction Networks. *Genome Research*, **13** (2003) 2498–2504. <https://doi.org/10.1101/gr.1239303>
30. O. Buß, P. C. F. Buchholz, M. Gräff, P. Klausmann, J. Rudat, & J. Pleiss, The  $\omega$ -Transaminase Engineering Database ( $\omega$ TAED): A navigation tool in protein sequence and structure space. *Proteins: Structure, Function, and Bioinformatics*, (2018) 1–15. <https://doi.org/10.1002/prot.25477>.
31. G. E. Crooks, G. Hon, J. Chandonia, & S. E. Brenner, WebLogo: a sequence logo generator. *Genome research*, **14** (2004) 1188–90. <https://doi.org/10.1101/gr.849004>.

## Chapter 6: In situ recycling of the amino donor for transaminase catalysed reactions



## 6.1. Introduction

## 6.2. Introduction

In transaminase catalysed reactions, when the equilibrium is not favourable for the desired amination, normally an excess of the amino donor is necessary to reach sensible conversions. For example, in the synthesis of sitagliptin, one of the highlights in transaminase biocatalysis, high concentrations of isopropyl amine were needed to achieve the formation of the amine product. As discussed in the Chapter 5, loss of the cofactor caused by high concentrations of the amino donor have been related to poor stability of transaminases. The amino donor can react with the PLP molecule to directly form a Schiff base, sequestering the cofactor from the active site and leaving a more unstable form of the enzyme, prone to inactivation by precipitation or unfolding [1]. As an alternative to this undesired high concentrations of the co-substrate, the possibility to use equimolar or even catalytic amounts of the donor and recycling it in situ has been explored [2-4]. One of the coupled reactions to recycle the amino donor with more promising perspectives is the recycling of amino acids, accepted by transaminases as the donor, catalysed by amino acid dehydrogenases (AADH).

AADHs are an extensive group of oxidoreductases which have found their niche in biocatalytic applications. Not only they can be used as recycling systems, but also for the direct synthesis of enantiopure amino acids and interesting derivatives, such as fluoro-alanine or norvaline [5], or ketoacids [6], which are chemically difficult to access.

From all different AADH known to date, *L*-alanine amine dehydrogenase (AlaDH) is one of the most commonly used and studied, both for its biological importance [5–7] as well as for its biocatalytic potential [3–4]. AlaDHs catalyse the deamination of alanine yielding pyruvate and ammonia but it can also perform the reverse reaction, where ammonia and pyruvate are combined to produce alanine, using an oxidised or reduced adenine cofactor, respectively (Figure 6.1A and 1B). Its capacity to act on both directions, allows the enzyme to be used

as a recycling system in reactions needing both the oxidized and reduced form of the cofactor with the added benefit that it acts on cheap and abundant starting materials [3–4]. More importantly to the focus of this chapter, as hinted before, AlaDH can also be used for the recycling of alanine, one of the most common amino donors used for transaminase catalysed reaction (Figure 6.1C and 6.1D).

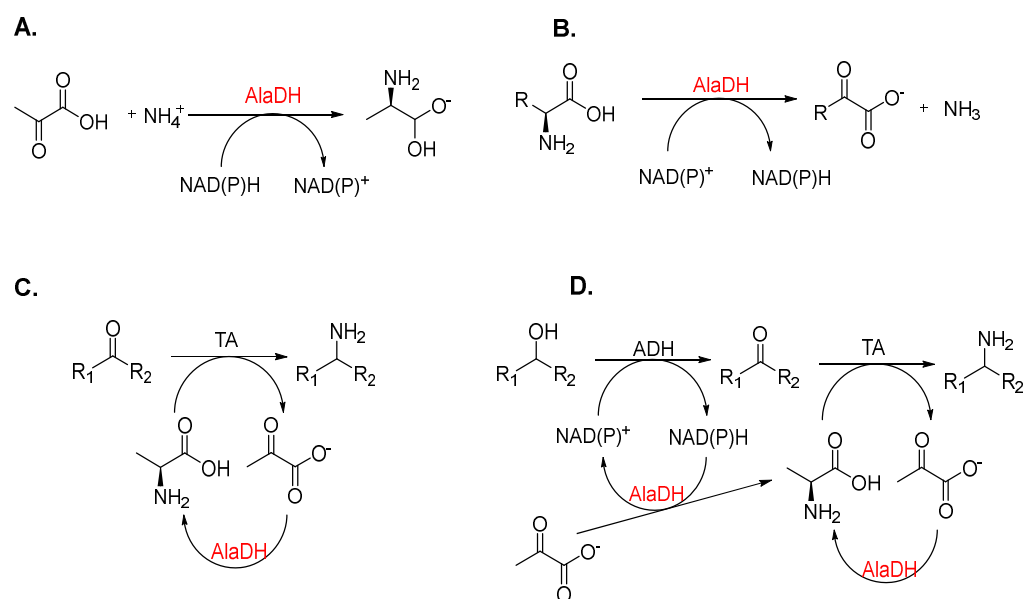


**Figure 6.1.** General scheme of the various applications of alanine dehydrogenases. **A** and **B** depict the use of alanine dehydrogenases for the direct synthesis of amino acids or ketoacids, respectively. In **C** and **D**, the alanine dehydrogenases are used as recycling systems for the main reaction; a transamination in **C** and the reductive amination of an alcohol in **D**.

Nevertheless, these coupled reactions also present some limitations. Among the most important, is the operational stability and reusability of the multiple biocatalysts needed, which depends on the reaction conditions and their intrinsic properties. Therefore, the search for more appropriate biocatalysts is still paramount for the successful application of biocatalytic routes.

Here the cloning and characterisation of a novel AlaDH from the halo adapted bacteria *Halomonas elongata* and its immobilisation is reported. Furthermore, the new AlaDH has been combined in multi-enzymatic cascade with HeTA (a transaminase from the same organism) and CbFDH (formate dehydrogenase from *Candida boidinii*) to access the amination of substrates with unfavourable equilibriums identified during

the initial characterisation of HeTA. The multi-enzymatic synthesis has also been studied in flow in a mixed packed-bed reactor.

The work presented in this chapter is my exclusive contribution unless otherwise stated. Zoya Nisar helped with the initial characterisation of HeAlaDH.

### 6.3. Alanine dehydrogenase cloning and characterisation:

A gene coding for a putative alanine dehydrogenase, helo\_3819, was identified in the genome of *Halomonas elongata* DSM2581. The gene was closely related to two previously characterised AlaDH from *Mycobacterium tuberculosis* [10] and *Bacillus subtilis* [11–12] with 72% and 71% similarity, respectively (56% and 58% of identity).

The gene was successfully cloned into pRSET-B expression vector and the protein expressed with an N-terminal His-tagged in Terrific Broth at 30°C. The protein was purified by IMAC chromatography to more than 90% purity with a yield of 7-8.5 mg/L of culture (

Figure 6.2).

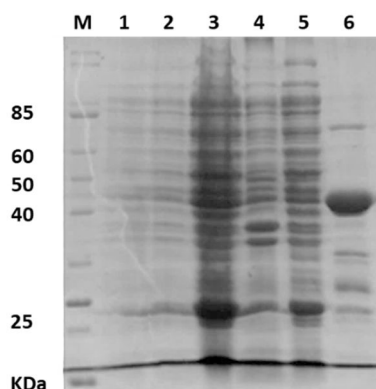
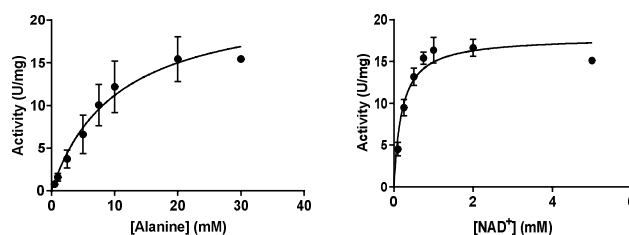


**Figure 6.2.** SDS-page analysis of HeAlaDH expression. M: molecular marker 1: Cell extract after expression; 2: Soluble fraction; 3: Insoluble fraction; 4: Flow through in IMAC; 5: Washing step; 6: Pure protein.

Following its successful expression, the enzyme quaternary structure was confirmed to be a hexamer by size exclusion chromatography, similarly to most alanine dehydrogenases whose oligomeric state and 3D-structure have been solved [13–15].

To functionally characterise the enzyme, kinetics in both directions, varying the concentrations of all substrates, were performed (Figure 6.3). For the cofactors, the amount of alanine was fixed at 40 mM and pyruvate at 2.5 mM. When measuring the kinetics for the natural substrates, 1 mM of NAD<sup>+</sup> or 0.1 mM of NADH were used. Cofactor kinetics were only performed with NAD(H) as HeAlaDH showed complete selectivity for it, with no detectable activity with NADP<sup>+</sup> or NADPH.

#### Oxidative deamination:



#### Reductive amination:

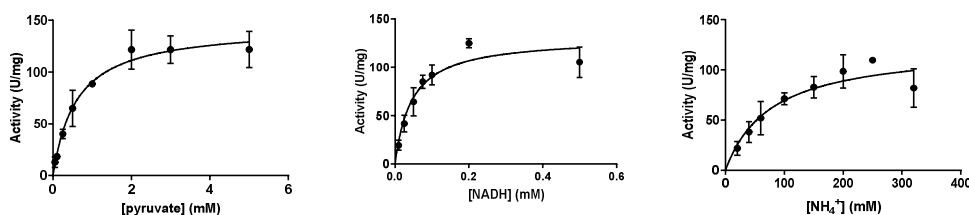


**Figure 6.3.** Kinetic characterisation of HeAlaDH in both the oxidative deamination and the reductive amination direction. Reactions in the oxidative direction were performed at pH 8 while the reductive deamination was performed at pH 10.

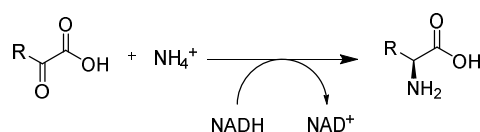
In the deamination direction, HeAlaDH exhibited a  $K_M$  for alanine of  $10.3 \pm 2.4$  mM and of  $0.20 \pm 0.04$  mM for NAD<sup>+</sup>, with specific activity of  $18 \pm 2$  U/mg at pH 8. In the reverse direction, the enzyme was much more active, with a specific activity of  $124 \pm 13$  U/mg at pH 10. Moreover, the affinities for the substrates in the reductive reaction were lower when compared to alanine ( $0.60 \pm 0.11$  mM for pyruvate,  $0.05 \pm 0.01$  mM for NADH) except for ammonia, for which the  $K_M$  was  $77.8 \pm 12.6$  mM. The affinity for the different substrates exhibited by HeAlaDH is very similar to those reported for the homologous proteins from *M. tuberculosis* and *B. subtilis* [16–17]. The only significant difference is for ammonia, for which HeAlaDH exhibits a  $K_M$  almost 2-fold higher than the two other AlaDHs.

Following the results of the kinetics, the standard conditions for the activity assays were defined as 40 mM alanine, 1 mM NAD<sup>+</sup> in phosphate buffer pH 10 in the oxidative reaction and 2.5 mM pyruvate, 250 mM NH<sub>4</sub><sup>+</sup> and 0.1 mM of NADH in carbonate buffer pH 8 in the reductive amination, similarly to the assays performed with the homologous enzymes [17-18].

As many amino acid dehydrogenases can accept structurally similar compounds to their natural substrates [18–19] and to assess HeAlaDH substrate promiscuity, the substrate scope of the new alanine dehydrogenase was explored with analogous compounds to alanine and pyruvate, as well as less related amino acids (Table 6.1).

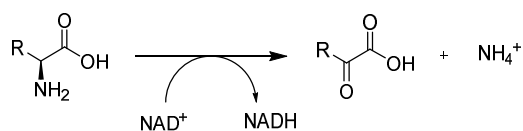
**Table 6.1.** Substrate scope of HeAlaDH in the reductive amination direction (**A**) and oxidative deamination (**B**). The activities were measured using the standard activity assay varying the concentration of the substrate when necessary. A scheme of the reaction is shown on top of the table.

**A.**



Substrate	Concentration (mM)	% activity
Pyruvate 	2.5	100
Hydroxy pyruvate 	2.5	22
Glyoxylate 	2.5	9.4

**B.**



Substrate	Concentration (mM)	% activity
L-alanine 	40	100
L-valine 	100	2.6



<i>L</i> -isoleucine	100	2.5
<i>L</i> -serine	100	1

HeAlaDH exhibited 22% of the activity detected with pyruvate with hydroxy pyruvate and almost 10% of the activity with glyoxylate in the reductive amination. Hydroxy pyruvate yields serine while glyoxylate would yield glycine. On the contrary, from the various amino acids tested, only with *L*-serine, *L*-isoleucine and *L*-valine some activity was detected. The activity was only apparent when using 100 mM of the substrate and HeAlaDH had less than a 3% of the activity exhibited with *L*-alanine. On the other hand, HeAlaDH did not show any activity for *D*-alanine or  $\beta$ -alanine, indicating the enzyme scope is restricted to *L*- $\alpha$ -amino acids. These results indicate that HeAlaDH is very specific for *L*-alanine in the deamination reaction, while for the reductive amination, closely related molecules to pyruvate could also be accepted.

To complete the characterisation, the performance of HeAlaDH under various conditions was measured. HeAlaDH exhibited an outstanding stability with most organic co-solvents (Figure 6.4). This dehydrogenase had a very good resistance to DMSO and various alcohols at 10% and even 20% (v/v) but more surprisingly, the enzyme was very resistant to the presence of MECN and THF at 10% (v/v), with more than 50% of the activity retained after 48h.

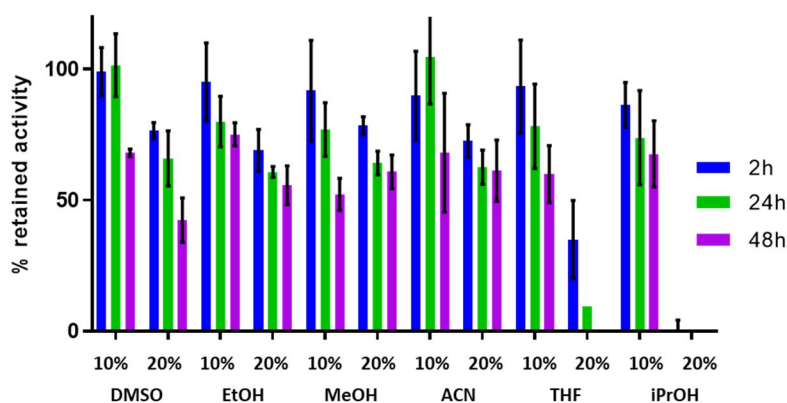


**Figure 6.4.** Cosolvent effect on the stability of HeAlaDH. 0.1 mg/mL of protein was incubated at 4°C for 48h in the presence of 10% or 20% (v/v) of the desired cosolvent.

Activity was tested at different time points using the standard activity assay. The values correspond to the average of 3 replicates.

As for the temperature optimum (Figure 6.5A), HeAlaDH had its maximum activity at 37°C which rapidly dropped by almost 50% at 40°C. Similarly, the enzyme exhibited good stability at temperatures lower than 37°C, with no apparent loss of activity after 48h at 30°C but at higher temperatures, it lost activity much faster as no activity could be detected after 2h at 55°C and only a 40% retained at 40°C after 48h (Figure 6.5B).

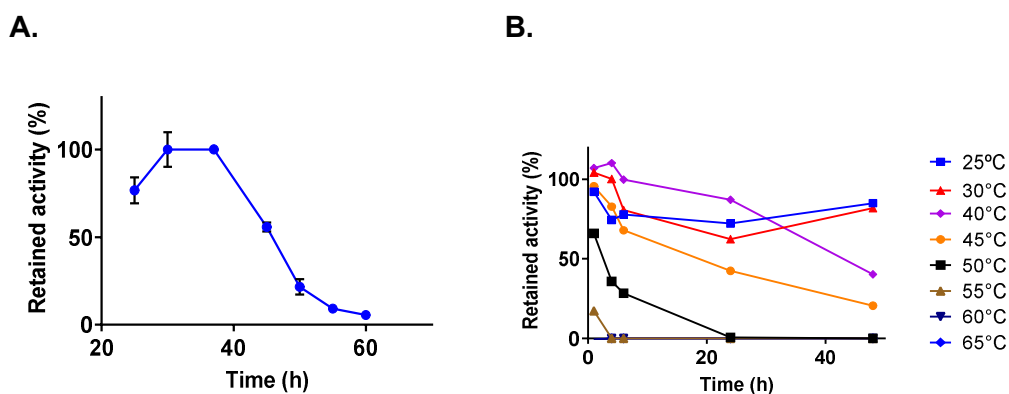


**Figure 6.5. A.** Temperature effect on the activity for He-AlaDH. The standard activity test was performed but all reaction components were incubated at the desired temperature apart from the protein **B.** Temperature stability at different temperatures. For the stability, 0.1 mg/mL of the protein were incubated at the desired temperature. The activity was tested using the standard activity assay at different time points.

Regarding the pH stability (Figure 6.6), HeAlaDH exhibited an excellent stability for 48h at pHs higher than pH 6, with no significant loss of activity observed over 48h between pH 6 and pH 10.

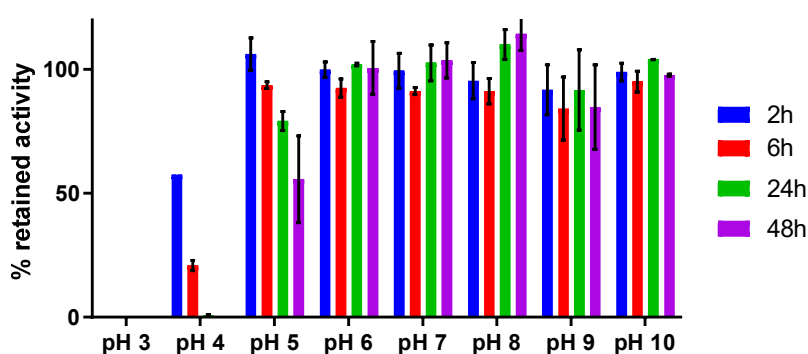


**Figure 6.6.** pH effect on the stability of HeAlaDH. The enzyme was incubated at 4°C for 48h and the activity determined at different time points using the standard activity assay. The values correspond to the average of 3 replicates.

In addition, since the enzyme comes from a halotolerant bacterium, its behaviour in high salt concentration was tested (Figure 6.7). In a similar manner to HeTA and to HeE, previously characterised in Chapter 4, HeAlaDH exhibited a very good activity and stability at molar concentrations of both NaCl and KCl. The activity of the enzyme was almost doubled when the reaction was performed in 1M KCl or NaCl and it exhibited a slight activation when stored for up to 48h in buffer containing 3M NaCl/KCl.

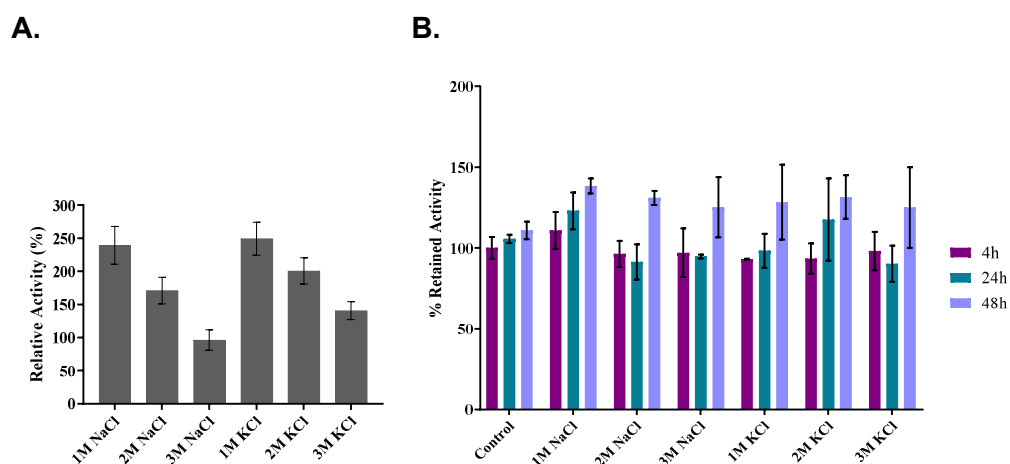


**Figure 6.7. A.** Salt concentration effect on the activity of He-AlaDH. Activity was determined with the standard activity assay with presence of the indicated concentration of salts. **B.** Salt concentration effect on the stability of He-AlaDH. 0.1 mg/mL of protein was incubated with the desired concentration of salt and the activity tested at different time points.

Overall, HeAlaDH exhibited excellent properties to be used in industrial biocatalysis. Specially, its resistance to organic co-solvents and basic pHs makes this enzyme a promising candidate to be applied in transaminase catalysed reactions, which normally require some organic co-solvent to enhance the solubility of the aldehyde or keto-containing substrate.

#### 6.4. Co-substrate recycling for TA catalysed reactions:

In order to exploit the characteristics of HeAlaDH, the transaminase from *Halomonas elongata* was selected. HeTA can accept *L*-alanine as amino donor and exhibits a broad substrate range. Excellent conversions were detected for benzaldehyde, glyoxylate and pyruvate (>95% over 24h) using (*S*)-methylbenzylamine (SMBA) as the amino donor, but more

moderate results were reported for vanillin and cinnamaldehyde, with only 45.5% and 56.1% of the aminated product was formed, respectively. These low conversions were also detected with some aliphatic ketones, such as cyclohexanone (30.5%) or 1,3-dihydroxyacetone (35.3%) [20]. The lower productions were explained by an unfavourable equilibrium and therefore, a method to shift it to the product side is ideal to try to enhance the final conversions.

Thus, with the aim of enhancing the capacity of HeTA to aminate the more challenging substrates, a coupled reaction of HeTA with HeAlaDH was tested. Initial tests were carried out with equimolar amount of NADH but to reduce the costs, a simple cofactor recycling system was added by coupling the reaction with a formate dehydrogenase from *Candida boidinii* (CbFDH) [21] (Figure 6.8). The presence of the sacrificing substrate (formate) did not affect the initial activity or stability of the other two enzymes present in the cascade, indicating good overall compatibility of the system.

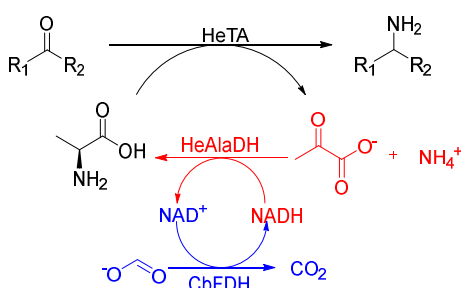


**Figure 6.8.** Scheme of the proposed multi-enzymatic reaction. HeAlaDH reaction is depicted in red and the cofactor recycling system in blue.

At first, to assess the capacity of HeTA to aminate vanillin with different equivalents of alanine, as well as the effect of the presence of the amino donor recycling system were tested with a fixed concentration of 10 mM of aldehyde (Figure 6.9).

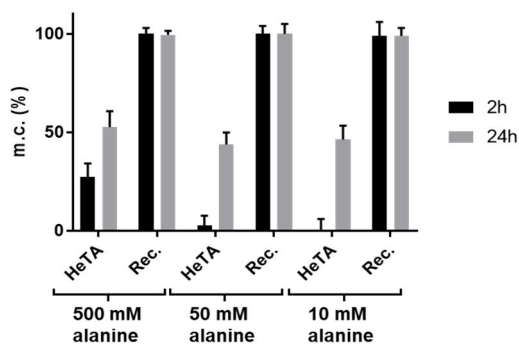


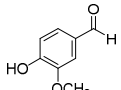
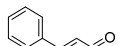
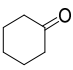
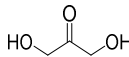
**Figure 6.9.** 10 mM of vanillin conversion in batch with different amounts of alanine with a fixed concentration of 1 mM of NAD<sup>+</sup>. Conversions are expressed as % of molar conversion. The presence of the alanine recycling system is indicated as Rec. in comparison to HeTA alone. The reactions contained 2 mg/mL of HeTA with 0.5 mg/mL of HeAlaDH, 1 mg/mL of CbFDH in the whole cascade assembly.

HeTA, in the absence of any concomitant enzymatic coupled reaction and independently of the amount of alanine used, reached the equilibrium when almost half of vanillin was converted. On the other hand, only when 50 equivalents of the amino donor were used (500 mM alanine), noticeable substrate consumption was detected after 2h of reaction ( $27 \pm 7\%$ ). With 5 or 1 equivalent, the reaction occurred much slower but reached the same equilibrium point. Remarkably, when the reaction was combined with HeAlaDH and CbFDH even with just equimolar amount of alanine, all the substrate was consumed during the first 2h. These results indicate that removing pyruvate and regenerating the amino donor, increases HeTA's capacity to aminate vanillin even faster than the presence of 50 equivalent of amino donor.

With the promising results obtained with vanillin, the substrate scope of the reaction was expanded to the other aldehydes and ketones. In some cases, optimisation of the aldehyde or ketone and the alanine concentration was needed (Table 6.2).

**Table 6.2.** Results of the amination of aldehydes and ketones by HeTA without (-) and in the presence (+) of the alanine recycling system. The reaction contained 2 mg/mL of HeTA, 0.5 mg/mL of HeAlaDH, 1 mg/mL of CbFDH with the desired concentration of the amino acceptor and alanine, with 1 mM NAD<sup>+</sup> in 100 mM phosphate buffer pH 8. Results are reported as percentage of conversion. The results from Cerioli *et al.* correspond to the biotransformation of 10 mM of substrate with equimolar amount of SMBA and 0.1 mg/mL of HeTA.

Substrate	L-Ala (mM)	m.c. conversion (%)	
		2h	24h

			HeAlaDH		HeAlaDH		Cerioni <i>et al.</i> 2015 [20]
			-	+	-	+	
Vanillin (10 mM)		10	>5 %	>99 %	46 %	>99 %	45.5
Cinnamaldehyde (10 mM)		10	39 %	>99 %	71 %	>99 %	56.1
Cyclohexanone (10 mM)		10	>5 %	28 %	>5 %	84 %	30.5
		100	6 %	56 %	7 %	95 %	
1,3-dihydroxyacetone (100 mM)		100	>5 %	>5 %	>5 %	24 %	35.3 <sup>2</sup>

<sup>2</sup>Conversion with 10 mM of the substrate.

For cinnamaldehyde, similar to what was observed for vanillin, the alanine recycling system not only pushed the reaction to completion but also diminished the reaction time significantly. After only two hours of reaction, complete conversion to cinnamyl amine was observed with the whole system, while only 39% of conversion is achieved using HeTA alone. As for the ketones, the system pushed the conversion of the cyclic ketone cyclohexanone from less than 10% to 84% when only one equivalent of alanine was used and to almost complete conversion when 10 equivalents of the amino donor were used. These conversions are almost a 3-fold improvement of the conversions obtained previously with 10 mM SMBA. For 1,2-dihydroxyacetone, no conversion was observed when only 10 mM of the substrate was used but increasing the concentration to 100 mM yielded 24% of conversion compared to <5% observed with HeTA alone. This conversion, though, was lower than that obtained with 1 equivalent of SMBA on a 10 mM scale (35.3 ± 1.5%). Thus, the multi enzymatic recycling of the amino donor was proved to be useful and applicable to three of the four substrates tested with excellent improvement of the final conversion and decreased reaction time.

Although equimolar amount of alanine offers already an advantage, since the system should be constantly producing alanine, the capacity of the multi-enzymatic system to operate with sub-stoichiometric amounts of alanine was tested (Figure 6.10). Amazingly, similar to what was

observed with 10 mM of alanine (1 eq.), with only 1 mM of alanine, the conversion of cinnamaldehyde was complete after only 1h of reaction.

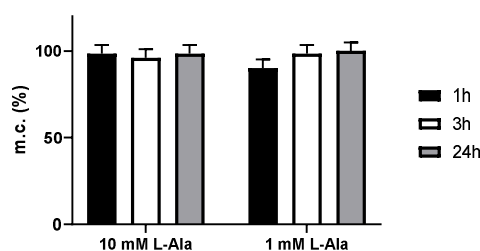


**Figure 6.10.** Amination of cinnamaldehyde equimolar and sub stoichiometric amount of the alanine as the amino donor. The reaction contained 1 mg/mL of HeTA, 0.5 mg/mL of HeAlaDH, 1 mg/mL of CbFDH with 10 mM of cinnamaldehyde and the desired concentration of alanine in 100 mM phosphate buffer pH 8. Results are reported as the percentage of conversion.

Following these encouraging results, to increase the sustainability and applicability of the system, immobilisation of the three enzymes was attempted. Immobilisation would allow for the recovery and reuse of the biocatalysts, and potentially translate in better productivities. At first, immobilisation of the three biocatalysts separately was attempted, as both HeTA and CbFDH immobilisation had been previously described. While co-immobilisation is known to enhance the overall reaction speed [22], at first, the focus was to achieve the maximum activity for the three enzymatic components of the reaction [23–24]. Thus, the focus was brought to HeAlaDH immobilisation.

### 6.5. HeAlaDH immobilisation:

Initial test for the immobilisation of HeALaDH were performed using the poly-methacrylate based resins from Resindion S.R.L. (for more details refer to Table 3.5 in Materials and Methods). Both resins with different pore size, functional groups and oxirane content were tested. In addition the loading of the protein was also varied in the same support to find the best immobilisation conditions (Figure 6.11).

A.

B.

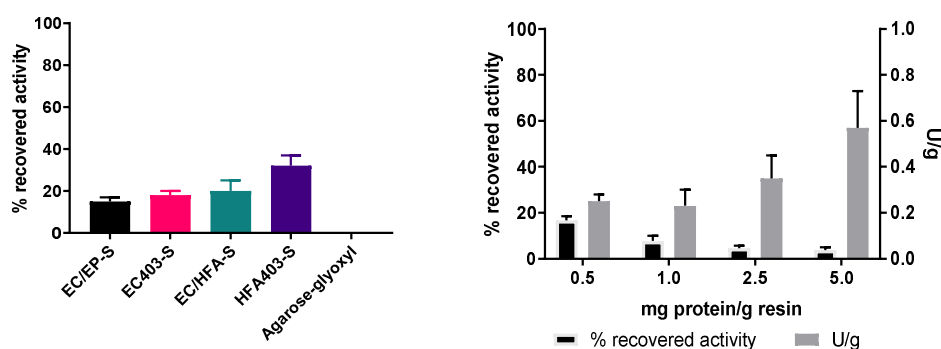


**Figure 6.11. A.** Results of the immobilisation of HeAlaDH in different supports and **B.** The effect of the loading in the recovered activity and the specific activity of the biocatalyst (U/g of resin).

The best result was obtained when immobilising onto HFA403-S, with up to  $32 \pm 2\%$  recovered activity. Differently from EC/EP-S or EC403-S, which showed the lowest recovered activities, HFA403-S and EC/HFA-S are derivatised with amino epoxy groups. Comparing the two amino-epoxy resins, the difference in the recovered activities between can be explained by their pore size, as HFA403-S pores are 3 times bigger than EC/HFA-S. This altogether indicates that HeAlaDH, probably due to its quaternary assembly as a hexamer, recovers most of its activity when the immobilisation is performed onto more flexible anchoring groups, such as amino epoxides, and less space-restrictive resins, indicated by its preference for bigger pores.

As per the loading (Figure 6.11B), although increasing it up to 5 mg/g of resin, increased the specific activity of the biocatalyst almost 3-fold compared to the 0.5 mg/g, the recovered activities dropped to less than 5% and did not correlate with the 10-fold higher loading of protein. The low recovered activities could be due to a distortion of the enzymatic structure due to the high density of anchoring groups, especially relevant in multimeric enzymes, as well as flexible proteins. Decreased flexibility not only affects the catalytic activity, but the proteins can lose their active conformation once immobilised. This loss of structure can be caused either by their interaction with the surface or by the covalent multi point attachment and it normally has a bigger effect when the multimeric unit is the catalytically active one, such as in HeAlaDH. Moreover, at high



loadings, diffusion problems might occur, diminishing the calculated activities. If the enzyme forms multilayers or enzymatic clusters, the impediment of the substrate diffusion, would provoke a portion of the immobilised enzyme to be catalytically inactive [25–27].

For these reasons, the loading was fixed at 0.5 mg/g of resin. Nonetheless when the same batch of immobilised enzyme was used repeatedly, another issue arose: the biocatalyst lost 50% of activity just after 3 cycles (Figure 6.12A).

The activity loss was confirmed to be due to protein leaching by boiling the resin for 10 minutes at 95°C (Figure 6.12B). This indicates that not all HeAlaDH subunits are covalently bound to the resin. Most likely, only a portion of the subunits are covalently attached through their superficial lysine while the rest are kept in position through the weaker inter subunit interactions. The loss of activity observed indicates that these weak interactions are not sufficient to keep the enzyme in its active conformation. This issue, has been previously reported for multimeric enzymes upon immobilisation and several strategies have been developed to avoid the subunit dissociation and the subsequent enzyme inactivation [28].

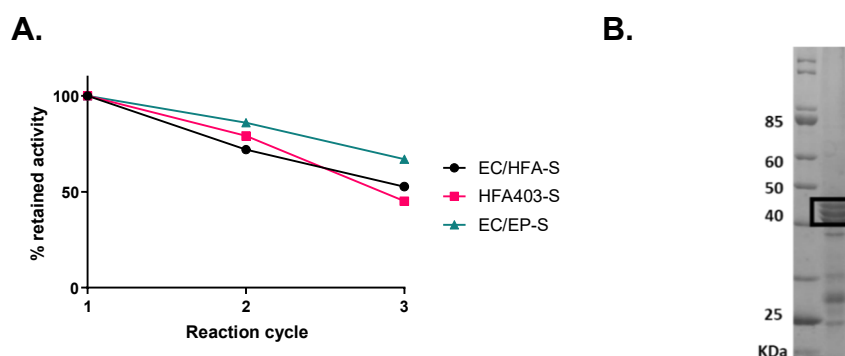


**Figure 6.12. A.** Operational stability of the biocatalyst during three cycles with different supports. 100% activity is referred as the initial activity of the biocatalyst. **B.** SDS-PAGE analysis of the HFA403-S. The first lane corresponds to the molecular markers and the second corresponds to the supernatant of a boiled sample (10 minutes at 95°C) of 20 mg of HFA403-HeAlaDH in 200  $\mu$ L. The band corresponding to HeAlaDH is indicated with a black box.

### 6.6. Post-immobilisation stabilisation:

One of broadly used strategies to avoid subunit dissociation is the coating of the enzyme with a polymer after immobilisation. These

techniques take advantage of poly-charged or functionalised polymers to interact with the surface of the different enzymatic subunits to crosslink them together and avoid their dissociation and/or enhance the resistance to harsh conditions [28–31][28][28].

For the stabilisation through ionic interactions, polyethyleneimine (PEI) is the most used polymer. PEI interacts with the negatively charged residues on the surface (glutamic acid and aspartic acid residues, mainly) to create a mesh that would keep the subunits together. Instead, for covalent coating, 50% oxidised dextran (dexCHO) and glutaraldehyde (GA) are the most common crosslinkers. Both dexCHO and GA have aldehyde groups which react with the free lysines on the surface of the enzyme to form a Schiff base that can be reduced to form a stable covalent link. It is important to note that the covalent linkers mentioned rely on the same reactivity as the immobilisation strategy used, where the epoxide or amino epoxide groups of the resin react with the superficial lysines of the enzyme. To evaluate the feasibility of both coatings, the distribution of these residues on the surface of HeAlaDH was analysed using a homology model based on *M. tuberculosis* (PDB id: 2VHW) [10] (Figure 6.13).

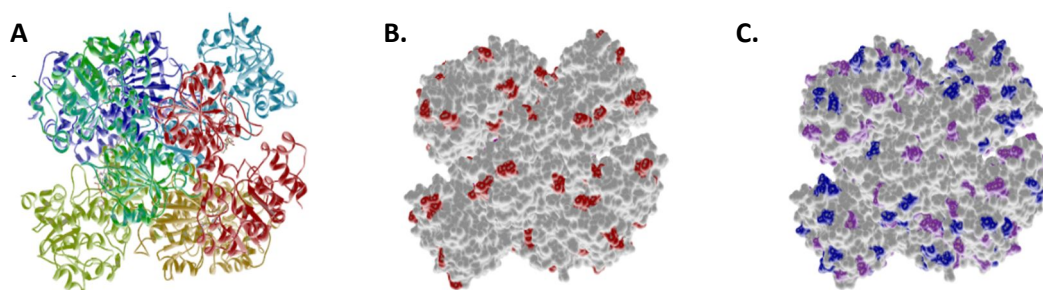


**Figure 6.13.** **A.** Three-dimensional structure of HeAlaDH. **B.** Three-dimensional surface representation where lysines on the surface are indicated in red colour. **C.** Three-dimensional surface representation of HeAlaDH where aspartic acid residues on the surface are coloured in blue while glutamic acid residues are coloured in purple.

As it can be seen, HeAlaDH presents several lysines on the surface of the hexameric unit, which could allow for the immobilisation and the post-immobilisation coating with poly-aldehyde polymers. Similarly, negatively charged residues are abundant on the surface, which enables the ionic-driven coating using the polycationic polymer PEI.

Hence, with an enzyme loading set at 0.5 mg/g of HFA403-S resin, the different post-immobilisation coating strategies were tested.

**Table 6.3.** Recovered activity for the different post-immobilisation techniques used with the HFA403-S resin with a loading of 0.5 mg enzyme/g of resin. The results correspond to the mean of two measurements.

<b>Resin + coating</b>	<b>% recovered activity</b>
<b>HFA403-S</b>	36 ± 7
<b>HFA403-S+GA</b>	21 ± 3
<b>HFA403-S+PEI</b>	27 ± 2
<b>HFA403-S+dexCHO</b>	31 ± 1
<b>HFA403-S+dexCHO+PEI</b>	39 ± 7
<b>HFA403-S+PEI+ dexCHO</b>	33 ± 3

The results, presented in Table 6.3, show that while glutaraldehyde had a negative effect, diminishing the recovered activity of the biocatalyst, dexCHO did not affect the biocatalyst activity compared to the control. Both dexCHO and GA have the same functionality and depend on the same reactivity, but their size is very different. dexCHO is a branched polysaccharide while GA is a small molecule that could intrude inside the enzyme structure and even the active site, possibly reacting with also internal lysines which could ultimately be affecting the enzyme structure and consequently, its activity. The coating with PEI also caused a slightly lower recovered activity compared to the untreated sample (27 ± 2% compared to 36 ± 7 %). Double coating was also tested, to evaluate if both polymers had a synergistic effect, but the calculated recovered activities were not different from the untreated sample or the dexCHO.

Following the recovered activity calculations, enzyme leaching as well as reusability of the immobilised enzyme were tested (Figure 6.14).

**A.**

**B.**

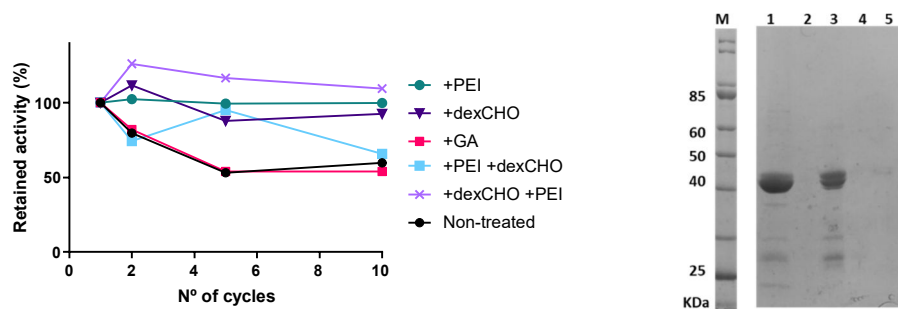


**Figure 6.14. A.** Operational stability expressed as the retained activity after 10 cycles of reaction. 100% is defined as the initial activity of each resin in the 1<sup>st</sup> cycle. **B.** SDS-PAGE analysis of the immobilised biocatalysts. The supernatant of a boiled sample (10 minutes at 95°C) of 20 mg of each sample in a final volume of 200 µL was loaded. M: molecular markers; 1: PEI; 2: dexCHO; 3: PEI+dexCHO; 4: dexCHO+PEI; 5: GA.

For the operational stability, treatment of the sample with either dexCHO or PEI increased the reusability of the biocatalyst with no loss of activity after 10 cycles, where the untreated sample lost almost half of its activity. This same behaviour was seen for the double coating when dexCHO was used first followed by PEI, while when inverting the order, the biocatalyst loses activity similarly to the untreated sample. Also, the sample treated with GA exhibits the same loss of activity at the 10<sup>th</sup> cycle as the biocatalyst with no post-immobilisation coating. Combined with the results of the SDS-PAGE analysis, it appears that the treatment with PEI stabilises the enzyme through weak interactions which are broken after boiling the sample but strong enough to keep the active unit of the enzyme through multiple reaction cycles. Instead, dexCHO and GA keep all the subunits attached to both the resin or to each other, with no protein detected in the gel even after boiling. Since the double coating using dexCHO and PEI does not seem to further enhance either the recovered activity or the operational stability, HFA403-S+HeAlaDH+dexCHO was selected for further experiments.

The behaviour of the heterogeneous biocatalyst under flow conditions (Figure 6.15) was then evaluated to see if the robustness exhibited after repeated batch reactions was maintained. Confirming the increased robustness, after more than 5h of continuous use with flow rates between 0.100 and 0.376 mL/min, the biocatalyst maintained 65% of its activity.

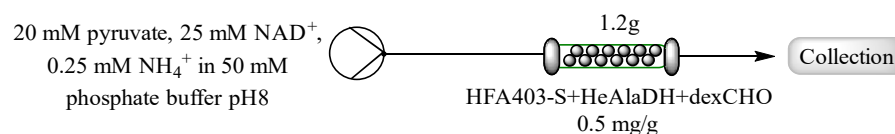


**Figure 6.15.** Scheme of the arrangement of the flow-assisted amination of pyruvate using the optimised immobilisation strategy for HeAlaDH.

### 6.6.1. Flow assisted amination with a mixed packed-bed reactor

With the optimised immobilisation strategy for HeAlaDH, the amination of the substrates presented in Table 6.2 were tested in flow with a mixed packed-bed reactor with each enzyme immobilised under its optimal conditions. The set up and the specifics about the immobilisation are detailed in Table 4. It is important to note that while the activity of the immobilised HeAlaDH is measured in the oxidative deamination direction for convenience, in the multi-enzymatic system HeAlaDH has to act in the reverse direction (aminating pyruvate) for which the free enzyme presents a specific activity of  $120 \pm 8$  U/mg, nearly 30 times higher than the calculated in the oxidative direction at pH 8.

Unfortunately, when tested under those conditions, no amination of any of the tested substrates could be detected. Since EC/HFA-S+CbFDH presented a low activity, to rule out the possibility that the cofactor recycling was the limiting step, the reaction was also carried out with equimolar amount of NADH, but no enhancement of the final conversions was observed. One of the explanations, could be the poor interaction between the three enzymes involved in the system. HeAlaDH needs to act on the pyruvate formed by HeTA during the transamination reaction and CbFDH is needed to keep the pool of reduced cofactor for HeAlaDH, therefore, efficient regeneration of the cofactor is crucial to keep HeAlaDH active and affect the equilibrium. In the literature, enhanced recycling of either co-substrates or cofactors has been previously related to the co-immobilisation of the enzymes involved [32–33]. Thus, in order to try to improve the cascade performance in flow, the co-immobilisation of the cofactor recycling system (HeAlaDH and CbFDH) was tested

**Table 6.4.** Recovered activities and specific activity of the biocatalysts of the three different enzymes. The flow set up and the reaction conditions are depicted above the table.

10 mM ketone or aldehyde,  
10 mM alanine, 1 mM NAD<sup>+</sup>,  
0.25 mM NH<sub>4</sub><sup>+</sup>, 0.1 mM PLP  
in 50 mM phosphate buffer pH8

Enzyme	Resin	Immobilised enzyme		
		Loading	Recovered activity	U/g
HeTA	EC403-S	5	40 %	8.4 ± 0.7
HeAlaDH	HFA403-S	1	32 %	1.2 ± 0.1
CbFDH	EC/HFA-S	5	12 %	0.8 ± 0.2

### 6.6.2. Co-immobilisation of AlaDH and FDH:

The co-immobilisation of the two dehydrogenases was tried with three different resins: the best for the immobilisation of HeAlaDH (HFA403-S), the best reported for CbFDH (EC/HFA-S) [24] and HFA112, which is also derivatised with amino epoxy groups but has a pore size which is in the middle of the other two (see Table 3.5 in Materials and Methods). Moreover, three different approaches for the immobilisation were tested: a sequential immobilisation, first either with CbFDH or HeAlaDH followed by immobilisation of the second enzyme, or simultaneous immobilisation, mixing both enzymes with the support at the same time. In all the preparations, a post-immobilisation coating with dextran was applied.

In the tested conditions, and with a loading of 1 mg of enzyme per gram of resin, all HeAlaDH got immobilised in the first 4h. On the contrary, with a loading of 5 mg/g of resin not all CbFDH got immobilised and even increasing the immobilisation time to 48h did not change the final yield (Table 6.5).

**Table 6.5.** Percentage of CbFDH immobilised in the different co-immobilisation strategies.

	Immobilisation yield (%)		
	Sequential immobilisation (CbFDH + HeAlaDH)	Sequential immobilisation (HeAlaDH + CbFDH)	Simultaneous immobilisation
HFA403-S	88 ± 1 %	64 ± 5%	46 ± 2 %
EC/HFA-S	26 ± 7 %	82 ± 11%	27 ± 1 %
HFA112-S	35 ± 9 %	40 ± 1%	29 ± 4 %

This difference in the immobilisation yield cannot be explained by the immobilisation strategy, as both proteins were immobilised with the same method directed by the His-tag. One of the explanations could be the reactivity and density of the surface lysines with the amino-epoxide groups in the support but curiously, both the distribution and number of lysines is similar in both HeAlaDH and CbFDH (Figure 6.16).

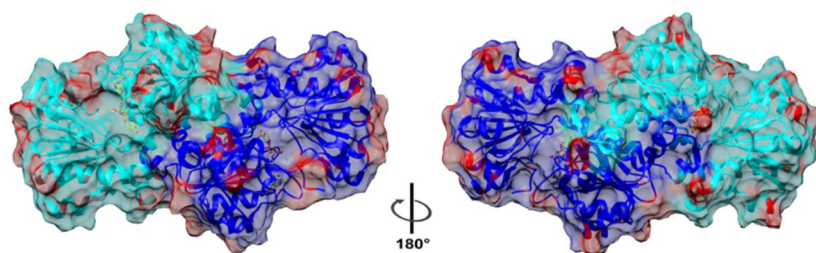


**Figure 6.16.** Representation of the surface of CbFDH based on its crystal structure (PDB: 5DN9) [34]. The two different chains are shown in different shades of blue. Lysines are coloured red and the cofactor is depicted in yellow.

Despite the low immobilisation yield recorded in some cases for CbFDH, the biocatalysts exhibited activity for both alanine and formate. All preparations yielded biocatalyst with similar specific activities (Figure 6.17). It is important to note that the activities for HeAlaDH were calculated in the deamination direction as the presence of CbFDH hampers the measurement of pyruvate reductive amination. To ensure that the proteins were covalently bound, similarly to the initial tests with HeAlaDH, 20 mg of resin in 200  $\mu$ L of 50 mM phosphate buffer pH 8 were incubated for 10 minutes at 95°C. Similarly to the results with HeAlaDH alone, with the dextran coating no protein leaching was detected in any of the preparations.

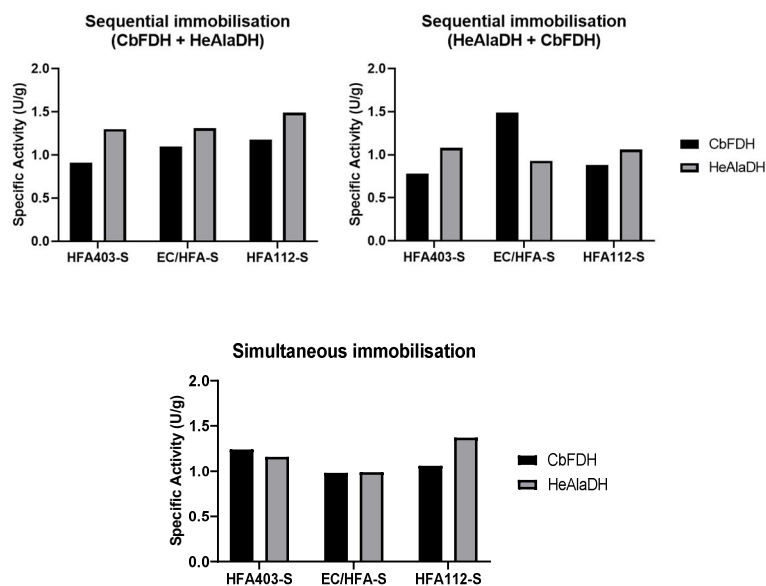


**Figure 6.17.** Specific activities of the heterogenous biocatalyst after immobilisation of both enzymes. The strategy of immobilisation is detailed in top of each graph. Activities were measured using the standard activity assay for each enzyme using the same sample.

From the results, the best biocatalyst from each strategy considering both the recovered activity of HeAlaDH and CbFDH (HFA112-S for the sequential immobilisation adding first CbFDH, EC/HFA-S for sequential immobilisation when HeAlaDH was added first and HFA403-S for the simultaneous immobilisation) were selected to be tried in flow as a mixed packed-bed reaction with EC403-S+HeTA, as depicted in Figure 6.18.

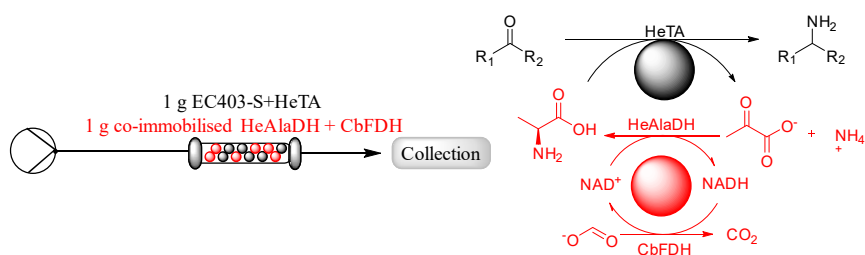


**Figure 6.18.** Flow set up for the amination of aldehydes or ketones with in-situ recycling of the cofactor. A scheme of the desired reaction is also shown.

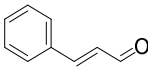
As a control, 1.5g of EC403-S+HeTA was tested alone under the same reaction conditions. Interestingly, only when using the simultaneous co-immobilised system, conversion of the desired aldehydes or ketones to amines was detected (Table 6.6).

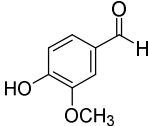
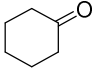


Not surprisingly, HeTA alone, with equimolar amount of alanine was not capable of aminating any of the tested substrates. For the tested aldehydes, previous attempts to aminate either of them, required 50 equivalents of alanine to observe any conversion. It is significant that for vanillin, even after two consecutive runs through the column with such an excess of the amino donor only yielded 50% of conversion [23]. Again, with HeTA alone, no conversion was observed with cyclohexanone at 10- or 20-minutes residence time.

The addition of the in-situ amino-donor recycling system indeed pushed the unfavourable equilibrium towards the amination of the products. For cinnamaldehyde, almost complete conversion was observed with a 10 minutes residence time and for the more challenging aldehyde, vanillin, 55% molar conversion was obtained with a 10 minutes residence time. At higher retention time, interestingly, the conversion dropped to 23%. It could be possible that the longer retention times promotes also the deamination of the formed substrate by HeTA, competing with HeAlaDH for the pyruvate and thus reducing the final amount of vanillin amine formed. Conversely, with cyclohexanone, while the batch reaction yielded more than 80% conversion at the 10 mM, the maximum conversion observed was 56% with a 20 minutes residence time.

**Table 6.6.** Results from the flow assisted amination using 1g of EC403-S+HeTA and 1g of simultaneously co-immobilised HeAlaDH and CbFDH in HFA403-S. The reactions were performed at 37°C with the desired concentration of substrate and equimolar amount of alanine, 0.1 mM PLP, 1 mM NADH, 250 mM NH<sub>4</sub><sup>+</sup>, 250 mM formate in 100 mM phosphate buffer pH 8.

Substrate	RT	Molar conversion (%)		
		HeTA	Rec.	
Cinnamaldehyde (10 mM) <sup>1</sup>		10 mins	< 5%	92 ± 4 %
Vanillin (10 mM) <sup>1</sup>	10 mins	< 5%	55 ± 12 %	

		20 mins	< 5%	23 ± 2 %
<b>Cyclohexanone (10 mM)</b>		10 mins	< 5%	42 ± 2 %
		20 mins	< 5%	56 ± 1%

<sup>1</sup>The aromatic substrates tested interacted with the resin. The conversions were calculated from the substrate depletion after at least 6 column volumes, when the substrate concentration was constant after collection.

In summary, in this chapter the successful cloning, characterisation and immobilisation of a new *L*-alanine dehydrogenase from *H. elongata* (HeAlaDH) is reported. Remarkably, the enzyme exhibited excellent resistance to both organic co-solvents and basic pH which highlighted its potential application in non-standard conditions. HeAlaDH, once immobilised, required a post-immobilisation coating to enhance its operational stability. From the three coatings tested, dextran was identified as the most favourable. Initial test in batch indicated the suitability of HeAlaDH combined with HeTA and CbFDH for the amination of challenging substrates with unfavourable equilibrium. For its application in flow, co-immobilisation of CbFDH and HeAlaDH was necessary to create a biocatalyst capable of recycling alanine and the adenine cofactor efficiently. Using only 1 equivalent of alanine, complete conversion to cinnamyl amine was achieved as well as more than 50% molar conversion for both vanillin amine and cyclohexylamine.

## **6.7. Experimental procedures**

### **6.7.1. Coating of immobilised HE-AlaDH with polyethyleneimine**

After the immobilisation, 10 volumes of 5 mg/mL PEI in 100 mM carbonate buffer pH 10 were mixed with the resin for 1h at RT. After that, the resin was filtered and washed thoroughly with water and 50 mM phosphate buffer pH 8 and stored at 4°C in the 50 mM phosphate buffer pH 8.

### **6.7.2. Coating of immobilised HE-AlaDH with glutaraldehyde**

After the immobilisation, 10 volumes of 5 mg/mL glutaraldehyde in 50 mM phosphate buffer pH 8 were mixed with the resin for 1h at RT. Sequentially, 1 mg/mL of sodium borohydride was added, and the mix shaken gently for 20 minutes. After that, the resin was filtered and washed thoroughly with water and 50 mM phosphate buffer pH 8 and stored at 4°C in the 50 mM phosphate buffer pH 8.

### **6.7.3. Coating of immobilised AlaDH with dextran poly-aldehyde:**

The coating method was modified from previously reported protocols [28-31]. For 100 mg of immobilised resin 500µL of 50 mM phosphate buffer pH 8 along with the appropriate amount of dextran poly-aldehyde were left stirring O/N. After that, 1 mg/mL of sodium borohydride was added along with 50µL of 900 mM bicarbonate buffer pH 10 and the mix was left stirring at 4°C for 25 minutes before it the biocatalyst was washed thoroughly with water and stored in 50 mM phosphate buffer pH 8.

### **6.7.4. Co-immobilisation of HeAlaDH and CbFDH:**

The co-immobilisation of HeAlaDH and CbFDH was tested with three different approaches:

- To the previously activated support, a loading of 5 mg/g of resin of CbFDH was added and left mixing overnight at room temperature. After that, the percentage of immobilised protein was assessed with both the remaining activity and the protein concentration in the supernatant. Then, 1 mg/g of resin of HeAlaDH was added and left mixing with the support for 4h, when

all the protein was immobilised. Desorption and blocking were performed as explained before for HeAlaDH.

- To the previously activated support, a loading of 1 mg/g of resin of HeAlaDH was added and left mixing for 4h at room temperature, when all the protein was immobilised. Then, 5 mg/g of resin of CbFDH was added and left mixing with the support for overnight and the percentage of immobilised protein was assessed with both the remaining activity and the protein concentration in the supernatant. Desorption and blocking were performed as explained before for HeAlaDH.
- To the previously activated support, a loading of 2 mg/g of resin of HeAlaDH and 5 mg/g of resin of CbFDH was added and left mixing with the support for overnight and the percentage of immobilisation of each protein was assessed with both the remaining activity and the protein concentration in the supernatant. Desorption and blocking were performed as explained before for HeAlaDH.

## 6.8. Bibliography

1. T. Börner, S. Rämisch, E. R. Reddem, S. Bartsch, A. Vogel, A. M. W. H. Thunnissen, P. Adlercreutz, & C. Grey, Explaining Operational Instability of Amine Transaminases: Substrate-Induced Inactivation Mechanism and Influence of Quaternary Structure on Enzyme-Cofactor Intermediate Stability. *ACS Catalysis*, **7** (2017) 1259–1269. <https://doi.org/10.1021/acscatal.6b02100>.
2. D. Koszelewski, I. Lavandera, D. Clay, G. M. Guebitz, D. Rozzell, & W. Kroutil, Formal asymmetric biocatalytic reductive amination. *Angewandte Chemie - International Edition*, **47** (2008) 9337–9340. <https://doi.org/10.1002/anie.200803763>.
3. N. Richter, J. E. Farnberger, D. Pressnitz, H. Lechner, F. Zepeck, & W. Kroutil, A system for  $\omega$ -transaminase mediated (*R*)-amination using *L*-alanine as an amine donor. *Green Chemistry*, **17** (2015) 2952–2958. <https://doi.org/10.1039/C4GC02363C>.
4. S. Klätte & V. F. Wendisch, Role of *L*-alanine for redox self-sufficient amination of alcohols. *Microbial Cell Factories*, **14** (2015) 1–10. <https://doi.org/10.1186/s12934-014-0189-x>.
5. S. Velasco-Lozano, E. S. da Silva, J. Llop, & F. López-Gallego, Sustainable and continuous synthesis of enantiopure *L*-amino acids using a versatile immobilised multi-enzyme system. *ChemBioChem*, **19** (2017) 395–403. <https://doi.org/10.1002/cbic.201700493>.
6. E. S. da Silva, V. Gómez-Vallejo, J. Llop, & F. López-Gallego, Structural, kinetic and operational characterization of an immobilized *L*-aminoacid dehydrogenase. *Process Biochemistry*, **57** (2017) 80–86. <https://doi.org/10.1016/j.procbio.2017.03.005>.
7. M. M. Giffin, L. Shi, M. L. Gennaro, & C. D. Sohaskey, Role of Alanine Dehydrogenase of *Mycobacterium tuberculosis* during Recovery from Hypoxic Nonreplicating Persistence. *PLoS ONE*,

- 11 (2016) 1–18. <https://doi.org/10.1371/journal.pone.0155522>.
8. J. H. Sattler, M. Fuchs, K. Tauber, F. G. Mutti, K. Faber, J. Pfeffer, T. Haas, & W. Kroutil, Redox self-sufficient biocatalyst network for the amination of primary alcohols. *Angewandte Chemie - International Edition*, **51** (2012) 9156–9159. <https://doi.org/10.1002/anie.201204683>.
  9. K. Tauber, M. Fuchs, J. H. Sattler, J. Pitzer, D. Pressnitz, D. Koszelewski, K. Faber, J. Pfeffer, T. Haas, & W. Kroutil, Artificial multi-enzyme networks for the asymmetric amination of sec-alcohols. *Chemistry - A European Journal*, **19** (2013) 4030–4035. <https://doi.org/10.1002/chem.201202666>.
  10. D. Ågren, M. Stehr, C. L. Berthold, S. Kapoor, W. Oehlmann, M. Singh, & G. Schneider, Three-Dimensional Structures of Apo- and Holo-I-Alanine Dehydrogenase from Mycobacterium tuberculosis Reveal Conformational Changes upon Coenzyme Binding. *Journal of Molecular Biology*, **377** (2008) 1161–1173. <https://doi.org/10.1016/j.jmb.2008.01.091>.
  11. A. Yoshida & E. Freese, Enzymic properties of alanine dehydrogenase of Bacillus subtilis. *Biochimica et Biophysica Acta (BBA) - Nucleic Acids and Protein Synthesis*, **96** (1965) 248–262. [https://doi.org/10.1016/0005-2787\(65\)90588-5](https://doi.org/10.1016/0005-2787(65)90588-5).
  12. A. Lerchner, A. Jarasch, & A. Skerra, Engineering of alanine dehydrogenase from Bacillus subtilis for novel cofactor specificity. *Biotechnology and Applied Biochemistry*, **63** (2016) 616–624. <https://doi.org/10.1002/bab.1414>.
  13. N. Itoh & R. Morikawa, Crystallization and properties of L-alanine dehydrogenase from streptomyces phaeochromogenes. *Agricultural and Biological Chemistry*, **47** (1983) 2511–2519. <https://doi.org/10.1080/00021369.1983.10865985>.
  14. S. M. Tripathi & R. Ramachandran, Crystal structures of the Mycobacterium tuberculosis secretory antigen alanine

dehydrogenase (Rv2780) in apo and ternary complex forms captures “open” and “closed” enzyme conformations. *Proteins: Structure, Function and Genetics*, **72** (2008) 1089–1095. <https://doi.org/10.1002/prot.22101>.

15. D. T. Gallagher, H. G. Monbouquette, I. Schröder, H. Robinson, M. J. Holden, & N. N. Smith, Structure of alanine dehydrogenase from *Archaeoglobus*: Active site analysis and relation to bacterial cyclodeaminases and mammalian mu crystallin. *Journal of Molecular Biology*, **342** (2004) 119–130. <https://doi.org/10.1016/j.jmb.2004.06.090>.
16. B. Hutter & M. Singh, Properties of the 40 kDa antigen of *Mycobacterium tuberculosis*, a functional L-alanine dehydrogenase. *Biochemical Journal*, **343** (1999) 669–672. <https://doi.org/10.1042/bj3430669>.
17. P. Fernandes, H. Aldeborgh, L. Carlucci, L. Walsh, J. Wasserman, E. Zhou, S. T. Lefurgy, & E. C. Mundorff, Alteration of substrate specificity of alanine dehydrogenase. *Protein Engineering, Design and Selection*, **28** (2015) 29–35. <https://doi.org/10.1093/protein/gzu053>.
18. A. Honorat-Pascal, F. Monot, & D. Ballerini, Comparative study of the enzymatic synthesis of L-valine by purified enzymes, crude extract, intact or permeabilized cells from *Bacillus megaterium*. *Applied Microbiology and Biotechnology*, **34** (1990) 236–241. <https://doi.org/10.1007/BF00166788>.
19. S. Nagata, H. Misono, S. Nagasaki, N. Esaki, H. Tanaka, & K. Soda, Gene cloning, purification, and characterization of the highly thermostable leucine dehydrogenase of *Bacillus* sp. *Journal of Fermentation and Bioengineering*, **69** (1990) 199–203. [https://doi.org/10.1016/0922-338X\(90\)90212-F](https://doi.org/10.1016/0922-338X(90)90212-F).
20. L. Cerioli, M. Planchestainer, J. Cassidy, D. Tessaro, & F. Paradisi, Characterization of a novel amine transaminase from *Halomonas*

- elongata. *Journal of Molecular Catalysis B: Enzymatic*, **120** (2015) 141–150. <https://doi.org/10.1016/j.molcatb.2015.07.009>.
21. H. Schütte, J. Flossdorf, H. Sahm, & M. -R Kula, Purification and Properties of Formaldehyde Dehydrogenase and Formate Dehydrogenase from *Candida boidinii*. *European Journal of Biochemistry*, **62** (1976) 151–160. <https://doi.org/10.1111/j.1432-1033.1976.tb10108.x>.
  22. J. Rocha-Martín, B. de las Rivas, R. Muñoz, J. M. Guisán, & F. López-Gallego, Rational Co-Immobilization of Bi-Enzyme Cascades on Porous Supports and their Applications in Bio-Redox Reactions with In Situ Recycling of Soluble Cofactors. *ChemCatChem*, **4** (2012) 1279–1288. <https://doi.org/10.1002/cctc.201200146>.
  23. M. Planchestainer, M. L. Contente, J. Cassidy, F. Molinari, L. Tamborini, & F. Paradisi, Continuous flow biocatalysis: production and in-line purification of amines by immobilised transaminase from *Halomonas elongata*. *Green Chem.*, **19** (2017) 372–375. <https://doi.org/10.1039/C6GC01780K>.
  24. J. M. Bolivar, L. Wilson, S. A. Ferrarotti, R. Fernandez-Lafuente, J. M. Guisan, & C. Mateo, Evaluation of different immobilization strategies to prepare an industrial biocatalyst of formate dehydrogenase from *Candida boidinii*. *Enzyme and Microbial Technology*, **40** (2007) 540–546. <https://doi.org/10.1016/j.enzmictec.2006.05.009>.
  25. J. C. Cruz, P. H. Pfromm, J. M. Tomich, & M. E. Rezac, Conformational changes and catalytic competency of hydrolases adsorbing on fumed silica nanoparticles: II. Secondary structure. *Colloids and Surfaces B: Biointerfaces*, (2010). <https://doi.org/10.1016/j.colsurfb.2010.06.005>.
  26. B. Kranz, J. Bürck, M. Franzreb, R. Köster, & A. S. Ulrich, Circular dichroism analysis of penicillin G acylase covalently immobilized

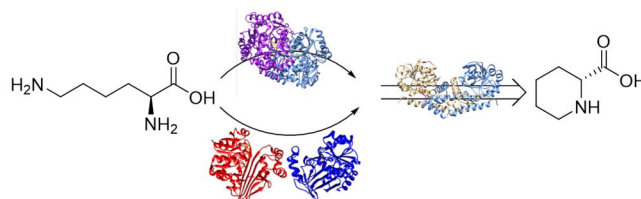


on silica nanoparticles. *Journal of Colloid and Interface Science*, (2007). <https://doi.org/10.1016/j.jcis.2007.08.062>.

27. G. A. Petkova, K. Záruba, & V. Král, Synthesis of silica particles and their application as supports for alcohol dehydrogenases and cofactor immobilizations: Conformational changes that lead to switch in enzyme stereoselectivity. *Biochimica et Biophysica Acta - Proteins and Proteomics*, (2012). <https://doi.org/10.1016/j.bbapap.2012.03.010>.
28. R. Fernandez-Lafuente, Stabilization of multimeric enzymes: Strategies to prevent subunit dissociation. *Enzyme and Microbial Technology*, **45** (2009) 405–418. <https://doi.org/10.1016/j.enzmictec.2009.08.009>.
29. F. Lopez-Gallego, L. Betancor, A. Hidalgo, G. Dellamora-Ortiz, C. Mateo, R. Fernández-Lafuente, & J. M. Guisán, Stabilization of different alcohol oxidases via immobilization and post immobilization techniques. *Enzyme and Microbial Technology*, (2007). <https://doi.org/10.1016/j.enzmictec.2006.04.021>.
30. R. Fernandez-Lafuente, J. M. Bolivar, J. Rocha-Martin, C. Mateo, F. Cava, J. Berenguer, & J. M. Guisan, Coating of Soluble and Immobilized Enzymes with Ionic Polymers: Full Stabilization of the Quaternary Structure of Multimeric Enzymes. *Biomacromolecules*, **10** (2009) 742–747.
31. L. Trobo-Maseda, A. H. Orrego, S. Moreno-Pérez, G. Fernández-Lorente, J. M. Guisan, & J. Rocha-Martin, Stabilization of multimeric sucrose synthase from *Acidithiobacillus caldus* via immobilization and post-immobilization techniques for synthesis of UDP-glucose. *Applied Microbiology and Biotechnology*, **102** (2018) 773–787. <https://doi.org/10.1007/s00253-017-8649-y>.
32. D. Brady & J. Jordaan, Advances in enzyme immobilisation. *Biotechnology Letters*, **31** (2009) 1639–1650. <https://doi.org/10.1007/s10529-009-0076-4>.

33. L. Betancor & H. R. Luckarift, Co-immobilized coupled enzyme systems in biotechnology. *Biotechnology and Genetic Engineering Reviews*, **27** (2010) 95–114. <https://doi.org/10.1080/02648725.2010.10648146>.
34. Q. Guo, L. Gakhar, K. Wickersham, K. Francis, A. Vardi-Kilshtain, D. T. Major, C. M. Cheatum, & A. Kohen, Structural and Kinetic Studies of Formate Dehydrogenase from *Candida boidinii*. *Biochemistry*, **55** (2016) 2760–2771. <https://doi.org/10.1021/acs.biochem.6b00181>.
35. C. Mateo, J. M. Palomo, L. M. Van Langen, F. Van Rantwijk, & R. A. Sheldon, A New, Mild Cross-Linking Methodology to Prepare Cross-Linked Enzyme Aggregates. *Biotechnology and Bioengineering*, **86** (2004) 273–276. <https://doi.org/10.1002/bit.20033>.
36. R. A. Sheldon, Cross-linked enzyme aggregates as industrial biocatalysts. *Organic Process Research and Development*, **15** (2011) 213–223. <https://doi.org/10.1021/op100289f>.

## Chapter 7: Synthesis of pipercolic acid by a multi-enzymatic cascade



## 7.1. Introduction

Pipecolic acid (PA) is a non-proteinogenic  $\alpha$ -amino acid found in all three domains of life with various functions [1–4]. In microorganisms and fungi, generally, PA serves as a building block for a plethora of biologically active secondary metabolites [5] and, in addition, PA can be used as a catalyst to perform stereoselective Mannich reactions [6]. PA is found in macrolides, such as rapamycin (an antifungal also used to prevent organ transplant rejection) [7] and the fungal metabolite apicidin (an antiprotozoal) [8]. The same molecule can also be found in smaller and simpler molecules, such as several amide anaesthetic drugs (i.e. Mepivacaine and Ropivacaine) (Figure 7.1). PA is also present in anticancer drugs (swainsonine), antibiotics (virginiamycin), and anthelmintic agents (macfortine). Noteworthy, in both ropivacaine and rapamycin, the *L* enantiomer of PA is present while Apicidin presents the *D* stereoisomer [9], highlighting the importance of the stereochemistry of PA.

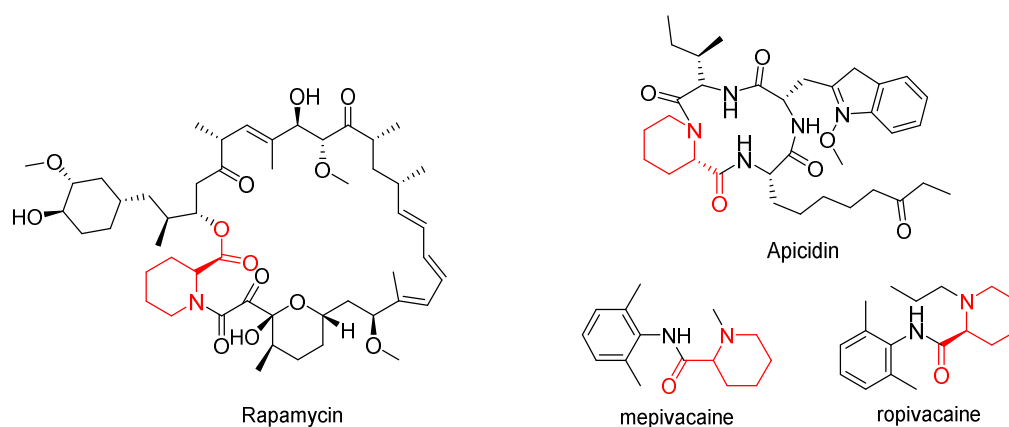


**Figure 7.1.** Structure of four drugs containing PA in their structure. PA is marked in red in each structure.

With such ubiquity in pharmaceuticals and bioactive molecules, the search for an efficient production of PA and its derivatives has gained momentum in the last few years. The chemical methods available normally involve harsh conditions and hazardous reagents despite recent efforts to develop more sustainable processes [10–11]. Alternatively, as it is a naturally occurring molecule, bioproduction has proved as an efficient alternative to the synthetic approaches. In nature,

normally, the pathway to produce PA is related to lysine metabolism. This bioconversion normally occurs in a two-step process, where lysine is deaminated in either the  $\alpha$  or  $\epsilon$  position by a lysine dehydrogenase or lysine oxidase, and after spontaneous cyclisation, the resulting product ( $\Delta^1$ -piperidine-2-carboxylic acid (P2C) or  $\Delta^1$ -piperidine-6-carboxylic acid (P6C)) is reduced by a specific reductase [12] to yield PA (Figure 7.2). More recently, the use of a single enzyme, a lysine cyclodeaminase which perform both the deamination and the reduction of the cyclic intermediate has been also described [13–14].

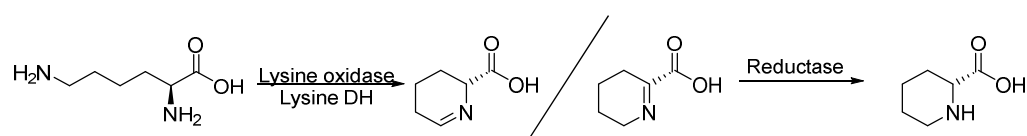


**Figure 7.2.** Biocatalytic approach for the synthesis of L-PA from L-Lysine by using a two-enzyme cascade. LysDH refers to lysine dehydrogenase.

From the different feasible approaches, combining a lysine-6-dehydrogenase with a pyrroline-5-carboxylate (P5C) reductase enzyme has been successfully applied as whole cell biocatalysis, and lysine cyclodeaminase production has been performed with soluble purified enzyme [15–16]. The combination of lysine dehydrogenase and P5C enzymes, is an appealing alternative as the cascade itself is redox neutral. This strategy has been further investigated to reach a productivity of 15 g/L using whole cell biocatalysis with *Corynebacterium glutamicum* over 70h fermentations [17].

Although the reaction consists in a deamination, no transaminase based approaches have been described to date, even if lysine- $\epsilon$ -aminotransferases have been identified in bacteria, fungi and animals and some  $\omega$ -transaminases exhibited activity with lysine [18–20]. In this chapter, exploiting the broad substrate range of the previously mentioned HeTA, a cascade reaction has been constructed by combining it with a novel P5C reductase isolated from the same organism, HeP5CR, for the synthesis of L-PA, L-proline and ethyl L-pipecolate from L-lysine, L-ornithine and L-lysine ester, respectively. In addition, the previously discussed redox neutral cascade, coupling a thermophilic lysine-6-

dehydrogenase (GsLys6DH) with HeP5CR has also been investigated. Co-immobilisation of GsLys6DH and HeP5CR has been optimised and this strategy has been successfully applied in flow as a packed-bed reactor to produce *L*-pipecolic acid.

All the work presented in this chapter is my own contribution unless stated otherwise. Liam Calvey performed the cloning and characterisation of GsLys6DH and initial studies to combine it with HeP5CR and Dr. Ana Isabel Benítez-Mateos performed the co-immobilisation of GsLys6DH and HeP5CR.

## 7.2. HeP5C cloning and characterization

A gene encoding for a putative pyrroline-5-carboxylate reductase (helo\_4115) was identified in the genome of *Halomonas elongata* DSM 2581 by BLAST using the sequence of the previously characterised P5CR from *Neisseria meningitidis* and *Streptococcus pyogenes* as probes [21]. The protein showed 55% and 51% sequence similarity, with identity values of 37% and 29%, respectively. The gene was amplified and successfully cloned into a pRSET-B expression vector. The His-tagged protein, named HeP5CR, was expressed in Terrific Broth media at 30°C and purified using IMAC with a yield of 15-17 mg/L of culture (Figure 7.3). The enzyme was identified as a dimer formed by monomers of 32 KDa by size exclusion chromatography, similarly to the previously characterised P5CR from *Neisseria meningitidis* [21].

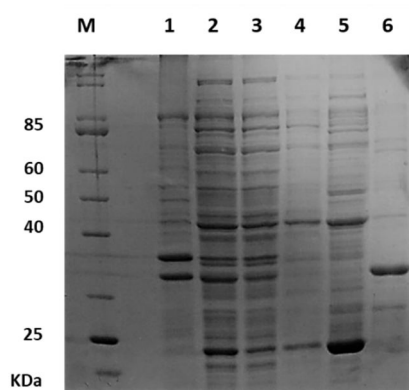


**Figure 7.3.** SDS-page analysis of HeP5CR expression. 1: Cell extract after expression; 2: Soluble fraction; 3: Insoluble fraction; 4: Flow through in IMAC; 5: Washing step; 6: Purified protein fraction.

Following the expression, basic kinetic characterisation of the protein was performed. As the substrate for the protein is not

commercially available, the six-membered ring derivative ( $\Delta^1$ -piperidine-6-L-carboxylate or P6C) was synthesized as reported previously by hydrolysis of allysine ethylene acetal by adding the polystyrene cation exchange resin Amberlyst-15 [22] (Figure 7.4).

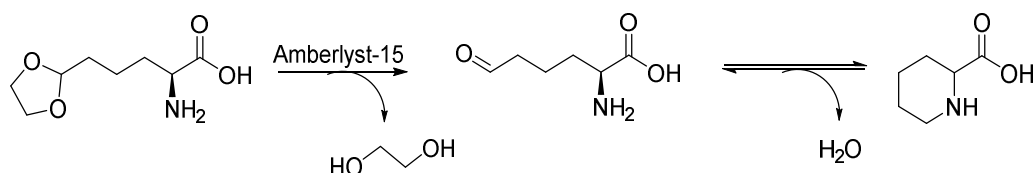


**Figure 7.4.** Scheme of the formation of P6C from the starting material allysine ethylene acetal.

According to literature, this reaction proceeds to completion at room temperature, but the concentration of the product was not quantifiable by either LC-MS or NMR. Consequently, this substrate was only used to characterise the cofactor affinity of HeP5CR by fixing the volume added. HeP5CR had dual affinity for the cofactor, being able to catalyse the reduction with both NADH and NADPH. It showed better affinity for NADH, with a  $K_M$  ten times lower than NADPH ( $0.013 \pm 0.004$  and  $0.17 \pm 0.03$  respectively). With both versions of the reduced cofactor, the  $V_{max}$  was similar, reaching  $2.06 \pm 0.14$  U/mg and  $1.87 \pm 0.18$  U/mg for NADH and NADPH, respectively.

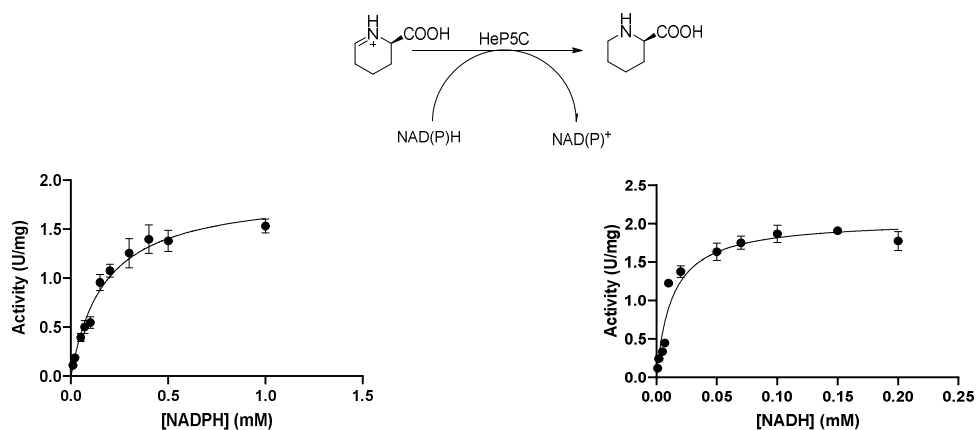


**Figure 7.5.** Kinetic characterisation of the cofactor dependence of HeP5CR with  $\Delta^1$ -piperidine-6-L-carboxylate. A scheme of the reaction is shown on top.

Normally, bacterial P5CRs are not only involved in the biosynthesis of proline, by reducing the pyrroline-5-carboxylate, but they also participate in detoxification processes by metabolising proline analogues, such as thioproline and 3,4-dehydro-L-proline [23]. Taking

advantage of their natural broad substrate range, the activity of these enzymes can also be monitored by their oxidative activity against the commercially available *L*-thiazolidine-4-carboxylate (T4C) [24]. To test the affinity for the cyclic substrates, the  $K_M$  for T4C was determined with  $NAD^+$  as cofactor (Figure 7.6). HeP5CR exhibited a  $K_M$  of  $4.3 \pm 0.3$  mM and a  $V_{max}$  of  $19.34 \pm 1.43$  U/mg. The affinity for T4C is in the same range as the one calculated for *E. coli* P5CR (1.32 mM) [24]. Not surprisingly, this values are almost ten times higher than the calculated affinities for the natural substrate (1-pyrroline-5-carboxylic acid), as reported for example for the P5CR from *M. tuberculosis* [25].

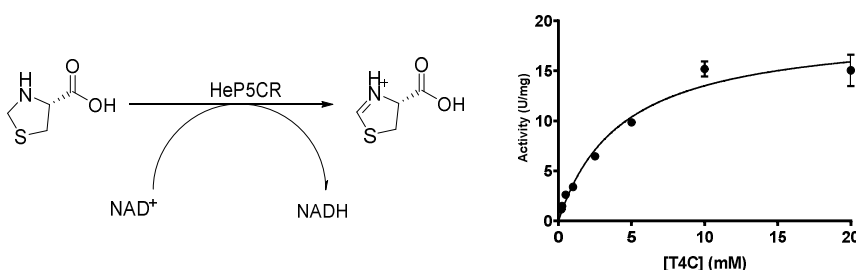


**Figure 7.6.** Kinetic characterisation of HeP5CR with the unnatural substrate, *L*-thiazolidine-4-carboxylate. A scheme of the reaction is shown on the left.

### 7.3. Combination of HeP5CR with HeTA catalysed reaction

Transaminases, as discussed in chapter 4, have a broad application in biocatalysis. Until recently, it was believed that almost all amino acids participate in transamination reactions mediated by specific amino acid transaminases a part from lysine, threonine, proline and hydroxyproline [26]. Discovery of lysine- $\epsilon$ -aminotransferases proved that statement wrong, and moreover activity with lysine was not limited to this specific group. HeTA, already extensively discussed in previous chapters, although not a member of the amino acid transaminase family, exhibited a broad substrate scope and accepts also lysine as the amino donor. This special characteristic exhibited by HeTA can be exploited to produce PA; the transamination can be performed with HeTA to yield the semialdehyde which spontaneously cyclises, forming P6C and this product can be further reduced by coupling the transamination reaction to HeP5CR, to yield PA (Figure 7.7).



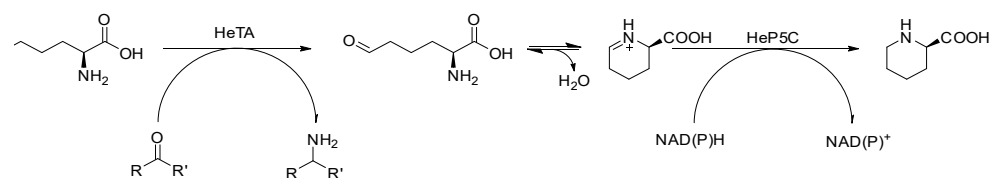


**Figure 7.7.** Representation of the enzymatic cascade proposed for the synthesis of PA from lysine. In the scheme, production of L-PA acid from L-lysine is depicted.

Initial tests were performed with three simple amino acceptors for which HeTA exhibited the highest activity: glyoxylate, pyruvate and benzaldehyde (Figure 7.8). While pyruvate and glyoxylate are soluble in the tested conditions, benzaldehyde required 10% DMSO as a cosolvent. The reactions were performed with both *L* and *D*-lysine, to evaluate both HeTA and HeP5CR stereoselectivity.

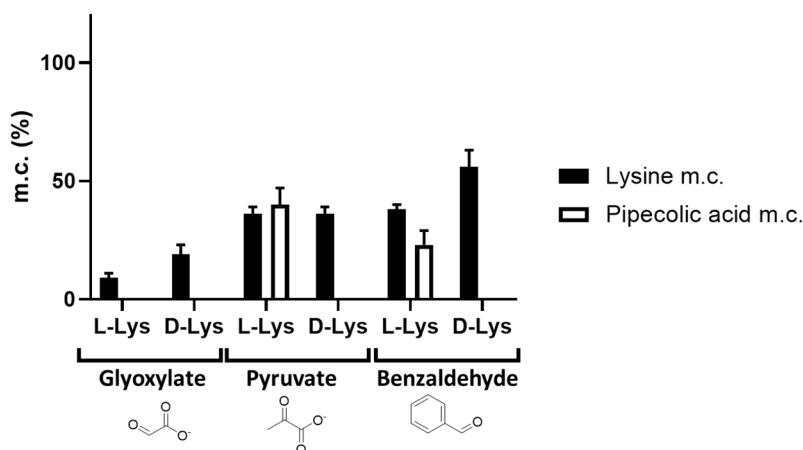


**Figure 7.8.** Conversion of lysine (black) and total conversion to PA (white). Reaction conditions are 2 mg/mL HeTA, 1 mg/mL HeP5C, 10 mM of lysine, 1 equivalent of amino acceptor, if not stated otherwise, 10 mM NADH, 0.1 mM PLP in 100 mM phosphate buffer pH 8 with equimolar concentration of the NADH. Conversions at 48h are shown.

In the initial tests, all three amino acceptors worked to some extent. The highest yields were obtained with benzaldehyde and pyruvate with a depletion of  $36 \pm 3\%$  and  $38 \pm 2\%$  of *L*-lysine. For glyoxylate, the yield obtained was much lower ( $9 \pm 2\%$ ). Interestingly, with both glyoxylate and benzaldehyde, the conversion of *D*-lysine was higher, up to  $56 \pm 7\%$  in the case of the aromatic amino acceptor and  $19 \pm 4\%$  with glyoxylate. With pyruvate, HeTA accepted equally well both *L*- and *D*-lysine as the amino donor with no significant difference. This indicates that while HeTA was extremely selective for other amino acids were it reacted with the  $\alpha$ -NH<sub>2</sub> [27], for lysine it shows no selectivity indubitably indicating that

rather than acting on the  $\alpha$  amino group, HeTA is acting on the  $\epsilon$  amino group of lysine, therefore yielding P6C which can be reduced by HeP5CR.

As for the second half of the reaction, HeP5CR exhibited complete enantioselectivity for the *L* enantiomer, with no PA formation observed when *D*-lysine was used as the substrate. Interestingly, while both pyruvate and benzaldehyde produced comparable amounts of the intermediate, only in the case of pyruvate the yield of *L*-PA was similar to the *L*-lysine depletion. With benzaldehyde, the conversion dropped from  $38 \pm 2\%$  of lysine to  $23 \pm 6\%$  of *L*-PA. To further investigate this issue, stability of HeP5CR was assessed in the presence of DMSO, benzaldehyde and benzylamine, the product of the transamination reaction (Figure 7.9).

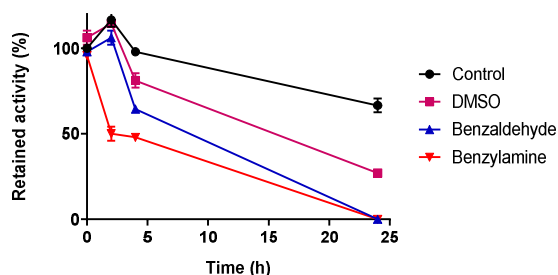


**Figure 7.9.** Stability of HeP5C in the reaction conditions with benzaldehyde as the amino acceptor. A solution of 0.25 mg/mL of HeP5CR was incubated with 10% DMSO or 10 mM benzaldehyde or benzylamine at 37°C for 24h.

As it can be seen in Figure 7.9, only after two hours, the presence of benzylamine provoked loss of half of the activity as opposed to the other tested conditions. After 24h, HeP5CR retained only 27% of the activity when in contact with DMSO, while the presence of both benzaldehyde and benzylamine triggered complete enzyme inactivation. These could explain the lower conversion to PA in the whole cascade reaction, because of decreased stability of HeP5CR with both benzaldehyde and more significantly, benzylamine.

HeP5CR, on the other hand, requires a reduced cofactor in equimolar amount to convert P6C into PA. To minimise the economic impact, a cofactor recycling system was incorporated into the reaction. As

HeP5CR exhibits dual affinity for the cofactors, with virtually identical performance with NADPH and NADH, the glucose dehydrogenase from *Bacillus megaterium* [28] (BmGDH), already available in the group, was incorporated. Using glucose as the sacrificial substrate, the cofactor can be recycled. Working under the same conditions as described in Figure 7.9, with 10 mM lysine, using 1 mM of NADP<sup>+</sup> and 1 mg/mL of BmGDH, the conversion to PA was not affected.

After the initial results obtained on a 10 mM scale with the recycling system incorporated, the scalability of the reaction up to the 50 mM was investigated. In this case, benzaldehyde was not trialed due to the negative effect on the stability of HeP5CR. Instead, to try and push the equilibrium towards the deamination of lysine, 2 equivalents of pyruvate to lysine were used. The results are shown in Figure 7.10.

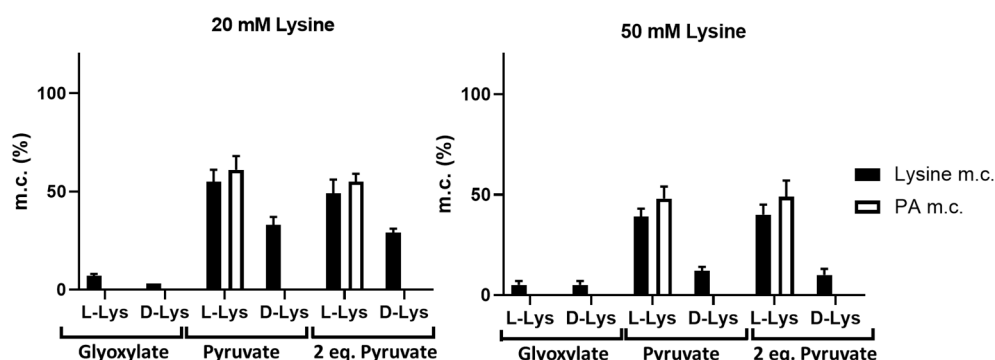


**Figure 7.10.** Conversion at 48h of lysine (black) and total conversion to PA (white). Reaction conditions are 2 mg/mL HeTA, 1 mg/mL HeP5C, 1 mg/mL BmGDH, 1 equivalent of amino acceptor, if not stated otherwise, 0.1 mM PLP in 100 mM phosphate buffer pH 8 with 1 mM NADP<sup>+</sup> was used.

Both at 20 mM and 50 mM scale, when glyoxylate was used as the amino acceptor, the conversions for both *L* and *D*-Lysine were less than 10%. As for pyruvate, conversions were proportional to what observed at the 10 mM scale. Interestingly, the addition of two equivalents of the acceptor did not affect the total conversion to PA. In agreement with previous results, only *L*-lysine led to the formation of PA, further confirming the complete enantioselectivity of HeP5CR. At higher substrates loading, the depletion of *D*-lysine is significantly lower than *L*-lysine, indicating that the conversion of the intermediate to *L*-PA shifts the equilibrium of the first step further. Once more, when pyruvate was

used as the amino acceptor, the amounts of PA formed corresponded to the amount of lysine depleted from the reaction, indicating that HeP5CR is able to reduce all available P6C to the final product. More importantly, the % of conversion to PA was consistent and at 50 mM scale it translates to 20 mM of product, a volumetric productivity of 0.054 g/L/h of PA, compared to 0.011 g/L/h at the 10 mM scale. The productivity at 50 mM substrate concentration is twice what was reported previously (0.025 g/L/h) with free enzymes [12], but still far from the 0.208 g/L/h [17] or 0.940 g/L/h [14] reported using whole cell transformations.

To further improve the yield, various reaction conditions were tested, and pH was the one that had a significant effect on the lysine conversion (Figure 7.11).

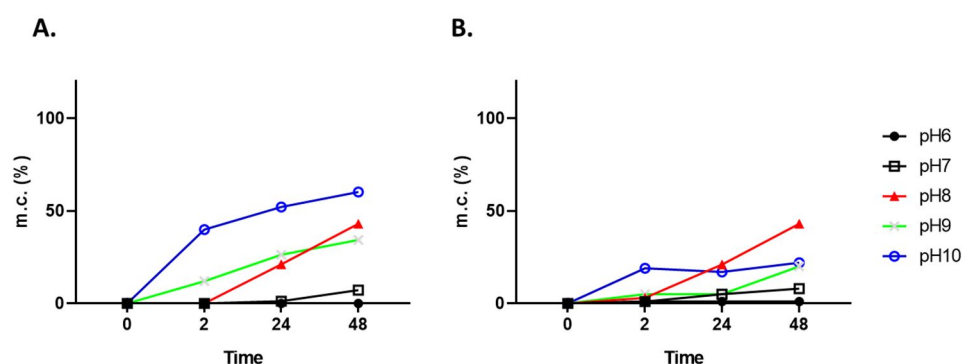


**Figure 7.11.** pH dependence of PA formation. Reaction conditions were 2 mg/mL HeTA, 1 mg/mL HeP5C, 1 mg/mL BmGDH, 50 mM Lysine, 50 mM pyruvate in the adequate buffer with 1 mM NADP<sup>+</sup>. **A.** Lysine conversion into P6C catalysed by HeTA at different pH. **B.** PA formation at different pH.

Compared to the initial conditions, at more basic pH the molar conversion of lysine was much higher, reaching 60% after 48h at pH 10. Not only that, but the reaction also happened much faster. Comparing the conversion observed after only 2h, at pH 8 the depletion of lysine is barely noticeable while at pH 9 it is already 10%, and at pH 10, remarkably, reaches 40%. The enhancement of the first reaction in the cascade correlates with the higher activity exhibited by HeTA at pH 10. Initial characterisation of the enzyme, performed by Cerioli *et al.*, indicated that while the enzyme is more stable at pH values around 8-9, the activity is three times higher at pH 10 [27].

This enhancement in the first half of the reaction, though, was not translated into higher molar conversion to PA. At pH 8, the formation of PA corresponded to the amount of lysine depleted, indicating that all the P6C intermediate was converted while at pH 9 and pH 10, the conversion of PA is only 20 and 22% respectively. This could be explained by inactivation of HeP5CR or BmGDH, at such high pH. Indeed, when the stability of the three enzymes was compared between pH 8 to 10, at more basic pHs, BmGDH exhibited nearly no activity after just half an hour (Figure 7.12). Explaining its low stability, BmGDH has a tetrameric assembly that has been previously reported to break apart at pH 9 [28]. Surprisingly, HeP5CR was not particularly affected by the change in pH, as no difference was observed between the incubation at pH 8 or pH 10. HeTA also lost activity much faster at basic pH, with only 10% of the activity retained after 4h and only 8.7% of the initial activity after 24h.

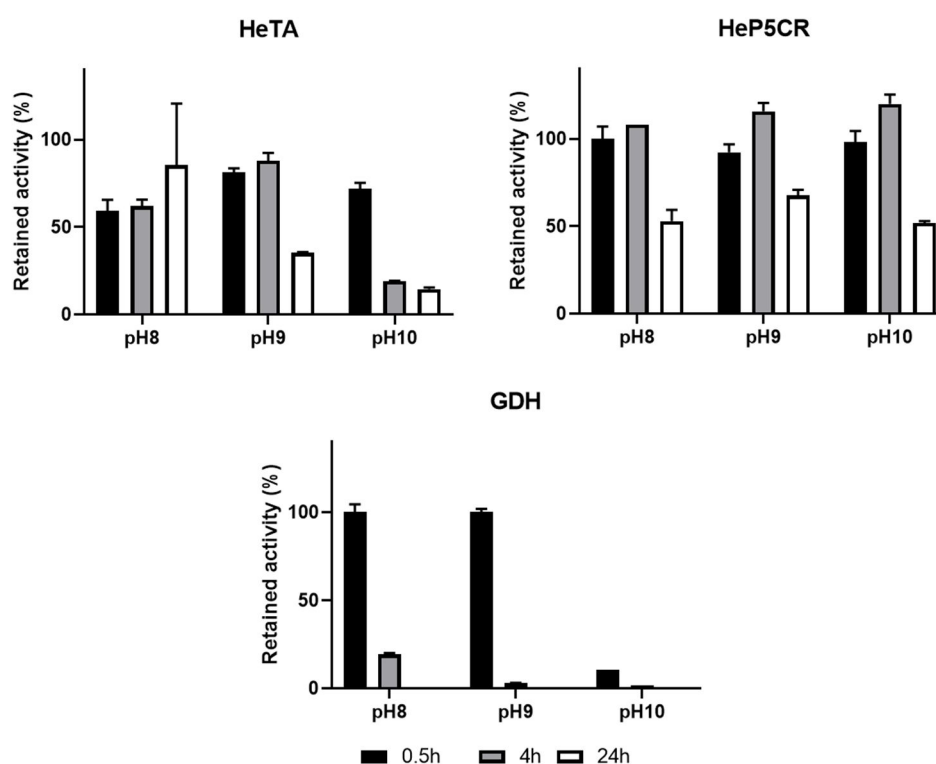


**Figure 7.12.** Stability of the three enzymes used in the cascade at pH 8 and pH 10. The reaction mixture was prepared without the addition of any substrate (2 mg/mL of HeTA, 1 mg/mL of HeP5CR and 1 mg/mL of BmGDH). The activity was checked by using the standard activity assay for each enzyme.

Altogether, these results suggest that while short time reactions at pH 10 could be applied for HeTA and HeP5CR, the incompatibility of

BmGDH is limiting its function in the intended cascade. Therefore, other enzymes used for the recycling of the cofactor were investigated.

Ideally, the sacrificing substrate has to meet certain requirements such as being inexpensive, easily separable from the product, favourable equilibrium and no cross-reactivity [29–30]. As a consequence, the NAD<sup>+</sup> dependant formate dehydrogenase from *Candida boidinii* [31] (CbFDH) was selected. This enzyme, previously used in hydrogen borrowing cascades [32] and in the previous chapter, exhibits good activity, better stability than BmGDH at higher pH [33] and the sacrificing substrate, formate, produces carbon dioxide which will not interact with either of the other enzymes and would simplify the purification of the product from the bulk reaction.

To assess the suitability of the new recycling system, CbFDH was tested in the whole cascade at pH 10, compared with GDH (both with NAD<sup>+</sup> and NADP<sup>+</sup>), and without the recycling system, with 50 mM of L-lysine and 1 mM of NAD(P)<sup>+</sup> cofactor and 50 mM of the cofactor for the reaction without recycling system (Table 7.1).

**Table 7.1.** Comparison of the molar conversions at 48h with the two cofactor recycling systems used.

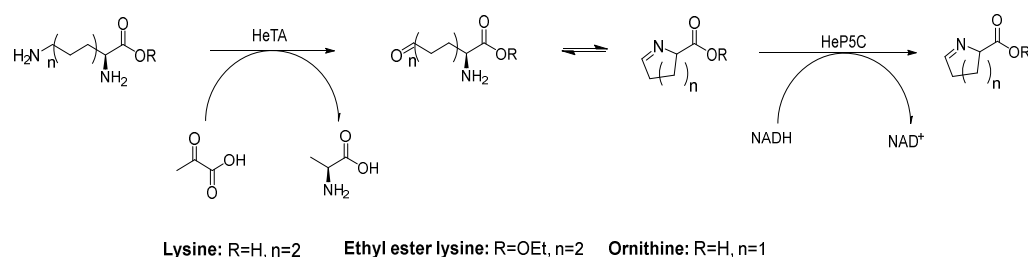
		<b>L-Lysine depletion (%)</b>	<b>L-PA (%)</b>
<b>CbFDH</b>	<b>NAD<sup>+</sup></b>	59 ± 1	58 ± 2
	<b>NADP<sup>+</sup></b>	27 ± 4	6 ± 1
<b>BmGDH</b>	<b>NAD<sup>+</sup></b>	57 ± 4	32 ± 2
	<b>NADP<sup>+</sup></b>	26 ± 4	14 ± 2
<b>No recycling</b>			

With the new recycling system, the depletion of lysine was not affected, reaching almost 60% of conversion. As for the PA formation, in the case of BmGDH in combination with NADP<sup>+</sup>, only half of the available P6C was reduced to PA. With NAD<sup>+</sup>, the preferred cofactor of HeP5C, in combination with BmGDH only 6% of PA was formed. As seen before, at the 50 mM scale, the formation of PA is necessary to push the equilibria towards the deamination of lysine. With the CbFDH recycling system, the lysine conversion was maintained at the 60% and all P6C intermediate

was converted, confirming CbFDH performs better in the desired conditions.

Once the full system was optimised and assembled, since HeTA exhibits a very wide substrate scope, ornithine and ethyl ester lysine were also tested at the 50 mM scale (Table 7.2).

**Table 7.2.** Substrate scope for the cascade reaction. The reaction mix contained 2 mg/mL HeTA, 2 mg/mL HeP5C, 1 mg/mL FDH, 50 mM Lysine, 100 mM pyruvate, 100 mM carbonate buffer pH 10, 1 mM NADH. Conversion shown are after 24h.



	Lysine depletion (%)	PA or proline formation (%)
<b>L-Lysine</b>	60 ± 2	57 ± 2
<b>L-Lysine ethyl ester</b>	55 ± 3	49 ± 3
<b>L-Ornithine</b>	99 ± 1	55 ± 2

Regarding the transamination reaction, ornithine appeared to be the preferred substrate for HeTA, with complete conversion after 24h. As for the lysine ester, the presence of the extra ethyl group in the  $\alpha$ -carboxyl does not affect the capacity of HeTA to deaminate the substrate, with conversion values similar to those obtained with *L*-lysine. In the second part of the reaction, it is important to note that while with lysine the conversion of the intermediate to PA is complete, with ornithine only half of the formed intermediate is reduced to proline. This indicates that either CbFDH is not sufficiently stable under the reaction conditions or HeP5CR is inhibited by the presence of the product. This last hypothesis was tested using the standard activity assay in the presence of different concentrations of the cyclic amino acid, but no significant inhibition was found at concentrations lower than 50 mM. The most plausible explanation thus, is the stability of the enzymatic system in the tested

reaction conditions. Surprisingly, the final yield from both lysine and lysine ethyl ester are comparable, indicating complete conversion of the intermediate formed. HeP5CR is therefore able to accommodate also the ethyl ester version of P6C in its active site in an active conformation, reducing it into ethyl pipercolinate, although it had been reported that the binding of the substrate to P5CR active sites depends highly on the hydrogen bonding to the carboxylic group [21].

Following the results obtained in batch reaction with free enzymes, to further improve the productivity and to reuse the catalysts, enzyme immobilisation was trialled. Apart from the reusability, in some cases, immobilisation can enhance the catalyst resistance to various factors, such as pH, which would be advantageous for the proposed system [34].

Initially, the reaction was carried out in batch using 100 mg of immobilised HeTA, either in EC-EP/S (for more details see Figure 3.5 in Materials and Methods), combined with soluble HeP5CR and CbFDH. After 48h, no conversion to PA or depletion to lysine was observed. The reason behind that, was clear when the stability of immobilised HeTA was assessed at pH 10 (Figure 7.13) as it was found that the immobilised enzyme exhibited in fact less stability than the free enzyme at pH 10.

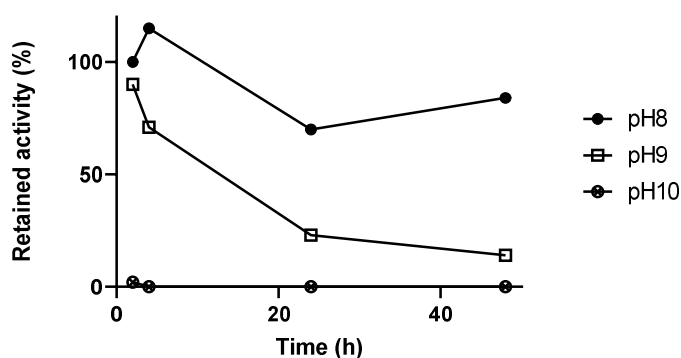


**Figure 7.13.** pH stability of immobilised HeTA in EC-EP/S polymethacrylate beads at pH ranging from 8 to 10. Activities are referred to the initial activity of the biocatalyst at pH 8 (9.1 U/g of resin).

The low stability of HeTA once immobilised at pH 10, limited the application of the proposed biocatalytic route with immobilised enzymes. Attempts to perform the reaction at milder conditions (pH 8 and pH 9), in



which the immobilised enzyme showed better stability at least for the first 24h, did not result any lysine depletion and consequently, no formation of pipercolic acid.

To sum up, for the transaminase catalysed reactions, the conversions observed in batch at pH 10, translate into productivities of 0.156 g/L/h for *L*-pipercolic acid, 0.160 g/L/h for *L*-ethyl pipercolinate and 0.132 g/L/h for *L*-proline. These values are closer to the best productivities obtained with whole cell biocatalysis using similar cascades for the production of pipercolic acid. More importantly, no example of the production of *L*-ethyl pipercolinate has been reported previously. Proline biosynthesis, on the other hand, has been widely investigated by fermentation using *Corynebacterium glutamicum*, with 0.42 g/L/h [35–36]. Whole-cell fermentations, while producing good amounts of *L*-proline also have a number of side reactions which not only complicate the purification of proline but also result in less mole percentage conversion (moles of substrate/moles of product x 100). This issue is surpassed with free enzymes in a batch reaction, as when ornithine is the sole substrate, no side products apart from the desired *L*-proline is formed. Therefore, the proposed route can serve as a good alternative to whole cell biocatalysis and fermentations with similar volumetric productivities.

#### **7.4. Combination of HE-P5C with Lys6DH**

##### **7.4.1. Lysine 6 dehydrogenase candidate selection and characterisation:**

As an alternative to the transaminase catalysed lysine deamination, this same chemical reaction can be performed with a specific enzyme for lysine: lysine-6-dehydrogenase (Lys6DH). This enzyme, opposed to transaminases, deaminates lysine in a NAD(P)<sup>+</sup> dependant manner with the release of ammonia. This cascade, which has been previously explored in literature [17,37], does not require the addition of a third enzyme to recycle the cofactor; the reaction catalysed by the Lys6DH creates the pool of reduced cofactor necessary for HeP5CR to reduce

the P6C intermediate into PA, creating a redox-neutral cascade (Figure 7.14).

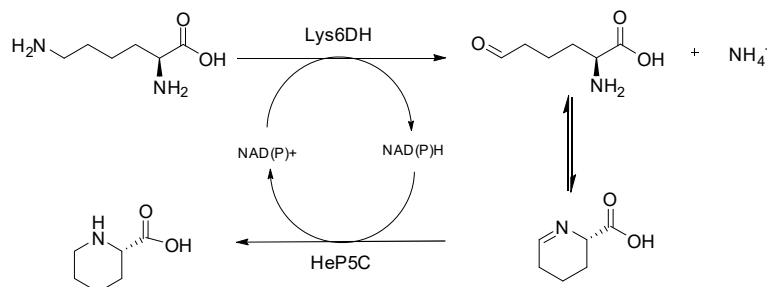


**Figure 7.14.** Cascade proposed for the synthesis of PA by coupling a lysine-6-dehydrogenase with HeP5CR.

The Lys6DH selected for this cascade was a previously characterised enzyme from *Geobacillus stearothermophilus* (GsLys6DH) [38]. This thermophilic enzyme was chosen as it had been previously expressed in *E. coli* and purified in the soluble fraction, unlike an homologous enzyme from *Pyrococcus horikoshii* [39], and exhibited excellent properties. GsLys6DH can be used at pH ranging from 7 to 10 and is very stable at neutral pH (7-9). Moreover, the enzyme resists at temperatures as high as 75°C. To that end, a synthetic gene coding for the GsLys6DH, optimised for expression in *E. coli*, was ordered and subcloned into a pRSET-B expression vector. The protein was successfully expressed in ZYP<sup>+</sup> autoinduction media and purified to more than 90% purity (Figure 7.15).

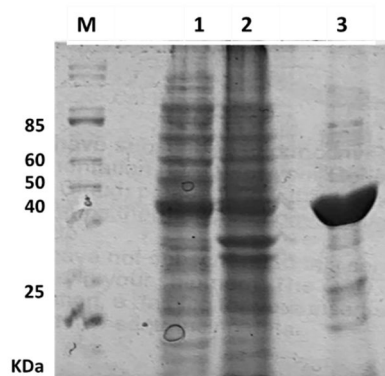


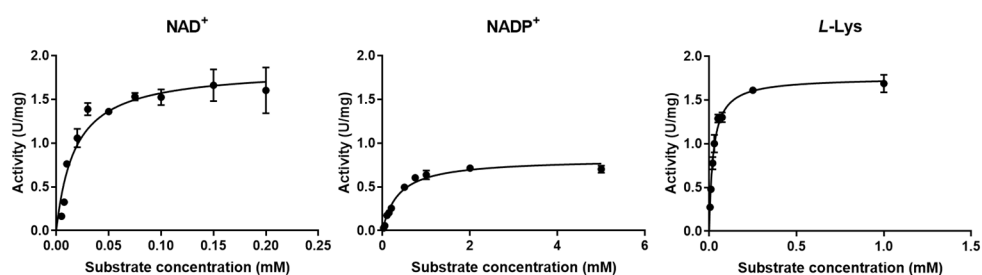
**Figure 7.15.** SDS-page analysis of GsLys6DH purification. M: molecular weight markers; 1: soluble fraction; 2: insoluble fraction; 3: pure protein.

When the activity of the His-tagged version of GsLys6DH was tested, it showed a specific activity lower than what previously reported ( $1.85 \pm 0.08$  U/mg compared to 7.81 U/mg). In the original protocol, two size

exclusion chromatography steps were necessary in order to get the pure protein, while in our case only an IMAC chromatography was performed. As it can be seen in Figure 7.15, the protein is not purified to complete homogeneity, which could be affecting the assessment of the specific activity. To further investigate this issue, basic molecular characterisation was performed to ensure the His-tag did not have any effect on the quaternary structure or affinity for the substrates of the enzyme.

As it can be seen in Table 7.3, the affinity for the cofactors did not change significantly but the  $K_M$  values were different from published values. Worth mentioning, the values reported by Heydari *et al.* were calculated using the Lineweaver-Burk plot, which is prone to error, while the kinetic parameters reported here were calculated by fitting the results to the Michaelis-Menten curve. Even with the differences, the results indicate the same behaviour:  $\text{NAD}^+$  was preferred to  $\text{NADP}^+$ , with a  $K_M$  value 20 times lower. The affinity for lysine was significantly different, as the estimated  $K_M$  of  $0.024 \pm 0.002$  mM is 30 times lower than the reported.

**Table 7.3.** Kinetic parameters of substrates for the GsLys6DH enzyme. Specific activity was calculated using the standard activity assay.  $K_m$  values were calculated from the graphs below, by fitting the data to the Michaelis-Menten equation.



Substrate	Specific activity (U/mg)		$K_m$ (mM)	
	Calculated	Heydari <i>et al.</i>	Calculated	Heydari <i>et al.</i>
$\text{NAD}^+$	$1.85 \pm 0.08$	7.81	$0.018 \pm 0.003$	0.088
$\text{NADP}^+$	$0.82 \pm 0.02$	1.72	$0.36 \pm 0.03$	0.48
<b>L-Lysine</b>	-	-	$0.024 \pm 0.002$	0.73

The enzyme was also confirmed to be a hexamer by size-exclusion chromatography and the activity maintained after this second purification, meaning that the difference in both activity and affinity for lysine cannot

be explained by a destabilisation or change in the quaternary structure or the presence of the extra proteins in the sample. Cleavage of the His-tag did not have any effect on the activity either. Consequently, the difference could not be attributable to any structural effect.

#### 7.4.2. Batch biotransformation of *L*-lysine into *L*-PA:

Once GsLys6DH was successfully characterised, the biocatalyst was tested in combination with HeP5CR to produce *L*-PA. Initial tests were performed with 10 mM *L*-lysine with both cofactors at pH 8. Although in the chosen conditions GsLys6DH does not have the highest reported activity, which was at pH 10, the stability of the enzyme is described to be better in milder conditions, and as a balance between activity and stability pH 8 was chosen. As for the cofactor, both NAD<sup>+</sup> and NADP<sup>+</sup> were tested at equimolar and sub-stoichiometric concentration, to investigate the capacity of both enzymes to act in a cooperative way for the cofactor recycling (Table 7.4).

**Table 7.4.** Percentage conversion of *L*-lysine to *L*-PA catalysed by both free enzymes in batch. Reaction conditions: 10 mM *L*-lysine, 0.5 mg/mL GsLys6DH and HeP5CR in 100 mM phosphate buffer pH 8 at 37°C.

Cofactor		Conversion to <i>L</i> -PA (%)		
		2h	4h	24h
NAD <sup>+</sup>	10 mM	80	97	98
	1 mM	89	100	99
NADP <sup>+</sup>	10 mM	57	81	97
	1 mM	26	57	83

In this cascade, most of the lysine was converted to *L*-PA after only 2h and complete conversion to *L*-PA was observed after only 4h, when using NAD<sup>+</sup>. Complete conversion was also achieved with sub-stoichiometric amount of the cofactor (1:10), indicating that the system is also self-recycling the cofactor efficiently. Even with NADP<sup>+</sup>, with which GsLys6DH only exhibited 40% of the activity, when 10 mM of the cofactor was used more than 50% of lysine was converted in the first 2h and 81% after 4h. In contrast, when only 1 mM of NADP<sup>+</sup> was added, the conversion dropped to 26% after the first two hours, clearly indicating that the recycling of NADP<sup>+</sup> is less efficient than for NAD<sup>+</sup>.

After the excellent results obtained with 10 mM of *L*-lysine, the reaction was scaled up to 100 mM of *L*-lysine with the same enzyme concentration and using 1 mM of the NAD<sup>+</sup> cofactor (Table 7.5).

**Table 7.5.** Percentage conversion of *L*-lysine to *L*-PA catalysed by both free enzymes. Reaction conditions were 50/100 mM *L*-lysine, 0.5 mg/mL GsLys6DH and HeP5CR, 1 mM NAD<sup>+</sup>, 100 mM phosphate buffer pH 8, 37°C

Substrate concentration (mM)	Conversion to <i>L</i> -PA (%)		
	2 hrs	4 hrs	24 hrs
50	18	25	100
100	9	12	62

The cascade showed excellent scalability, being able to convert 50 mM of lysine over 24h. At the 100 mM scale, the conversion was lower, but as much as 62% of the substrate was converted after one day, with no further increase. These conversions, when expressed in volumetric yield are higher than the ones obtained with the transaminase catalysed reaction: more than 5 fold at both 50 mM and 100 mM scale (0.269 g/L/h and 0.333 g/L/h, respectively) when compared to HeTA at the 50 mM scale (0.054 g/L/h).

### 7.5. Immobilisation of GsLys6DH and HeP5C:

To further improve the productivity of the system and enable the recycling of the biocatalyst, immobilisation of both proteins onto epoxy or amino-epoxy derivatised polymethacrylate beads with variable pore size, and oxirane content (for more details see Figure 3.5 in Materials and Methods) were tested with a fixed loading of 2 mg/g of resin (Table 7.6).

**Table 7.6.** Recovered activity measured for both enzymes immobilised on each type of resin.

Enzyme	Recovered activity			
	EC/EP-S	EP403-S	ECHFA-S	HFA403-S
GsLys6DH	63 %	79 %	47 %	36 %
HeP5CR	3 %	4 %	3 %	4 %

When immobilised, GsLys6DH recovers in the best case, almost 80% of the activity, while the same strategy for HeP5CR provokes the loss of

more than 90% of its activity. Nonetheless, the specific activities of the biocatalyst are not that different. Free GsLys6DH exhibited a specific activity of 1.9 U/mg while HeP5CR has an activity of 19 U/mg in the oxidative way with T4C, and consequently once immobilised, the biocatalysts exhibited activities of 1.46 U/g of resin for GsLys6DH and 0.76 U/g of resin for HeP5CR. These biocatalysts were used in flow as a mixed bed packed-bed reactor, using 0.65g of each (Figure 7.16). The reaction, when using sub-stoichiometric amount of cofactor, only yielded 8% of pipercolic acid at the 10 mM scale and only when the amount of cofactor was increased to 10 mM, 28% conversion to pipercolic acid was observed with 64% lysine depletion. Varying the reaction temperature to promote GsLys6DH activity did not enhance significantly the final yield. This indicated that further optimisation of the system was needed, especially for the HeP5CR immobilisation.

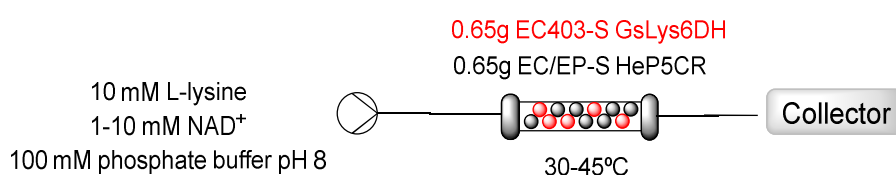


**Figure 7.16.** Schematic representation of the flow set up for the mixed packed-bed reactor containing both HeP5CR and GsLys6DH.

### 7.6. Optimisation of HeP5CR immobilisation, co-immobilisation with GsLys6DH and flow-assisted synthesis of L-PA:

To better understand the factors governing the loss of activity, a homology model of HeP5CR was created based on previously crystallised P5CR [21–40] using Phyre2 web service [41]. The monomer model, was then assembled as a dimer, based on *N. meningitidis* P5CR to mimic as much as possible its native form (Figure 7.17). Highlighting the importance of the dimeric structure in HeP5CR, the active site is located at the interface of the two subunits, close to the conserved cofactor binding motif. The two monomers interact through 4  $\alpha$ -helix which invade the other subunit and the cofactor, bound on one chain, participates in the catalysis of the substrate hosted by the other subunit. The substrate binding site is formed by seven residues, from Val230 to

Thr237 with which the substrate is thought to be stabilised through multiple hydrogen bonds [21–42].

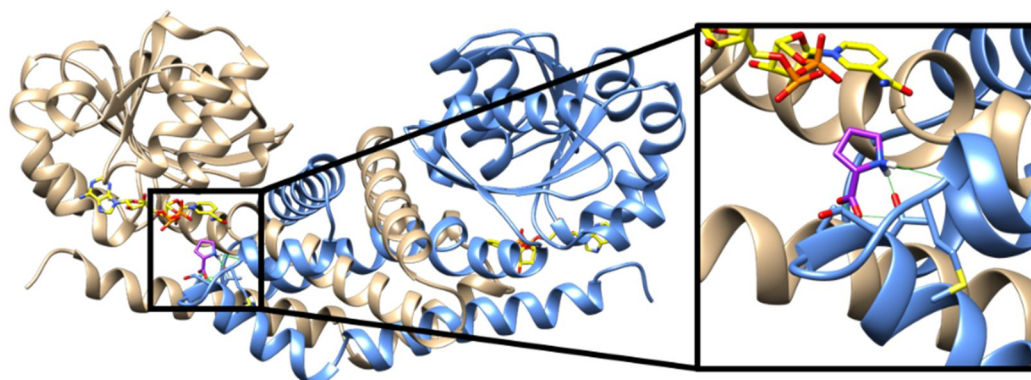


**Figure 7.17.** HeP5CR model. The two chains are shown in beige and blue. NAD<sup>+</sup> is shown in yellow and the proline substrate, docked into the active site, in purple. Hydrogen bonds between proline and the substrate binding residues are shown in green.

Although directed by the His-tag, the covalent immobilisation strategy used is based on the reactivity of superficial lysines with the epoxide groups. In this kind of immobilisation, as seen previously with HeAlaDH, distortion of the quaternary can cause the disruption of important interactions which keep the enzyme in its active form [43–44]. As shown in Figure 7.18, HeP5CR has only a few superficial lysines and 4 of them are in the dimeric interface. If those lysines interact with the epoxide, the rupture of the dimer could explain the low recovered activity of the reductase once immobilised.

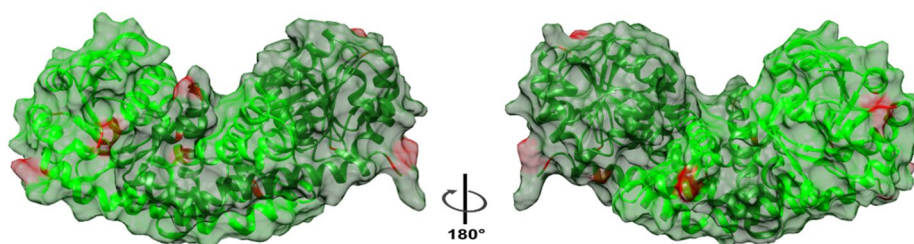


**Figure 7.18.** Image of the homology modelled HeP5CR. The two different chains are shown in two different shades of green with their corresponding surface representation. The lysine residues in red.

It has been previously described that subunit dissociation of immobilised enzymes can be prevented through pre or post-immobilisation coating with charged polymers, such as polyethyleneimine (PEI), a cationic polymer. Moreover, the post-

immobilisation coating with PEI also prevents the dissociation of the subunits in multimeric enzymes, if not all subunits interact directly with the resin [45–46]. Following this rationale, immobilisation of HeP5CR was attempted with simultaneous addition of different amounts of PEI. The cationic polymer was added during the immobilisation process also to promote competition between the enzyme and PEI for the epoxides, expecting PEI to occupy some epoxides and preventing the enzyme to form excessive links to the resin, which could affect also its activity by decreasing its flexibility (Figure 7.19).

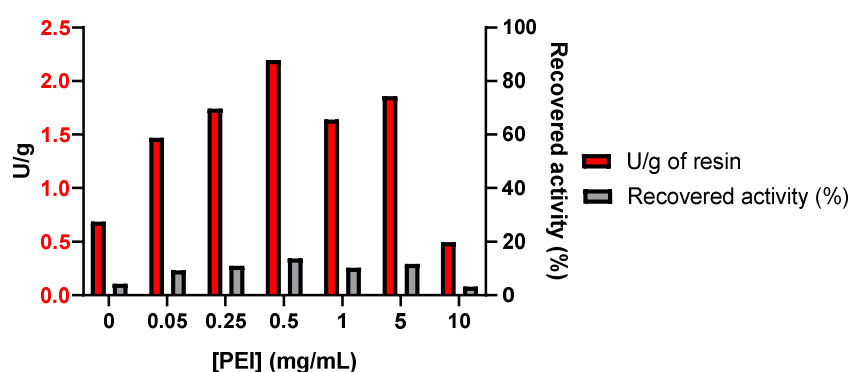


**Figure 7.19.** Results after immobilisation in presence of PEI of HeP5CR. A fixed loading of 2 mg of HeP5CR per g of resin of EP403/S was used. Specific activity of the biocatalyst is shown in red bars while the recovered activity is shown in grey bars.

Clearly, addition of low concentrations of PEI (from 0.05 to 0.5 mg/mL) during immobilisation, enhanced the recovered activity and therefore the specific activity of the biocatalyst. Using higher concentrations of the cationic polymer, provoked a decrease in activity, explained by lower immobilisation yields. As both the protein and PEI are competing for the same pool of epoxides, higher concentration of PEI might be counter-productive as instead of stabilising the enzyme it may hamper its immobilisation. The maximum value was obtained when using 0.5 mg/mL of PEI during immobilisation which delivered a biocatalyst with 13% recovered activity and 2.2 U/g, a 4-fold improvement compared to the initial values.

Once the activity of the biocatalyst was optimised, a new strategy to promote the cofactor recycling during the reaction was attempted by co-immobilisation of GsLys6DH and HeP5CR. It has been previously



reported that co-immobilisation of enzymes implicated in a cascade eases the substrate diffusion from one enzyme to the second one and therefore, has the potential to improve the production of the final product [47]. In this cascade, not only HeP5CR needs the product of GsLys6DH but also both enzymes are complementary in the cofactor recycling. Thus, 2 mg/g of support of GsLys6DH were firstly immobilised followed by the addition of HeP5CR in combination with 0.5 mg/mL of PEI as shown in Figure 7.20.

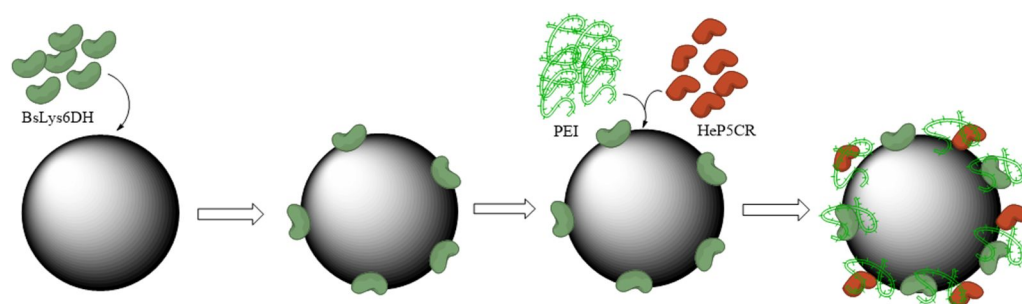


**Figure 7.20.** Schematic representation of the co-immobilisation strategy used for GsLys6DH and HeP5CR in combination with PEI.

Following the sequential co-immobilisation, the recovered activity of both enzymes, as well as the effect of PEI was assessed. Moreover, batch reactions were performed to investigate the capacity of the system to recycle the cofactor and catalyse the formation of *L*-PA with 10 mM *L*-lysine (Table 7.7).

**Table 7.7.** Characterisation of the co-immobilised system composed by GsLys6DH and HeP5CR with and without addition of PEI in two different polymethacrylate resins. The production of pipercolic acid of a batch reaction, consisting in 10 mM *L*-lysine, 0.1 mM NAD<sup>+</sup> performed with 40 mg of biocatalyst in 200  $\mu$ L is reported.

	EP403		EP113	
<b>GsLys6DH recovered activity (%)</b>	61 ± 2		53 ± 7	
<b>PEI (mg/mL)</b>	-	0.5	-	0.5
<b>HeP5CR recovered activity (%)</b>	2 ± 0.1	8 ± 1	0.3 ± 0.1	9 ± 1
<b><i>L</i>-PA m.c. (%)</b>	17 ± 2	98 ± 1	<5	91 ± 1

GsLys6DH, when immobilised in the two polymethacrylate resins (EP403-S and EP113-S), exhibited more than 50% of recovered activity in both cases. After co-immobilisation, the recovered activity for HeP5CR

were comparable to the ones depicted in Figure 7.19. The presence of PEI not only enhanced the recovered activity of HeP5CR as before, but also massively increased the production of *L*-PA and the system capacity to recycle the cofactor. When PEI was added, with both supports, the conversion of lysine into *L*-PA was almost complete after 24h of reaction with only catalytic amount of cofactor (0.1 mM). On the other hand, when no PEI was added the final production was not detectable with EP112/S and only 17% conversion was observed with EP403/S.

Following the excellent results obtained in batch, the co-immobilisation in EP403/S was scaled up in order to use it in a packed-bed reactor (Figure 7.21). Unexpectedly, mimicking the same conditions used in batch with a residence time of 10 minutes, no conversion was observed and increasing the cofactor concentration to 1 mM, only 6% conversion of 10 mM lysine was detected. The obtained results suggested that while the addition of PEI enhanced the recovered activity of HeP5CR, the improvement was not enough to recycle the cofactor when used in a continuous mode.

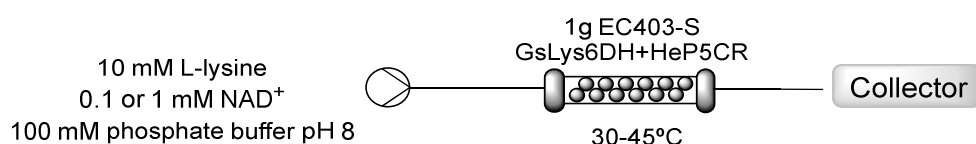


**Figure 7.21.** Schematic representation of the flow set up for the packed-bed reactor containing co-immobilised HeP5CR and GsLys6DH in EC403-S.

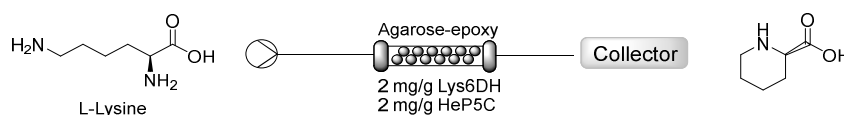
Since all the tested resins up until now were poly-methacrylate based, the support was changed to agarose to assess the effect of the matrix nature in the recovered activity and applicability of the biocatalyst. To keep the same immobilisation protocol and chemistry, agarose CL6B was derivatised with epoxide groups as previously described (Ep-Ag) [48]. Co-immobilisation onto agarose using the same conditions, generated a biocatalyst with  $91 \pm 4\%$  recovered activity for GsLys6DH and even better for HeP5CR with  $25 \pm 2\%$  compared to the  $11 \pm 1\%$  obtained with EP403/S (Table 7.8). The new biocatalyst, like EP403-S, also exhibited complete conversion of *L*-lysine to *L*-PA at the 10 mM scale after 24h in a batch reaction with just 0.1 mM of NAD<sup>+</sup>.

**Table 7.8.** Recovered activities obtained in the co-immobilisation of GsLys6DH and HeP5CR onto a polymethacrylate based resin (EP403/S) and an agarose CL6B support (Ep-Ag).

Enzyme	Loading (mg/g resin)	Recovered activity (%)	
		EP403/S	Ep-Ag
Lys6DH	2	61 ± 2	91 ± 4
HeP5C	2	11 ± 1	25 ± 2

Next, the agarose-based biocatalyst was tested as packed-bed reactor in flow. The retention time was increased to 20 or 30 minutes while the amount of cofactor was varied to investigate the capacity of the system to self-recycle the cofactor with 10 mM of lysine (Table 7.9).

**Table 7.9.** Flow assisted bioconversion of L-lysine into L-PA. A scheme of the reaction is shown.



	R.T. (min)	L-PA formation (%)
10 mM L-Lys, 1 mM NAD+	20	58 ± 1 %
10 mM L-Lys, 1 mM NAD+		100 ± 9 %
10 mM L-Lys, 0.5 mM NAD+	30	70 ± 3 %
10 mM L-Lys, 0.1 mM NAD+		28 ± 1 %

With this new biocatalyst, with a 20 minutes residence time and 1 mM of the cofactor, almost 60% of lysine was converted to L-PA. More importantly, with the same amount of cofactor but a longer retention time, up to half an hour, complete conversion was observed. In order to test the capacity of the system to recycle the cofactor, keeping the same retention time, lower amounts of cofactors were provided. Not surprisingly, when the amount of cofactor was reduced, the overall conversion to L-PA was also diminished. When the cofactor concentration was 0.5 mM, the conversion went down to 70% and with lowest tested concentration of cofactor, 0.1 mM, less than 30% conversion was obtained. Although the decreased conversions, this

proves this system has potential for the production of *L*-PA using only 0.01 equivalents of NAD<sup>+</sup>.

Remarkably, proving the beneficial properties of flow assisted biotransformations for process intensification, the productivity of the system with the co-immobilised enzymes combined with the continuous flow synthesis, was 2.5 g/L/h. This productivity is much higher than that obtained in batch using the same system with higher concentration of lysine (0.269 g/L/h at 50 mM scale and 0.333 g/L/h at 100 mM scale). Moreover, the covalent immobilisation allowed the recovery of the heterogeneous biocatalyst and its reuse. The same biocatalytic system was used for more than 5h at flow rates between 66 and 100  $\mu$ L/min without affecting the conversion to *L*-PA or the activity of the resin. Thus, the system presents a robust biocatalyst with excellent time-space yield for the synthesis of *L*-PA. Moreover, since both GsLys6DH and HeP5C exhibited activity against *L*-lysine-ethyl ester, this system presents the opportunity to synthesize derivatives of *L*-PA readily from modified lysine. Unlike what was observed with HeTA, GsLys6DH did not show any activity against ornithine in the tested conditions.

As for the immobilisation of HeP5CR, the addition of PEI during the immobilisation process and the high conversions obtained, indicated the ability to recycle the cofactor is sufficient and opens up the possibility to create biocatalyst with co-immobilised cofactor [49]. This strategy, which would generate a self-sufficient system in all senses, has been previously applied for the synthesis of chiral alcohols and proved that co-immobilisation of the cofactor increased both the cost-effectiveness and the applicability of the system in large scale.

In conclusion, in this chapter two different enzymatic cascades have been investigated for the production of *L*-pipecolic acid and derivatives starting from *L*-lysine, ornithine or lysine ethyl ester. By coupling a transamination reaction catalysed by HeTA with HeP5CR and FDH, volumetric productivities of 0.156 g/L/h, 0.160 g/L/h and 0.132 g/L/h were achieved for *L*-PA, *L*-proline and ethyl *L*-pipecolate respectively. This

cascade though, could not be satisfactorily applied in the synthesis of PA as the immobilised enzymes showed reduced stability at basic pH. On the other hand, coupling the deamination catalysed by GsLys6DH with HeP5CR reduction step, and by co-immobilisation on agarose of both enzymes was successful and the system was applied in a continuous mode as packed-bed reactor, increasing the productivity of *L*-PA to 2.5 g/L/h, a 10 fold improvement on the highest reported using sugar-fermentation in *C. glutamicum* (0.208 g/L/h).

## **7.7. Experimental procedures**

### **7.7.1. Synthesis of pyrroline-6-carboxylate:**

To 1mL of distilled water, 18.9 mg of allysine ethylene acetal were dissolved, followed by the addition of 40 mg of Amberlyst-15. The reaction was left stirring for 2h at 30°C.

### **7.7.2. Co-immobilisation of BsLys6DH and HeP5CR:**

To the previously activated support, a loading of 2 mg/g of resin of BsLys6DH was added and left mixing for 4 hours at room temperature, when all the protein was immobilised. After that, 2 mg/g of resin of HeP5CR with 0.5 mg/mL of PEI was added and left mixing for 4 hours at room temperature. Desorption was performed as explained before, but the blocking step was done with 10 mL/g of resin of 10 mg/mL of PEI in 50 mM phosphate buffer pH 8. The suspension was left in agitation O/N and the sample thoroughly washed with water before keeping the biocatalyst at 4°C in 50 mM phosphate buffer pH 8.

## 7.8. Bibliography

1. M. Nishizawa, M. Shimizu, H. Ohkawa, & M. Kanaoka, Stereoselective production of (+)-trans-chrysanthemic acid by a microbial esterase: cloning, nucleotide sequence, and overexpression of the esterase gene of *Arthrobacter globiformis* in *Escherichia coli*. *Applied and environmental microbiology*, **61** (1995) 3208–15.
2. H. Návarová, F. Bernsdorff, A.-C. Döring, & J. Zeier, Pipecolic Acid, an Endogenous Mediator of Defense Amplification and Priming, Is a Critical Regulator of Inducible Plant Immunity. *The Plant Cell*, **24** (2012) 5123–5141. <https://doi.org/10.1105/tpc.112.103564>.
3. Y. -F Chang, Lysine Metabolism in the Rat Brain: the Pipecolic Acid-Forming Pathway. *Journal of Neurochemistry*, **30** (1978) 347–354. <https://doi.org/10.1111/j.1471-4159.1978.tb06536.x>.
4. V. Vranova, L. Lojkova, K. Rejsek, & P. Formanek, Significance of the Natural Occurrence of L- Versus D-Pipecolic Acid: A Review. *Chirality*, **25** (2013) 823–831. <https://doi.org/10.1002/chir.22237>.
5. T. Schwecke, J. F. Aparicio, I. Molnár, A. König, L. E. Khaw, S. F. Haydock, M. Oliynyk, P. Caffrey, J. Cortés, & J. B. Lester, The biosynthetic gene cluster for the polyketide immunosuppressant rapamycin. *Proceedings of the National Academy of Sciences of the United States of America*, **92** (1995) 7839–43. <https://doi.org/10.1073/pnas.92.17.7839>.
6. P. H. Y. Cheong, H. Zhang, R. Thayumanavan, F. Tanaka, K. N. Houk, & C. F. Barbas, Pipecolic acid-catalyzed direct asymmetric Mannich reactions. *Organic Letters*, **8** (2006) 811–814. <https://doi.org/10.1021/ol052861o>.
7. A. Gaumann, H. J. Schlitt, & E. K. Geissler, Immunosuppression and tumor development in organ transplant recipients: The emerging dualistic role of rapamycin. *Transplant International*, **21**

(2008) 207–217. <https://doi.org/10.1111/j.1432-2277.2007.00610.x>.

8. J. W. Han, Seong Hoon Ahn, Seung Hee Park, So Young Wang, G. U. Bae, D. W. Seo, H. K. Kwon, S. Hong, Hoi Young Lee, Y. W. Lee, & H. W. Lee, Apicidin, a histone deacetylase inhibitor, inhibits proliferation of tumor cells via induction of p21(WAF1/Cip1) and gelsolin. *Cancer Research*, **60** (2000) 6068–6074.
9. S. J. Darkin-Rattray, A. M. Gurnett, R. W. Myers, P. M. Dulski, T. M. Crumley, J. J. Allocco, C. Cannova, P. T. Meinke, S. L. Colletti, M. A. Bednarek, S. B. Singh, M. A. Goetz, A. W. Dombrowski, J. D. Polishook, & D. M. Schmatz, Apicidin: A novel antiprotozoal agent that inhibits parasite histone deacetylase. *Proceedings of the National Academy of Sciences*, **93** (1996) 13143–13147. <https://doi.org/10.1073/pnas.93.23.13143>.
10. L. A. Watanabe, S. Haranaka, B. Jose, M. Yoshida, T. Kato, M. Moriguchi, K. Soda, & N. Nishino, An efficient access to both enantiomers of pipercolic acid. *Tetrahedron: Asymmetry*, **16** (2005) 903–908. <https://doi.org/10.1016/j.tetasy.2005.01.017>.
11. A. Cant & A. Sutherland, Asymmetric Synthesis of Pipercolic Acid and Derivatives. *Synthesis*, **44** (2012) 1935–1950. <https://doi.org/10.1055/s-0031-1289767>.
12. T. Fujii, M. Mukaihara, H. Agematu, & H. Tsunekawa, Biotransformation of L-Lysine to L-Pipercolic Acid Catalyzed by L-Lysine 6-Aminotransferase and Pyrroline-5-carboxylate Reductase. *Bioscience, Biotechnology, and Biochemistry*, **66** (2002) 622–627. <https://doi.org/10.1271/bbb.66.622>.
13. H. Ying, J. Wang, Z. Wang, J. Feng, K. Chen, Y. Li, & P. Ouyang, Enhanced conversion of L-lysine to L-pipercolic acid using a recombinant *Escherichia coli* containing lysine cyclodeaminase as whole-cell biocatalyst. *Journal of Molecular Catalysis B: Enzymatic*, **117** (2015) 75–80.

<https://doi.org/10.1016/j.molcatb.2015.05.001>.

14. Y. Tani, R. Miyake, R. Yukami, Y. Dekishima, H. China, S. Saito, H. Kawabata, & H. Mihara, Functional expression of l-lysine  $\alpha$ -oxidase from *Scomber japonicus* in *Escherichia coli* for one-pot synthesis of l-pipecolic acid from dl-lysine. *Applied Microbiology and Biotechnology*, **99** (2015) 5045–5054. <https://doi.org/10.1007/s00253-014-6308-0>.
15. M.-L. Wu, J.-H. Chen, C.-T. Ho, & T.-C. Huang, Synthesis of 1-Piperidine-6-carboxylic Acid Produced by  $\epsilon$ -lysine- $\epsilon$ -aminotransferase from the *Streptomyces clavuligerus* Gene Expressed in *Escherichia coli*. *Journal of Agricultural and Food Chemistry*, **55** (2007) 1767–1772. <https://doi.org/10.1021/jf062975u>.
16. S. M. Byun, S. W. Jeong, D. H. Cho, & Y. H. Kim, Optimized conversion of L-lysine to L-pipecolic acid using recombinant lysine cyclodeaminase from *Streptomyces pristinaespiralis*. *Biotechnology and Bioprocess Engineering*, **20** (2015) 73–78. <https://doi.org/10.1007/s12257-014-0428-3>.
17. F. Pérez-García, J. Max Risse, K. Friehs, & V. F. Wendisch, Fermentative production of L-pipecolic acid from glucose and alternative carbon sources. *Biotechnology Journal*, **12** (2017) 1–12. <https://doi.org/10.1002/biot.201600646>.
18. H. H. Lo, S. K. Hsu, W. De Lin, N. L. Chan, & W. H. Hsu, Asymmetrical synthesis of L-Homophenylalanine using engineered *Escherichia coli* aspartate aminotransferase. *Biotechnology Progress*, **21** (2005) 411–415. <https://doi.org/10.1021/bp049756i>.
19. B. A. Kern, D. Hendlin, & E. Inamine, L-lysine epsilon-aminotransferase involved in cephamycin C synthesis in *Streptomyces lactamdurans*. *Antimicrobial Agents and Chemotherapy*, **17** (1980) 679–685.



<https://doi.org/10.1128/AAC.17.4.679>.

20. J. C. Fothergill & J. R. Guest, Catabolism of L-Lysine by *Pseudomonas aeruginosa*. *Journal of General Microbiology*, **99** (1977) 139–155. <https://doi.org/10.1099/00221287-99-1-139>.
21. B. Nocek, C. Chang, H. Li, L. Lezondra, D. Holzle, F. Collart, & A. Joachimiak, Crystal structures of  $\Delta^1$ -pyrroline-5-carboxylate reductase from human pathogens *Neisseria meningitidis* and *Streptococcus pyogenes*. *Journal of Molecular Biology*, **354** (2005) 91–106. <https://doi.org/10.1016/j.jmb.2005.08.036>.
22. A. Rumbero, J. Fco. Martín, M. Angeles Lumbreras, P. Liras, & C. Esmahan, Chemical synthesis of allysine ethylene acetal and conversion in situ into 1-piperideine-6-carboxylic acid: Key intermediate of the  $\alpha$ -amino adipic acid for  $\beta$ -lactam antibiotics biosynthesis. *Bioorganic and Medicinal Chemistry*, **3** (1995) 1237–1240. [https://doi.org/10.1016/0968-0896\(95\)00110-3](https://doi.org/10.1016/0968-0896(95)00110-3).
23. I. Pérez-Arellano, F. Carmona-Álvarez, A. I. Martínez, J. Rodríguez-Díaz, & J. Cervera, Pyrroline-5-carboxylate synthase and proline biosynthesis: From Osmotolerance to rare metabolic disease. *Protein Science*, **19** (2010) 372–382. <https://doi.org/10.1002/pro.340>.
24. C. E. Deutch, J. L. Klarstrom, C. L. Link, & D. L. Ricciardi, Oxidation of L-thiazolidine-4-carboxylate by  $\delta^1$ -pyrroline-5-carboxylate reductase in *Escherichia coli*. *Current Microbiology*, **42** (2001) 442–446. <https://doi.org/10.1007/s002840010245>.
25. Y. Yang, S. Xu, M. Zhang, R. Jin, L. Zhang, J. Bao, & H. Wang, Purification and characterization of a functionally active *Mycobacterium tuberculosis* pyrroline-5-carboxylate reductase. *Protein Expression and Purification*, **45** (2006) 241–248. <https://doi.org/10.1016/j.pep.2005.08.007>.
26. N. V. Bhagavan, C.-E. Ha, N. V. Bhagavan, C.-E. Ha, & P. Fürst, Protein and Amino Acid Metabolism. *Nutr. Support Crit. Ill Patient*

- (Academic Press, 2005), pp. 27–47.  
<https://doi.org/10.1201/9781420039191.ch3>.
27. L. Cerioli, M. Planchestainer, J. Cassidy, D. Tessaro, & F. Paradisi, Characterization of a novel amine transaminase from *Halomonas elongata*. *Journal of Molecular Catalysis B: Enzymatic*, **120** (2015) 141–150. <https://doi.org/10.1016/j.molcatb.2015.07.009>.
  28. K. Yamamoto, G. Kurisu, M. Kusunoki, S. Tabata, I. Urabe, & S. Osaki, Crystal Structure of Glucose Dehydrogenase from *Bacillus megaterium* IWG3 at 1.7 Resolution. *Journal of Biochemistry*, **129** (2001) 303–312. <https://doi.org/10.1093/oxfordjournals.jbchem.a002858>.
  29. W. Liu & P. Wang, Cofactor regeneration for sustainable enzymatic biosynthesis. *Biotechnology Advances*, **25** (2007) 369–384. <https://doi.org/10.1016/j.biotechadv.2007.03.002>.
  30. X. Wang, T. Saba, H. H. P. Yiu, R. F. Howe, J. A. Anderson, & J. Shi, Cofactor NAD(P)H Regeneration Inspired by Heterogeneous Pathways. *Chem*, **2** (2017) 621–654. <https://doi.org/10.1016/j.chempr.2017.04.009>.
  31. H. Schütte, J. Flossdorf, H. Sahm, & M. R. Kula, Purification and Properties of Formaldehyde Dehydrogenase and Formate Dehydrogenase from *Candida boidinii*. *European Journal of Biochemistry*, **62** (1976) 151–160. <https://doi.org/10.1111/j.1432-1033.1976.tb10108.x>.
  32. S. Velasco-Lozano, E. S. da Silva, J. Llop, & F. López-Gallego, Sustainable and continuous synthesis of enantiopure L-amino acids using a versatile immobilised multi-enzyme system. *ChemBioChem*, **19** (2017) 395–403. <https://doi.org/10.1002/cbic.201700493>.
  33. A. V. Mesentev, V. S. Lamzin, V. I. Tishkov, T. B. Ustinnikova, & V. O. Popov, Effect of pH on kinetic parameters of NAD<sup>+</sup>-dependent formate dehydrogenase. *Biochemical Journal*, **321**

(1997) 475–480. <https://doi.org/10.1042/bj3210475>.

34. A. Dinçer & A. Telefoncu, Improving the stability of cellulase by immobilization on modified polyvinyl alcohol coated chitosan beads. *Journal of Molecular Catalysis B: Enzymatic*, **45** (2007) 10–14. <https://doi.org/10.1016/j.molcatb.2006.10.005>.
35. V. F. Wendisch, J. M. P. Jorge, F. Pérez-García, & E. Sgobba, Updates on industrial production of amino acids using *Corynebacterium glutamicum*. *World Journal of Microbiology and Biotechnology*, **32** (2016). <https://doi.org/10.1007/s11274-016-2060-1>.
36. J. V. K. Jensen & V. F. Wendisch, Ornithine cyclodeaminase-based proline production by *Corynebacterium glutamicum*. *Microbial Cell Factories*, **12** (2013) 1–10. <https://doi.org/10.1186/1475-2859-12-63>.
37. H. Ying, S. Tao, J. Wang, W. Ma, K. Chen, X. Wang, & P. Ouyang, Expanding metabolic pathway for de novo biosynthesis of the chiral pharmaceutical intermediate l-pipecolic acid in *Escherichia coli*. *Microbial Cell Factories*, **16** (2017) 52. <https://doi.org/10.1186/s12934-017-0666-0>.
38. M. Heydari, T. Ohshima, & N. Nunoura-kominato, Highly Stable l-Lysine 6-Dehydrogenase from the Thermophile *Geobacillus stearothermophilus* Isolated from a Japanese Hot Spring: Characterization, Gene Cloning and Sequencing, and Expression. **70** (2004) 1–7. <https://doi.org/10.1128/AEM.70.2.937.942.2004>.
39. K. Yoneda, J. Fukuda, H. Sakuraba, & T. Ohshima, First crystal structure of L-lysine 6-dehydrogenase as an NAD-dependent amine dehydrogenase. *Journal of Biological Chemistry*, **285** (2010) 8444–8453. <https://doi.org/10.1074/jbc.M109.084384>.
40. Z. Meng, Z. Lou, Z. Liu, M. Li, X. Zhao, M. Bartlam, & Z. Rao, Crystal Structure of Human Pyrroline-5-carboxylate Reductase.

*Journal of Molecular Biology*, **359** (2006) 1364–1377.  
<https://doi.org/10.1016/j.jmb.2006.04.053>.

41. L. A. Kelly, S. Mezulis, C. Yates, M. Wass, & M. Sternberg, The Phyre2 web portal for protein modelling, prediction, and analysis. *Nature Protocols*, **10** (2015) 845–858.  
<https://doi.org/10.1038/nprot.2015-053>.
42. E. M. Christensen, S. M. Patel, D. A. Korasick, A. C. Campbell, K. L. Krause, D. F. Becker, & J. J. Tanner, Resolving the cofactor-binding site in the proline biosynthetic enzyme human pyrroline-5-carboxylate reductase 1. *Journal of Biological Chemistry*, **292** (2017) 7233–7243. <https://doi.org/10.1074/jbc.M117.780288>.
43. R. A. Sheldon, Enzyme immobilization: The quest for optimum performance. *Advanced Synthesis and Catalysis*, **349** (2007) 1289–1307. <https://doi.org/10.1002/adsc.200700082>.
44. U. Hanefeld, L. Gardossi, & E. Magner, Understanding enzyme immobilisation. *Chem. Soc. Rev.*, **38** (2009) 453–468.  
<https://doi.org/10.1039/B711564B>.
45. J. M. Bolivar, J. Rocha-Martín, C. Mateo, & J. M. Guisan, Stabilization of a highly active but unstable alcohol dehydrogenase from yeast using immobilization and post-immobilization techniques. *Process Biochemistry*, **47** (2012) 679–686.  
<https://doi.org/10.1016/j.procbio.2012.01.012>.
46. L. Trobo-Maseda, A. H. Orrego, S. Moreno-Pérez, G. Fernández-Lorente, J. M. Guisan, & J. Rocha-Martín, Stabilization of multimeric sucrose synthase from *Acidithiobacillus caldus* via immobilization and post-immobilization techniques for synthesis of UDP-glucose. *Applied Microbiology and Biotechnology*, **102** (2018) 773–787. <https://doi.org/10.1007/s00253-017-8649-y>.
47. J. Rocha-Martín, B. de las Rivas, R. Muñoz, J. M. Guisán, & F. López-Gallego, Rational Co-Immobilization of Bi-Enzyme Cascades on Porous Supports and their Applications in Bio-Redox

Reactions with In Situ Recycling of Soluble Cofactors. *ChemCatChem*, **4** (2012) 1279–1288. <https://doi.org/10.1002/cctc.201200146>.

48. C. Mateo, V. Grazu, J. M. Palomo, F. Lopez-Gallego, R. Fernandez-Lafuente, & J. M. Guisan, Immobilization of enzymes on heterofunctional epoxy supports. *Nature Protocols*, **2** (2007) 1022–1033. <https://doi.org/10.1038/nprot.2007.133>.
49. A. I. Benítez-Mateos, E. San Sebastián, N. Ríos Lombardía, F. Morís, J. González-Sabín, & F. Lopez-Gallego, Asymmetric reduction of prochiral ketones by using self-sufficient heterogeneous biocatalysts based on NADPH-dependent ketoreductases. *Chemistry - A European Journal*, (2017). <https://doi.org/10.1002/chem.201703475>.

## Chapter 8: Conclusions and final remarks

In this work, the central theme has been to identify and address some of problems which still hamper the industrial use of flow biocatalysis. The main problems identified and discussed are: (I) the use of enzymes with difficult immobilisation, (II) the bioconversion of water-insoluble substrates, (III) the stability of the biocatalyst and (IV) the use of expensive cofactors, such as PLP or NAD(P).

In chapter 4, a new esterase from *Halomonas elongata* has been characterised. In addition, the problematic immobilisation was addressed for BS2m. A new covalent immobilisation strategy to enhance the recovered activity of this carboxylesterase with industrial potential, through the creation of a fusion protein was developed. The heterogeneous biocatalyst had comparable activity with the commercially available Novozym435® with a much lower loading (7.5 mg/g compared to 82 mg/g), reducing the overall costs. In addition, this new biocatalyst was used in flow in a packed-bed reactor for the enantioselective cleavage of naproxen butyl esters. To overcome the issues arising from the use of water-insoluble substrates in a flow reactor, addition of surfactant to the sample allowed complete solubilisation of up to 5 mM of the ester substrate. On a 5 mM scale, the optimised reaction yielded 24% molar conversion with 80% enantioselectivity. The biocatalyst also exhibited good resistance to the reaction conditions, with almost 60% of the initial activity retained after 6h of use in flow.

For the transaminase catalysed reactions, the PLP affinity has been identified as one of the major factors to consider for their industrial application due to the cost associated with the requirement of high amounts of exogenous cofactor needed, and for its effect on the protein stability. To better understand the factors governing the PLP binding, in chapter 5, the PLP binding pocket of three different class-III  $\omega$ -transaminases (HeTA, CvTA and PfTA) was studied. From the three, HeTA exhibited a higher affinity for PLP when used in flow with co-immobilised PLP. To increase our structural understanding of these

enzymes, firstly, the structure of PfTA, was solved and the enzyme identified as a tetramer, unlike HeTA and CvTA which are dimers. Next, through the analysis of the PLP-binding pocket, a single residue difference was identified in HeTA; an asparagine with potential to interact with the PLP either directly or indirectly, by polarising the acidic residue conserved in the PLP binding site that interacts with the pyridinium nitrogen. The homologous position was occupied by a valine in the two other studied enzymes. The role of this asparagine and its relation to both functional and structural parameters was studied for the three enzymes by single-point mutagenesis. While in PfTA the substitution did not affect the PLP binding, it seemed to destabilise the enzyme, probably affecting its quaternary assembly. On the other hand, for the two dimeric transaminases the variants containing the asparagine exhibited a better affinity for PLP and consequently higher temperature stabilities to their counterparts with a valine. Moreover, these new variants proved to retain more efficiently PMP. In CvTA no change in its thermodynamic behaviour was observed, indicating that the folding of the protein was not affected. In HeTA, substitution of the asparagine for a valine, affected also the midpoint denaturation point of the protein, indicating PLP binding is of utmost importance for the correct folding and maintenance of the structure.

Likewise, another important issue in transaminase catalysed bioconversion was addressed in Chapter 6. When working with substrates with an unfavourable equilibrium for their amination, normally high concentrations of the amino donor are needed. This affects the stability of the transaminase by either forming an imine of PLP-amino donor or PMP, which are no longer covalently bound to the enzyme and therefore can leak from the active site. Therefore, an in-situ recycling of the amino donor is beneficial as it provides a strategy to shift the equilibrium without affecting the stability of the main catalyst. To harness the beneficial behaviour exhibited by halo-tolerant proteins, a new alanine dehydrogenase from *Halomonas elongata* was cloned, characterised and immobilised to create a robust biocatalyst. In addition,

HeAlaDH was co-immobilised with a formate dehydrogenase to create a biocatalyst which could self-recycle the NAD-cofactor required in this step, and used in combination with HeTA, as a mixed packed-bed reactor. This system, with only one equivalent of the amino donor, delivered almost complete conversion of cinnamaldehyde, more than 50% of vanillin and 60% of cyclohexanone, opposed to HeTA alone which yielded no conversion. Further optimisation of the system could be applied by co-immobilising the three enzymes, and possibly the cofactor, in the same support to enhance the efficient recycling. Moreover, when the aromatic substrates were used, interaction with the resin was detected and an investigation of more hydrophilic supports, as well as further screening of the reaction conditions, could increase their yield and facilitate their purification.

In Chapter 7, a more synthetic based problem was addressed: the synthesis of pipercolic acid from lysine. Here, a pyrroline-5-reductase from *H. elongata* (HeP5CR) was successfully cloned, characterised and its immobilisation optimised through the addition of PEI. This new enzyme was firstly combined with HeTA, which is capable of deaminating lysine on its  $\epsilon$ -position. Once deaminated, the product undergoes spontaneous cyclisation in water yielding pyrroline-6-carboxylate which can be reduced by HeP5CR. To make the system more cost-effective, two different recycling systems for the NAD(P)-cofactor were studied. By using this method in the optimised conditions, volumetric productivities matching the state-of-art transformation with free enzymes were obtained for *L*-pipercolic acid (0.156 g/L/h), *L*-proline (0.160) g/L/h and, for the first time, the biosynthesis of *L*-ethyl pipercolinate (0.132 g/L/h). This cascade reaction could not be applied in a flow reactor as the immobilised biocatalyst exhibited low stability in the desired reaction conditions. As an alternative, a redox neutral cascade was constructed combining HeP5CR with a thermophilic lysine-6-dehydrogenase (GsLys6DH). Co-immobilisation of both enzymes allowed for the system to be applied as packed-bed reactor with excellent volumetric yields to produce *L*-pipercolic acid, 2.5 g/L/h, a 10-fold improvement compared to



the highest reported by whole cell fermentation. Moreover, co-immobilisation of the cofactor is now being studied to develop an entirely self-sufficient biocatalyst for *L*-PA production at industrial scale.

## Acknowledgments

First, I would like to express my deepest gratitude to my supervisor Prof. Francesca Paradisi for giving me the opportunity to do my PhD in her group which has been a marvellous experience, both professionally and personally. I would also like to thank her for being always available and for her guidance and counselling. I would also like to specially thank Dr. Martina Contente, who during my first year in Nottingham took me under her wing and taught me most of what I know about flow-chemistry. Thank you, Marti, for your time, your patience and for your caring toughness when needed. Special thanks also to Eimear Hegarty, with whom I shared this journey from the very first day. Thank you for listening to my (many) complains, my problems and always being there. To Matteo Planchestainer and Alessandro Orlandini for taking care of me during my unforgettable first year in Nottingham. To Lidia Delgado for her support and particularly for bearing with my noisy manners in the office, which often ended with a deserved “serpientazo”. To Maria Romero for her insights in protein immobilisation and, more importantly, proving that being always happy and optimistic is possible and the best way to face everything. Thanks also to the other members of the group, Valentina, Irene, Nourah, Candice, Chris and Nick for the beautiful environment we always had in the lab. Special thanks also to the many friends I had the opportunity to meet in Nottingham. They have been my family here and they always will have a place wherever I am.

And last, thanks to the biggest gift the PhD experience has given me: meeting Ana. Because sometimes, it's when you are not seeking anything that you actually find everything. No hay palabras suficientes para agradecer todo lo que has hecho por mí en estos dos años. Gracias por estar siempre ahí, por hacerme sonreír en los momentos más grises a pesar de la distancia, porque es lo que me daba fuerza para continuar adelante. De todo lo que me ha dado el doctorado, sé que tú eres lo más importante. T'estimo!